ELECTRIC FIELD MANIPULATION OF POLYMER NANOCOMPOSITES: PROCESSING AND INVESTIGATION OF THEIR PHYSICAL CHARACTERISTICS

A Dissertation

by

SUMANTH BANDA

Submitted to the Office of Graduate Studies of
Texas A&M University
in partial fulfillment of the requirements for the degree of

DOCTOR OF PHILOSOPHY

December 2008

Major Subject: Materials Science & Engineering

ELECTRIC FIELD MANIPULATION OF POLYMER NANOCOMPOSITES: PROCESSING AND INVESTIGATION OF THEIR PHYSICAL CHARACTERISTICS

A Dissertation

by

SUMANTH BANDA

Submitted to the Office of Graduate Studies of
Texas A&M University
in partial fulfillment of the requirements for the degree of

DOCTOR OF PHILOSOPHY

Approved by:

Chair of Committee,	Zoubeida Ounaies
Committee Members,	Dimitris Lagoudas
	Jim Boyd
	Hung-Jue Sue
	Jaime Grunlan
Intercollegiate Faculty Chair,	Tahir Cagin

December 2008

Major Subject: Materials Science & Engineering

ABSTRACT

Electric Field Manipulation of Polymer Nanocomposites: Processing and Investigation of Their Physical Characteristics. (December 2008)

Sumanth Banda, B.Tech, Jawaharlal Nehru Technological University;

M.S., Virginia Commonwealth University

Chair of Advisory Committee: Dr. Zoubeida Ounaies

Research in nanoparticle-reinforced composites is predicated by the promise for exceptional properties. However, to date the performance of nanocomposites has not reached its potential due to processing challenges such as inadequate dispersion and patterning of nanoparticles, and poor bonding and weak interfaces. The main objective of this dissertation is to improve the physical properties of polymer nanocomposites at low nanoparticle loading. The first step towards improving the physical properties is to achieve a good homogenous dispersion of carbon nanofibers (CNFs) and single wall carbon nanotubes (SWNTs) in the polymer matrix; the second step is to manipulate the well-dispersed CNFs and SWNTs in polymers by using an AC electric field.

Different techniques are explored to achieve homogenous dispersion of CNFs and SWNTs in three polymer matrices (epoxy, polyimide and acrylate) without detrimentally affecting the nanoparticle morphology. The three main factors that influence CNF and SWNT dispersion are: use of solvent, sonication time, and type of mixing. Once a

dispersion procedure is optimized for each polymer system, the study moves to the next step. Low concentrations of well dispersed CNFs and SWNTs are successfully manipulated by means of an AC electric field in acrylate and epoxy polymer solutions. To monitor the change in microstructure, alignment is observed under an optical microscope, which identifies a two-step process: rotation of CNFs and SWNTs in the direction of electric field and chaining of CNFs and SWNTs. In the final step, the aligned microstructure is preserved by curing the polymer medium, either thermally (epoxy) or chemically (acrylate). The conductivity and dielectric constant in the parallel and perpendicular direction increased with increase in alignment frequency. The values in the parallel direction are greater than the values in the perpendicular direction and anisotropy in conductivity increased with increase in AC electric field frequency. There is an 11 orders magnitude increase in electrical conductivity of 0.1 wt% CNF-epoxy nanocomposite that is aligned at 100 V/mm and 1 kHz frequency for 90 minutes. Electric field magnitude, frequency and time are tuned to improve and achieve desired physical properties at very low nanoparticle loadings.

DEDICATION

To my parents and grandparents

ACKNOWLEDGEMENTS

I would like to acknowledge several people for their help in completing this dissertation. First and foremost, I want to thank Zoubeida Ounaies, my doctoral advisor for the advice, guidance and support that she continuously provided to me throughout my graduate work. Her words of encouragement and careful reading of all my writing will never be forgotten. She is one of the rare advisors that students dream that they will find. Without her support, I could not have done what I was able to do. I also extend my thanks to my doctoral committee, Dimitris Lagoudas, Jim Boyd, Hung-Jue Sue, and Jaime Grunlan, for their guidance and support throughout the course of this research.

My thanks to all my colleagues at Electroactive Materials Characterization Laboratory, especially Ricardo Perez, Sanjay Kalidindi, Sujay Deshmukh, Ainsley VanRooyen and Casey Whalen who helped me with my doctoral work. This work was supported in part by NSF-DMI and NASA URETI Texas Institute for Intelligent Bio-Nano Materials and Structures for Aerospace Vehicles (TIIMS).

Graduate life can be stressful and tiring sometimes, this would have not been possible without the support of all family members and friends. I would like to thank my parents, grandparents, sister, brother in law and friends for their encouragement and support. Special thanks to my uncle Ramesh Chamala who encouraged me to pursue my doctoral studies and provided me with a lot of support. Finally, I would like to thank my fiancé

Pavani Reddy for all the love, support and encouragement that she provided during difficult times.

NOMENCLATURE

DMAc	N, N- dimethylacetamide
βCN-APB	Bi(3-amino phenoxy benzo nitrile)
ODPA	Oxydiphthalic anhydride
UDMA	Urethane dimethacrylate
HDDMA	1, 6 Haxanediol dimethacrylate
DEP	Dielectrophoretic
q	Charge
V	Volume
ε’	Dielectric constant
σ’	Electrical conductivity
ε_0	Dielectric constant in vaccum
ε_m	Dielectric permittivity of medium
ε_p	Dielectric permittivity of particle
σ_m	Conductivity of medium
σ_p	Conductivity of particle
E	Electric field
K	Clausius Mossoti factor
w	Frequency
D	Diffusion constant
f	Friction factor

k	Boltzman's constant
T	Absolute temperature
ρ_p	Density of particle
ρ_m	Density of medium
g	Acceleration due to gravity
τ	Torque
τ^E	Electrical torque
τ^V	Viscous torque
μ	Dipole moment
θ	Angle between the particle axis and the electric field
OM	Optical microscopy
SEM	Scanning electron microscopy
t	Thickness
A	Area
C	Capacitance
E'	Storage modulus
E"	Loss modulus
DMA	Dynamic mechanical analysis
σ	Stress
γ	Strain
Tan δ	Loss tangent

TABLE OF CONTENTS

Page

Page

LIST OF FIGURES

FIGURE Page

FIGURE Page

FIGURE Page

FIGURE Page

FIGURE Page

FIGURE Page

LIST OF TABLES

1. INTRODUCTION

1.1 Problem statement

Polymer-based composites are widely used in aerospace applications due to the following advantages: lightweight, flexibility, high strength, corrosion resistance, easy processability and relatively low cost. This unique combination of characteristics motivated their use in military and commercial aircrafts as well as spacecrafts. Recent research has focused on complementing their structural characteristics with added functionalities such as electrical conductivity, thermal conductivity, self-sensing and actuation. One approach used to achieve this 'multifunctionality' is to embed nanoparticles with exceptional properties in the polymer composites. Some of the potential aerospace applications are health monitoring of space vehicles and aircraft, electrostatic discharge, electric current mitigation in response to lightning strikes in the atmosphere[5], electromagnetic interference shielding [6, 7], and inflatable structures like satellites and space mirrors.

Although the high prospect for applications outlined above justifies the extensive research focusing on polymer nanocomposites, to date the performance of polymer nanocomposites has been limited by processing challenges such as difficulty in dispersing and manipulating nanoparticles, and poor bonding and weak interfaces.

This dissertation follows the style of *Advanced Functional Materials*.

Efforts have been made to improve dispersion and interaction between the polymer matrix and nanoparticles [4, 8-23], hence enhancing mechanical [17-20] and electrical [21-23] properties. But even in these cases, although homogeneous dispersion is achieved at low nanoparticle loadings, it remains a major challenge to separate the nanoparticle agglomerates and attain a homogeneous dispersion and good interaction at high loadings. Another challenge at high nanoparticle loadings is processability where the polymer viscosity increases drastically. One approach to achieve large improvements in physical properties while maintaining a low concentration of nanoparticles is to orient the nanoparticles at low concentration, resulting in large improvements in properties in the direction of alignment. Aligned polymer nanocomposites have shown improvements in physical properties like electrical and dielectric properties [24-27], but a comprehensive description of different mechanisms that drive the network formation and the impact of the modified microstructure on the physical properties of polymer nanocomposites is still lacking. This gap in analysis provides a strong motivation to investigate and understand the effect of electric field manipulation of nanoparticles on the microstructure and physical properties of polymer nanocomposites.

The broad goal of this research is to improve the physical properties of polymer nanocomposites while maintaining good interaction between nanoparticles and the polymer matrix. The study focuses on manipulation of a low concentration of well-dispersed nanoparticles in polymers by means of an external AC electric field. A fundamental study of different mechanisms associated with electric field-driven

manipulation is very important. This enables us to achieve spatial control of nanoparticle distribution while optimizing mechanical and electrical contrast throughout the material. In this work single wall carbon nanotubes (SWNTs) and carbon nanofibers (CNFs) are dispersed in epoxy, acrylates and polyimides.

It is a major challenge to disperse SWNTs and CNFs in polymers, as they tend to agglomerate and form bundles due to the high van der Waals forces of attraction. Bad dispersion of SWNTs in the polymer matrix results in poor electric, dielectric and mechanical properties. Non-solvent and solvent-based dispersion approaches along with a combination of mechanical stirring and sonication are used to break the nanoparticle agglomerates and achieve homogeneous dispersion in the polymer. The resulting polymer nanocomposites at varying nanoparticle concentrations are assessed for dispersion by optical microscopy, electrical conductivity and dielectric constant measurements. An AC electric field is used to manipulate a low concentration of well-dispersed SWNTs and CNFs in acrylates and epoxies respectively. CNFs and SWNTs are aligned in liquid polymer to investigate the effect of electric field magnitude, frequency and time on the behavior of SWNT and CNF bundles, and to quantify the effect of AC electric field frequency and time on the microstructure and physical properties. Possible electrokinetic forces acting on SWNTs and CNFs that result in the change in microstructure are discussed, along with the effect of electric field magnitude, frequency and time on these forces. In-situ electrical measurements are done to quantify the extent of SWNT and CNF alignment as a function of the above parameters. This

understanding enables us to alter the physical properties of polymer nanocomposites, by controlling AC electric field magnitude, frequency and duration of applied electric field. In the next step, the polymer is cured while the electric field is ON. Curing the polymer immobilizes the aligned nanoparticles which 'freezes' the polymer composite microstructure. The resulting microstructure and the extent of alignment of electric field-manipulated nanoparticles are assessed by measuring electrical conductivity, dielectric constant and storage modulus as a function of different alignment conditions to asses the impact of alignment on the properties and understand the relationship between processing parameters and resulting morphology.

In summary, the objectives of this study are: 1) to disperse CNFs and SWNTs in three types of polymers: epoxy, acrylates and polyimides, 2) to manipulate them using AC electric field and determine the key parameter(s) that affect alignment, and 3) to characterize the electric field manipulated polymer nanocomposites by measuring the electrical, dielectric and mechanical properties to assess the impact of alignment on the physical properties.

1.2. Background

1.2.1. Nanoparticles: Carbon nanofibers and single wall carbon nanotubes

A particle having one or more dimensions of the order of 100nm or less is defined as a nanoparticle[28]. This work focuses on carbon based metallic or semiconducting nanoparticles, namely CNFs and SWNTs. SWNTs are long, slender fullerene tubes that

are capped at both ends with C_{60} fullerene hemispheres. SWNT can be visualized as a graphene sheet that has been rolled into a tube, as shown in Figure 1.1a. The most common form of CNFs is a long cylindrical structure with multiple graphene layers with a lot of structural defects. CNFs can also be made of graphene layers that are arranged as stacked cones as shown in Figure 1.1b. SWNTs and CNFs are forms of carbon formed by sp^2 hybridization. Like graphite, SWNTs and CNFs are also sp^2 bonded; however, the curvature and cylindrical symmetry cause very important modifications compared with planar graphite.

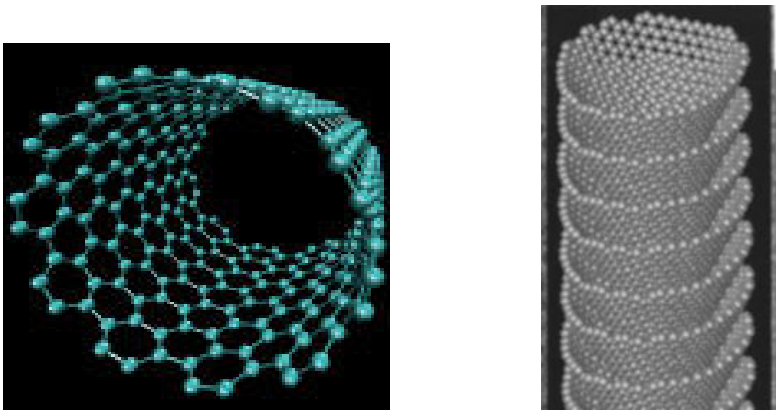

(a) (b)

Figure 1.1 (a) Image of SWNT [29] and (b) image of CNF with stacked cups [30].

Since the discovery of SWNTs in 1993 by Iijima [31] through the electric arc discharge method there have been different techniques in producing SWNTs and CNFs. The different methods to synthesize SWNTs and CNFs include arc-discharge [32-36] and laser ablation [37], which are very expensive techniques requiring very high temperatures and resulting in nanoparticles with a range of diameters and lengths. Chemical vapor

deposition (CVD) from hydrocarbons [38-40] is commonly used as it facilitates large scale production with uniform diameters and lengths. Two other methods developed on the basis of CVD are gas phase catalytic growth from carbon monoxide known as high pressure carbon monoxide (HiPCO) to produce SWNTs [41] and floating reactant method using ferrocene or iron pentacarbonyl as a catalyst precursor, hydrogen sulfide as a co-catalyst, and natural gas as the carbon source to produce cup stacked CNFs [42]. In this study HiPCO processed SWNTs and CVD grown CNFs are used.

SWNTs and CNFs have exceptional properties and high surface to volume ratio. These properties are a consequence of their symmetric structure, topology and highly anisotropic nature. The chirality and the tube diameter introduce significant changes in the electronic density of states and hence provide unique electronic character for the SWNTs [43, 44]. The other factor is topology, or the closed geometry of the SWNT [45, 46], which has a profound effect on the physical properties. The combination of size, structure, and topology endows these nanoparticles with important and unique mechanical (stability, strength, stiffness, and elastic deformability), transport (coherent electron transport), and surface properties [47]. SWNTs are very small, their diameters are 1-10 nm and their length is 1-2 μm. SWNTs have a tensile modulus that ranges from 270 GPa to 1 TPa and a tensile strength ranging from 11 to 200 GPa which is 10 to 100 times higher than the strongest steel at a fraction of the weight [48, 49]. They have a very low density of ~1.3 g/cm^3, this is due to their hollow structure. SWNTs also exhibit exceptional thermal and electrical properties. They are thermally stable up to 2800ºC in

vacuum and their thermal conductivity is about twice as high as that of diamond; these high values are due to the large phonon mean free paths present in SWNTs and the fact that their electric-current carrying capacity is 1000 times higher than that of copper wires [50]. CNFs have similar properties as the SWNTs but they are much bigger than the SWNTs; their diameters range from 70 to 200 nm and they are 50 to 100 μm long. CNFs have a tensile modulus of 400 to 600 GPa and a tensile strength of 2.7 to 7 GPa. They also have good electrical and thermal conductivity. CNFs have a thermal conductivity of 20 to 1950 W/m-K. They have a low density of 1.8 g/cm^3, since they too are hollow [51]. These exceptional electrical, mechanical and thermal properties along with high surface to volume ratio and low density comparable to that of polymers have motivated their use in polymer composites. Dispersion, nanoparticle-polymer adhesion, and manipulation or positioning of nanoparticles are some of the major challenges encountered when added to the polymer matrix [52].

1.2.2. Dispersion of nanoparticles

Dispersion of nanoparticles in polymers is very challenging as there is significant agglomeration due to high intrinsic van der Waals forces of attraction. Surface of most nanoparticles is non reactive resulting in poor interaction with the polymer, which could lead to small or no improvement in physical properties. There have been many studies that have focused on achieving homogeneous dispersion of nanoparticles in polymers to improve the physical properties of polymer nanocomposites.

Different methods have been used to efficiently disperse nanoparticles like SWNTs, multiwall carbon nanotubes (MWNTs) and CNFs in polymer matrices. Nanoparticles are ultra sonicated in a solvent to disperse them before they are added to the polymer matrix or before another dispersion technique is applied [53-56]. Melt mixing and extrusion [1, 3, 57-66] are mechanical methods that minimizes the aggregate formation by applying large shear to the polymer composite. Ultrasonication is a very effective method used to break the large nanoparticle agglomerates in a solvent before it is added to a polymer matrix. Safadi et al [54] dispersed MWNTs in toluene using an ultrasonic wand dismembrator at 300 W for 30 min. The MWNT suspensions are then mixed with Polystyrene (PS) to yield 1 wt%, 2 wt% and 5 wt% PS/MWNT solutions. These mixtures are further homogenized in an ultrasonic bath for 30 min. Conductivity measurements showed homogeneous dispersion, as the composite samples exhibited percolation threshold at less than 0.5% MWNTs. Composites at 5 wt% MWNT loading exhibited a 120% increase in elastic modulus and 33% increase in tensile strength. Figure 1.2 shows SEM micrograph of 5 wt% MWNT-PS fracture surface. MWNTs are homogenously distributed in the PS polymer matrix with no large agglomerates.

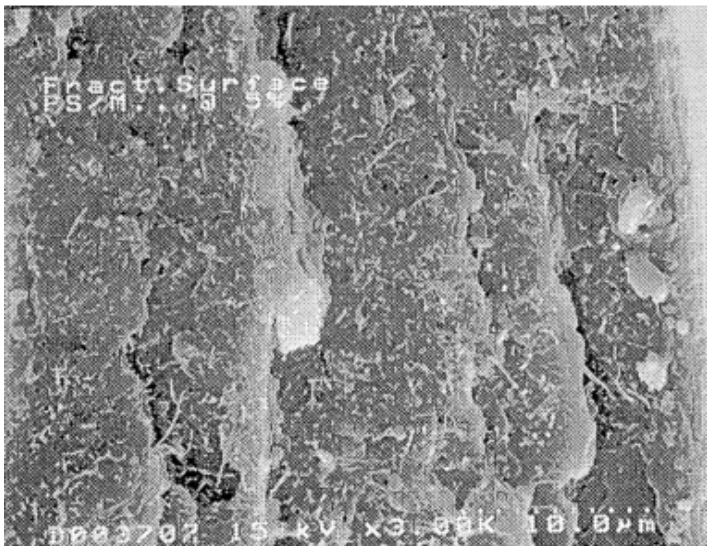

Figure 1.2. SEM micrograph of 5 wt% MWNT-PS fracture surface.

Du et al [53] used a new and versatile fabrication method called coagulation method to achieve a homogenous dispersion of SWNTs in PMMA matrix. The SWNTs are sonicated in DMF at 45 kHz for 24 hours to disperse the SWNTs and then a desired quantity of PMMA is dissolved in the SWNT and DMF solution. The suspension is then dipped into a large amount of distilled water in a blender. PMMA precipitates immediately because of its insolubility in the DMF and water mixture. The precipitating PMMA chains entrap the SWNTs and prevent SWNTs from bundling again. Optical and SEM micrographs show homogeneous distribution of SWNTs up to 7 wt% loading. Figure 1.3 shows uniform SWNT distribution in 1 wt% SWNT-PMMA composite film. Elastic modulus increased by 90% and electrical conductivity by 11 orders of magnitude for 2 wt% SWNT loading.

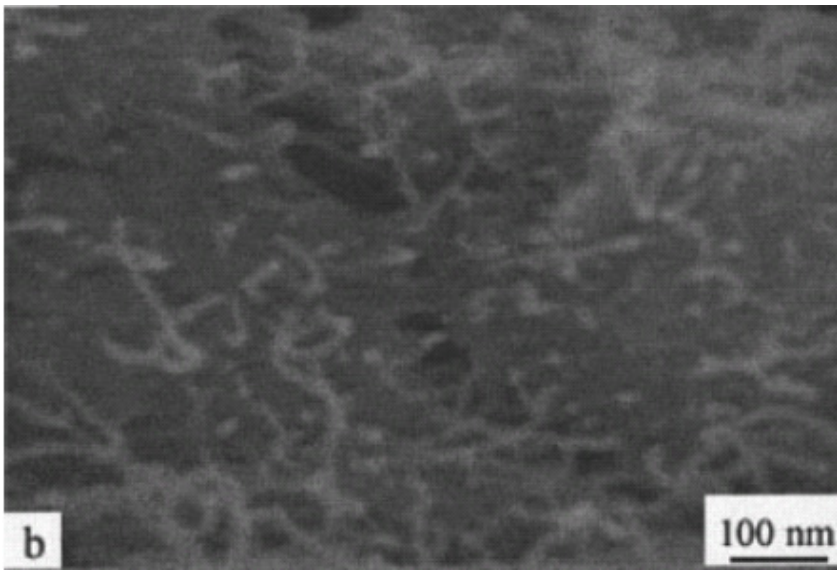

Figure 1.3. SEM showing uniform SWNT distribution in 1% SWNT-PMMA composite film fabricated by the coagulation method. [53]

Microcompounder and twin screw extruder are used to obtain the high shear mixing necessary to disentangle and disperse large concentrations of SWNTs [57-60, 66] and CNFs in polymers [1, 2, 67]. SWNTs were compounded with poly(acrylonitrile-co-butadieneco-styrene) (ABS) to create composite materials from melt mixing and extrusion[66]. SWNTs and dried ABS were mixed using a Banbury type mixer bowl. The material was mixed at 60 rpm and 140ºC for 10 minutes and then molded into sheet using a heated press at 150ºC. SWNTs were homogeneously dispersed and well distributed in the polymer matrix as shown in Figure 1.4. There was a 32% increase in tensile strength and 93% increase in elastic modulus at 5 wt% SWNT loading.

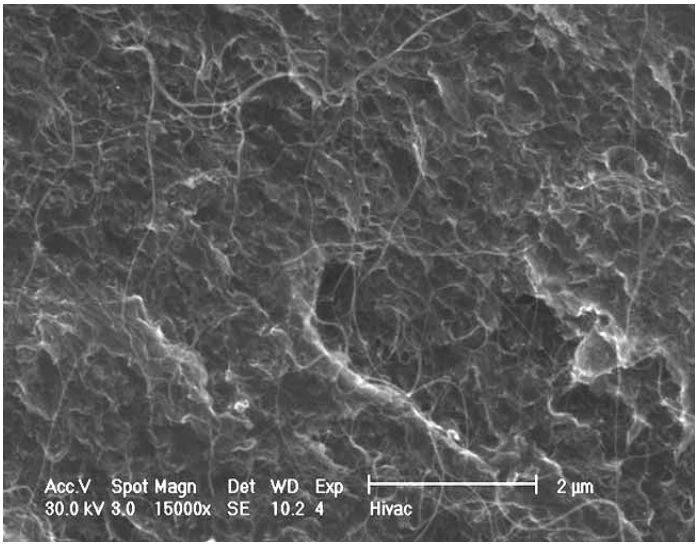

Figure 1.4. SEM micrograph of 5wt% SWNT-ABS composite. [66]

A number of methods have been used: in general, a combination of solution mixing and sonication to disperse SWNTs. They disperse as small bundles resulting in modest improvement in mechanical properties. Impact of SWNT bundles on electrical properties seems more pronounced.[13, 56, 68, 69] Dual wall carbon nanotubes (DWNT) are homogenously dispersed in PVDF polymer matrix with no large agglomerates as shown in Figure 1.5. A large increase in conductivity around 9 orders of magnitude is seen at 0.4 vol% loading and a low percolation threshold value of 0.23 vol% is reported. Using the percolation threshold and the excluded volume approach, data indicates the presence of DWNT bundles, which consist of around 7 individual tubes. A similar study where SWNTs were dispersed in polyimide polymer matrix also showed the presence of SWNT bundles, which consist of around 7 individual SWNTs.[69]

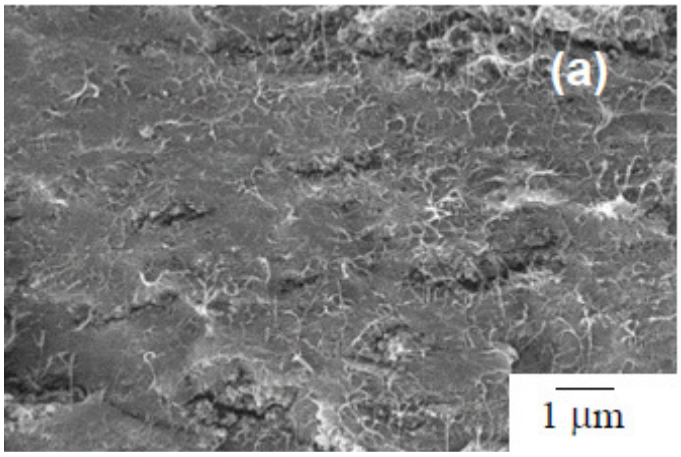

Figure 1.5. SEM image of 2.28 vol% DWNT-PVDF sample.

CNFs were dispersed in polypropylene (PP) and polycarbonate (PC) by melt mixing using a microcompounder [1]. Different amounts of CNFs (5 wt% - 25 wt%) were added at set temperatures of 230ºC at screw speeds of 50 rpm and 150 rpm for 20 minutes. CNFs were dispersed as individual fibers as shown in Figure 1.6. There was a 90% increase in Young's modulus at 15wt% CNF loading. Volume resistivity also decreased from 10^{13} Ωcm to 10^{5} Ωcm with less than 10 wt% CNF loading. Conductivity of CNF-PC showed slightly lower conductivity values of 10^{7} Ωcm and 10^{6} Ωcm at 7.5 wt% and 10 wt% respectively compared to CNF-PP composite. However for both polymer composites percolation threshold was between 5wt% and 10 wt%. Conductivity results and SEM image indicates good homogeneous distribution of CNFs. In Figure 1.7 there are holes and cavities that are visible, which indicates poor adhesion and interaction between CNFs and the polymer matrix. This mechanical methods improves dispersion of

nanoparticles, but does not improve the interfacial interaction between the polymer matrix and the nanoparticle.

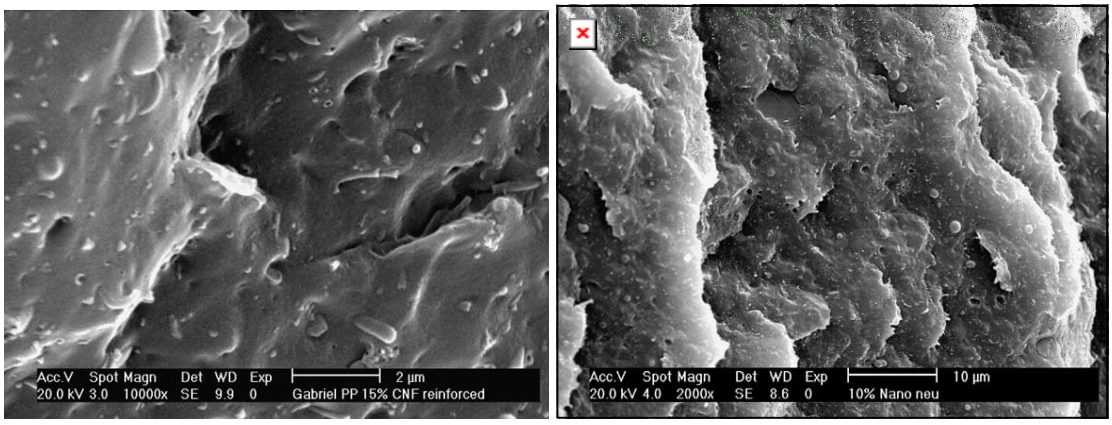

(a) (b)

Figure 1.6. SEM micrographs of CNF-PP composites prepared by melt mixing. (a) 15 wt% CNF and (b) 10 wt% CNF. [1]

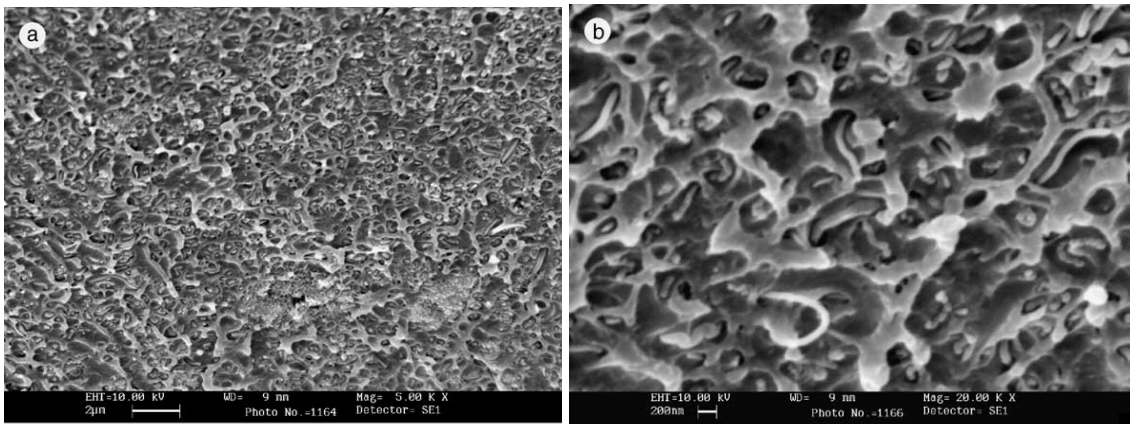

(b) (b)

Figure 1.7. SEM micrographs of fractured 7.5 wt% CNF-PC composites prepared by melt mixing. (a) low magnification and (b) high magnification. [1]

In order to improve both dispersion of nanoparticles and interfacial interaction between nanoparticles and polymer matrix, functionalization methods like covalent functionalization and non-covalent functionalization are used. Covalent functionalization is based on covalent linkage of functional entities onto the surface of the nanoparticle. In covalent functionalization there can be different degrees of functionalization where there is very little or no damage to the side wall of SWNTs or functional groups are attached to the sidewalls of SWNTs causing damage to most of the SWNT structure. Figure 1.8a shows functional groups like carboxylic acid groups are attached to the ends of SWNTs and Figure 1.8b shows functional groups are attached to the sidewalls of SWNTs. These functionalized SWNTs react with other chemical functionalities in solvents or polymers, which results in better dispersion and good adhesion and interaction with the host polymer matrix [8-10].

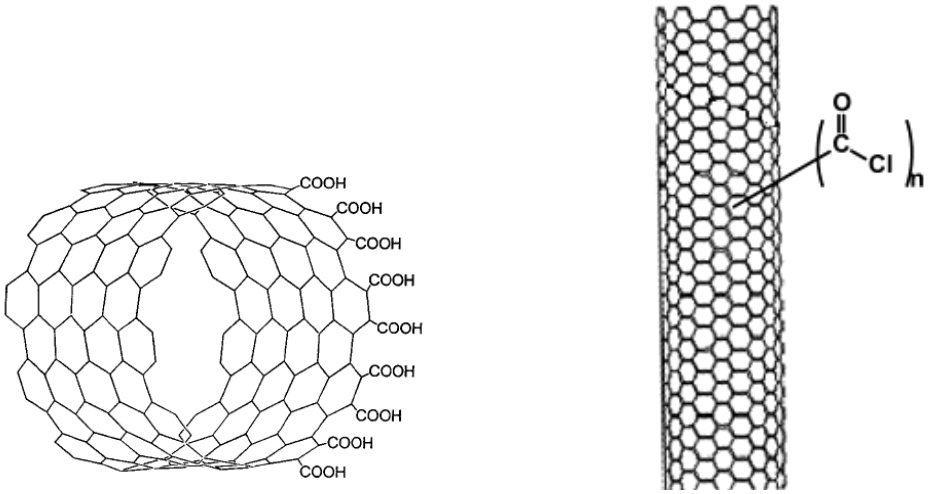

(a) (b)

Figure 1.8. Functional groups are attached to (a) ends of SWNTs and (b) side wall of SWNTs. [70, 71]

The first report of extensive sidewall functionalization of SWNTs was by fluorination of SWNTs [10]. Acid treated SWNT bucky paper was reacted with elemental fluorine under temperatures ranging from 150°C to 600°C by the method described in detail by Mickelson et al [10]. Raman spectroscopy and infrared results indicate that fluorine was covalently attached to the side wall of the SWNTs. Epoxy nanocomposites were processed by adding 1 wt% fluorinated SWNTs to the epoxy polymer [72]. The fluorine group that is covalently attached to the SWNT wall interacts with the amine curing agent during the curing process of epoxy system, resulting in good interfacial bonding between the epoxy and SWNT. There was a moderate increase in the mechanical properties, elastic modulus by 30% and tensile strength by 18% at 1 wt% SWNT loading. Figure 1.9 shows well distributed SWNTs in epoxy matrix with absence of large SWNT agglomerates.

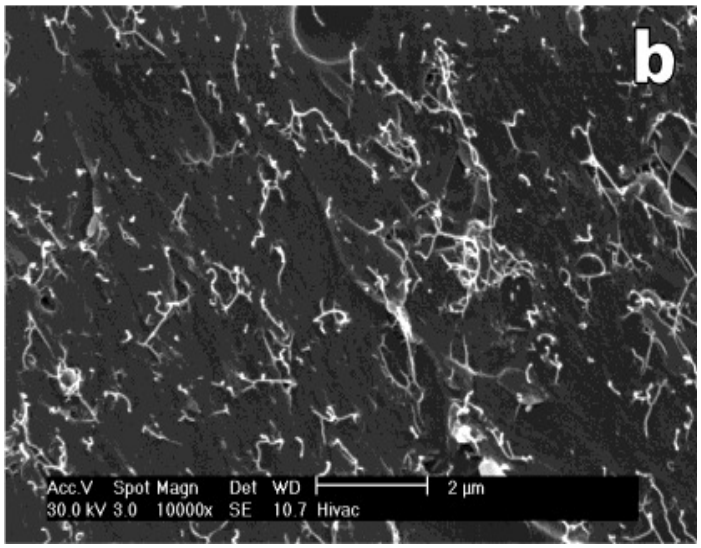

Figure 1.9. SEM images of fracture surfaces of 1 wt %SWNT-epoxy polymer composite showing dispersed individual nanotube ropes.[72]

In another method to further improve physical properties of SWNT polystyrene composite, side walls of SWNTs were functionalized with 4-(10-Hydroxydecyl)aminobenzoate. Polystyrene nanocomposites were prepared by mixing functionalized SWNTs with PS polymer in toluene, details of composite processing are given by Mitchell et al [73]. UV-vis spectroscopy, Raman spectroscopy and thermo gravimetric analysis results indicate bonding between the polymer and the functional group on SWNT side wall. The dispersion of functionalized SWNTs in polystyrene matrix was analyzed by melt state rheology. The rheological data suggest that the extent of reinforcement and state of dispersion are considerably better for the functionalized SWNTs in PS as compared to the pristine SWNT in PS. Further, clear evidence for the formation of a percolated filler network structure is observed for the functionalized SWNTs at loadings as low as 1.5 wt % and there was a 2 orders of magnitude increase in shear modulus, which indicates bonding between SWNTs and the polymer matrix have improved the mechanical properties.

In order to further improve the mechanical properties SWNTs were functionalized with functional groups that were similar to the host polymer, resulting in dissolution of both the SWNTs and the host polymer in the same solvent [71, 74, 75]. In one such attempt SWNTs and MWNTs were functionalized with polyvinyl alcohol (PVA) in carbodiimide activated esterfication reactions [75]. The resultant functionalized nanotubes were soluble in water and dimethyl sulfoxide (DMSO), similar to the parent PVA. The composite thin films were of high optical quality, transparent and homogeneous distribution of MWNTs

(Figure 1.10). This method of functionalization allowed the PVA-functionalized SWNTs and MWNTs to be soluble in the same solvent as the neat PVA, thus allowing good mixing with the matrix polymer. Amide-functionalized SWNTs were dispersed in PMMA polymer matrix by mixing and sonication.[76] There was an 85% increase in storage modulus of this composite due to the covalent functionalization of SWNTs and the polymer matrix. In parallel there was only a 15% increase in the storage modulus of pristine SWNT polymer composites.

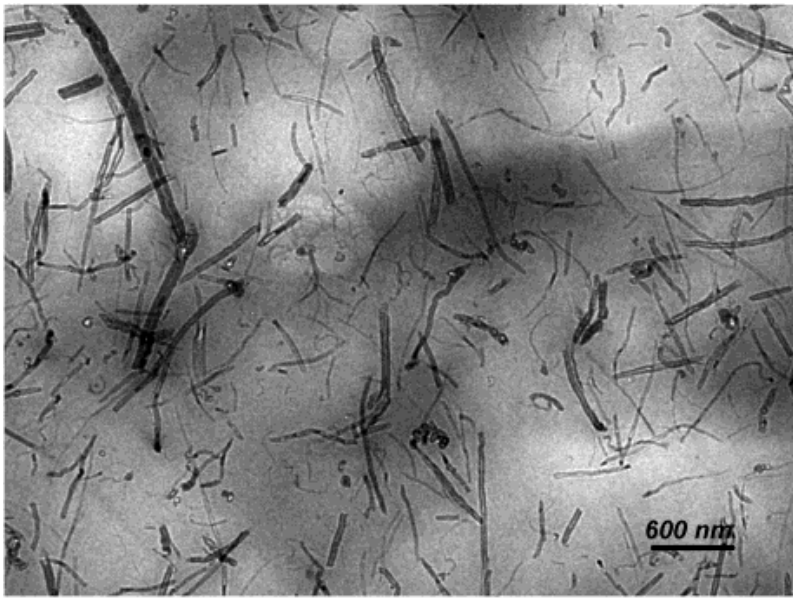

Figure 1.10. TEM image of a crosssectional microtome of MWNT-PVA composite film. [75]

Covalent functionalization led to improvement in mechanical properties of all the above polymer nanocomposites. Raman spectra on these SWNT-polymer composites showed the presence of D band, which corresponds to the sp^3 carbon hybridization peak and this

indicates that the sidewalls of the SWNTs are modified [72, 73, 77-80]. Change in carbon hybridization of SWNTs from sp^2 to sp^3 results in the loss of electrical properties. The functional groups on the surface of SWNTs act as defects in the Fermi level, which results in the loss of electronic properties [78, 81, 82]. The effect of covalent functionalization on the electrical conductivity of epoxy nanocomposites was studied by Kim et al [83]. Multiwall carbon nanotubes (MWNTs) were subjected to strong and mild oxidation by changing variables like acid, temperature and time. Concentrated aqueous acids introduce O_2 containing functional groups at sidewalls and ends caps of MWNTs. Electrical percolation thresholds of the composites prepared with MWNTs with different degree of functionalization was measured from the electrical conductivity. The results indicate that the stronger the oxidation conditions, the higher the percolation threshold of the composite, which indicates lower conductivity. Sidewall functionalization modifies the π electron system on the SWNT surface responsible for the exceptional electronic properties, which was the reason for the high electrical percolation threshold for MWNTs treated with strong oxidation conditions. There was a small decrease in electrical conductivity with mild functionalization, but strong sidewall and end cap functionalization deteriorate electrical properties due to sp^3 hybridization and reduce the electrical conductivity from 10^{-6} S/cm to 10^{-14} S/cm. In summary, covalent functionalization increases the adhesion between the SWNT and the polymer matrix, which results in improving the mechanical properties of the polymer nanocomposite, but there is a loss in the electrical properties. This method can not be used to improve both mechanical and electrical properties of polymer composites.

Non-covalent functionalization of nanotubes to aid dispersion is gaining popularity amongst researchers because, in theory, it promises to achieve the desired dispersion and mechanical properties while keeping the electronic properties of the nanotubes unchanged. Non-covalent functionalization is mainly based on weak secondary bonding between nanotubes and the dispersing matrix. A study was carried out by Chen et al.[84] to aid dispersion and mechanical property improvement of SWNT polymer nanocomposites. They have used noncovalent functionalization for efficient dispersion. Rigid and conjugate macromolecules, poly(p-phenylene ethynylene)s (PPEs), are used to non-covalently functionalize and solubilize the SWNTs and attain good dispersion in the polymer (Parmax) matrices. The non-covalent interaction was attributed to a π–π interaction between the carbon nanotube walls and the backbone of PPE, which was determined by H NMR spectra[85]. Gong et al[11] have reported the role of surfactants which function as a dispersing agent in processing of CNT epoxy composites. Polyoxyethylene 8 lauryl ($C_{12}EO_8$) is used as the surfactant, which is a nonionic surfactant containing an oxyethylenated hydrophilic segment, a hydrocarbon which is a hydrophobic segment and a good dispersant for carbon. The mixture of $C_{12}EO_8$ and acetone is added to SWNTs. The hydrocarbon repels the SWNTs and the oxyethylenated traps the SWNTs. SWNT bundles are separated because of this attraction and repulsion between the surfactant and SWNTs. Epoxy is then added to the well separated SWNT mixture resulting in homogeneous dispersion. In Figure 1.11a SWNTs are well distributed due to the presence of the surfactant and in Figure 1.11b there are large agglomerates with inhomogeneous distribution of SWNTs due to the absence of the

surfactant. The storage modulus increased by more than 30% with 1 wt% SWNT loading.

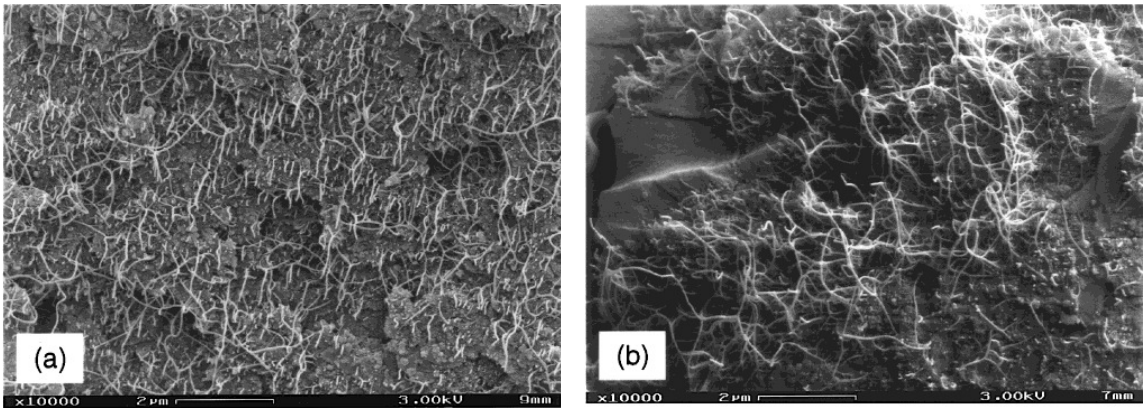

Figure 1.11. SEM micrographs of fracture surfaces (a) with surfactant and (b) without surfactant.

SWNTs were dispersed in 1 wt% polyacrylic acid (PAA) using sonication by Grunlan et al. [86] The pH of the solution was varied from 2.9 to 9.2 to achieve a stable well dispersed suspension of SWNTs in PAA. SWNT aggregation in PAA decreases and are better embedded in PAA matrix as the pH increases. At low pH values there are large SWNT aggregates and also SWNTs are pulled out of the matrix indicating a weak interaction between SWNT and PAA, as shown in Figure 1.12a. At high pH values there is better SWNT exfoliation and there is no evidence of SWNT detachment from the PAA matrix, as shown in Figure 1.12b. PAA becomes more negatively charged as the pH is raised due to deprotonation of its carboxylic acid groups. This change in PAA strengthens the interaction with the suspended SWNTs, which leads to the break up of SWNT bundles into more individual tubes. The electrical conductivity increases with

increase in SWNT concentration for the composites prepared with low and high pH values. But composites at low pH value had a high percolation threshold of 0.45 wt% due to SWNT aggregation compared to a low percolation threshold of 0.046 wt% at high pH value due to the highly networked structure.

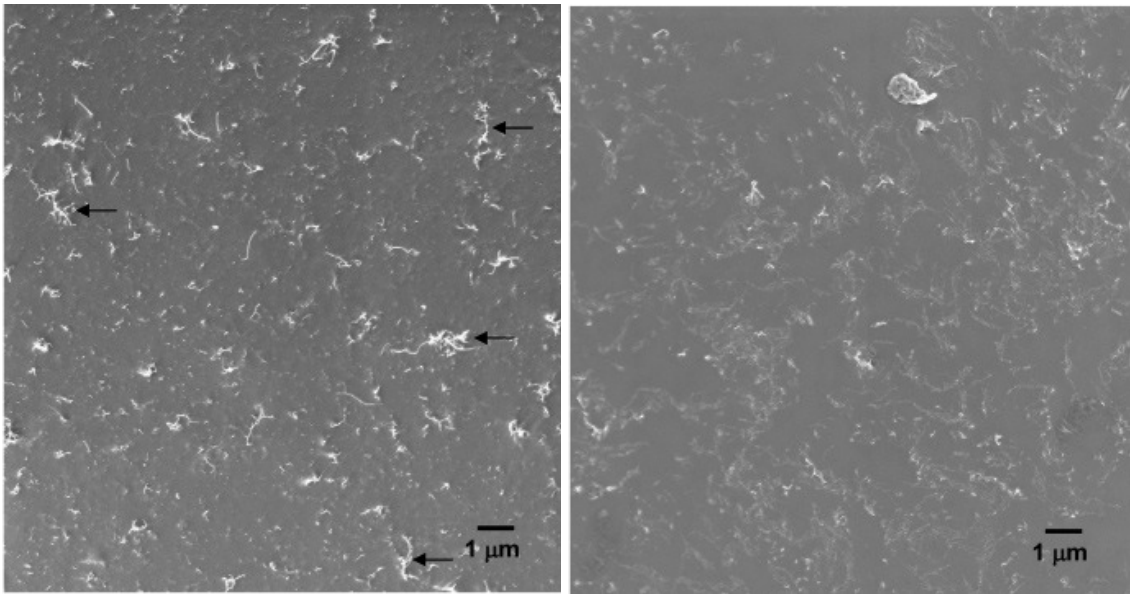

Figure 1.12. SEM micrographs of fractured PAA with 1 wt% SWNTs. Aqueous mixtures with (a) pH of 2.9 and (b) pH of 9.2.

Another method to disperse SWNTs by non covalent functionalization is by in situ polymerization in which SWNTs are added while the polymerization is in process [56, 87]. Li et al [87] have reported the fabrication of SWNT/PANI composites by in situ polymerization of an aniline solution containing different SWNT contents. SWNT ranging from 1 wt% to 8 wt% is added to 5 ml of aniline. The original colorless aniline solution first became brownish and then turned dark red indicating that SWNTs have been dissolved into aniline. Polymerization is started by adding a solution of HCL to

aniline with dissolved SWNTs in various mixture ratios. Ammonium persulfate in HCL added and the mixture is then left for polymerization. The color of the solution changes to green, indicating polymerization of aniline with dissolved SWNTs. UV vis adsorption spectra showed a peak at 320nm, which was due to the π–π transition of the benzene rings and also suggested charge transfer between SWNT and aniline. TEM image showed very good adhesion between the SWNT and the polymer matrix as shown in Figure 1.13. Raman spectra indicated no damage on the SWNT structure, thus preserving the electronic properties. There was also an increase in conductivity of the polymer by 14 times at 8wt% SWNTs.

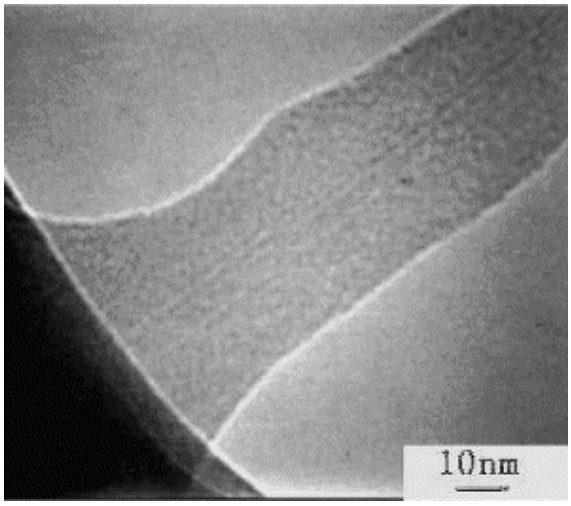

Figure 1.13. TEM image of SWNT covered with polymer matrix.

In summary, non-covalent interaction preserves the electronic structure of SWNTs and also improves SWNT dispersion in polymer nanocomposites. In this research, a combination of sonication, mechanical methods and non covalent functionalization

techniques will be used to achieve homogeneous dispersion of SWNTs and CNFs in different polymer systems as we are interested in enhancing both electrical and mechanical properties.

1.2.3 Manipulation of nanoparticles

Nanoparticles can be directly manipulated by using an atomic force microscope (AFM)), where the AFM is used to manipulate the nanoparticles by pushing, pulling, picking, placing and positioning them using the AFM tip [88]. Alternately, nanoparticles dispersed in a polymer can be manipulated by applying an external force, such as a mechanical, a magnetic or an electric field. Detailed reviews on some of these different nanomanipulation methods have been given by Sitti [89] and Li [90].

1.2.3.1 Mechanical manipulation

Mechanical force is used to align nanoparticles. Alignment of nanoparticles is either driven by the shear flow of the polymer [91-93] or by extrusion of the polymer [58, 66]. A doctor blade was used to induce shear flow alignment of MWNTs in polyfurfuryl alcohol (PFA) polymer[91]. SEM images indicate MWNT alignment in the flow direction as shown in Figure 1.14. Electrical conductivity was measured for composites with 5wt% to 15 wt% MWNT loading. Conductivity increased by 6 orders of magnitude compared to the unaligned composite at 5wt% MWNT loading.

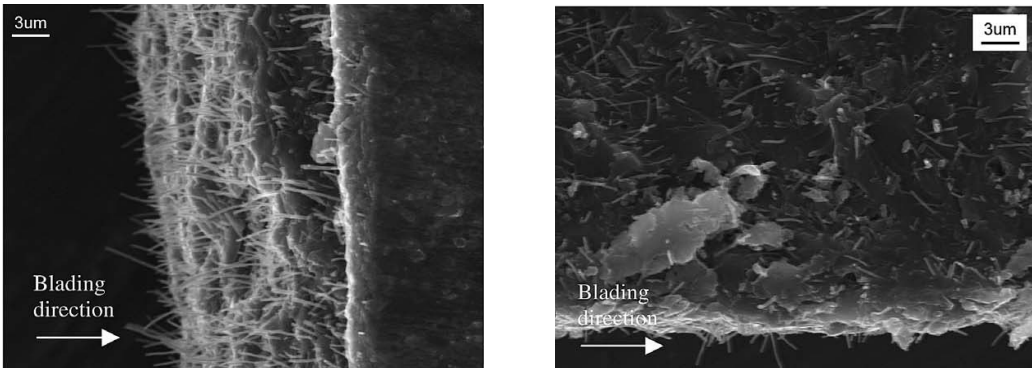

Figure 1.14. SEM micrographs of the cross sections of the film.

CNFs were manipulated in poly(acrylonitrile-co-butadiene-co-styrene) (ABS) by extrusion of the mixture through a die [66]. SEM images in Figure 1.15 show alignment of CNFs in the extrusion direction. At 5 wt% CNF loading there was a 44% increase in the elastic modulus compared to the pure polymer and there was no increase in the tensile strength. In another attempt MWNTs were aligned by extrusion of MWNT-PS mixture [58]. The polymer melt is extruded through a rectangular die and drawn under tension before solidification. Micrographs from transmission electron microscope (TEM) show overall alignment of MWNTs in the drawing direction. Aligned composites showed a 50% increase in the storage modulus at 5 wt% MWNT loading.

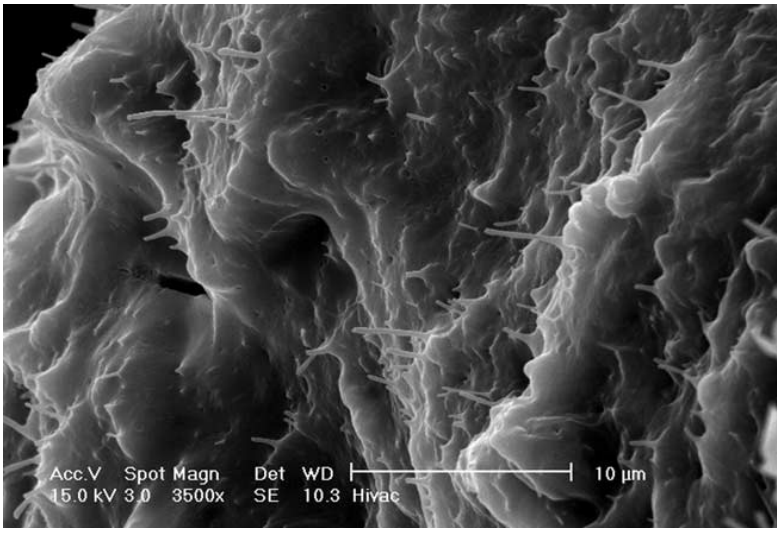

Figure 1.15. SEM micrograph of CNF-ABS composite, CNFs are aligned in the extrusion direction.

The advantage of melt mixing and extrusion techniques is that these methods disperse and align the nanoparticles in polymers at large concentrations. The major drawback is that only a small improvement in the physical properties has been achieved compared to the unaligned polymer with large nanoparticle loading.

1.2.3.2 Magnetic field manipulation

A high magnetic field is used by Kimura et al [94] to align the MWNTs in a polystyrene polymer matrix. Under a constant magnetic field of 10 T, the monomer is polymerized by adding a radical indicator. Polymerizing this MWNT monomer dispersion under the magnetic field freezes the alignment of MWNTs in the polyester matrix. High resolution TEM images, sliced in a parallel direction to the magnetic field had relatively long MWNTs (Figure 1.16a), which were not seen in the images perpendicular to the

magnetic field (Figure 1.16b). The conductivity parallel to the magnetic field is one order of magnitude higher than that measured perpendicular to the field at 1 wt% MWNT concentration. The elastic modulus measured in the parallel direction was 11% greater than the perpendicular direction. Anisotropy in conductivity and elastic modulus show alignment of MWNTs in the polyester composite.

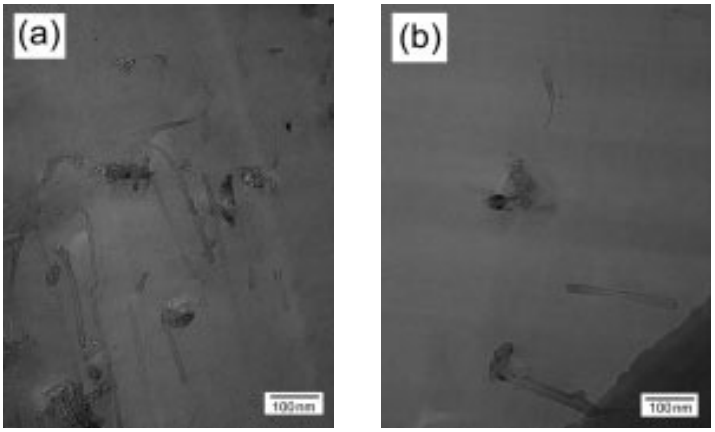

Figure 1.16. TEM images of aligned MWNTs. (a) Parallel and (b) perpendicular to the magnetic field direction.

Smith et al [95, 96] used a higher magnetic field (25 T) to make thick aligned SWNT films. A magnetic field is applied across a syringe filter, in which suspended tubes deposit under axial flow onto a filter membrane normal to the syringe axis. Resistance is measured parallel and perpendicular to the direction of alignment. The resistance in the parallel and perpendicular directions showed anisotropy. The parallel resistance value was 0.095 mΩ cm and perpendicular resistance was 2.3 mΩ cm. Anisotropy in resistance indicates alignment of SWNTs. The major disadvantage in using magnetic field

alignment is access to very high magnetic fields, which are not readily available. Also, a relatively small anisotropy in conductivity is achieved.

1.2.3.3 Electric field manipulation

Electric field is widely used to manipulate nanoparticles in various systems. A great amount of work on electric field manipulation of particles has been done in the colloids community. In general, the focus has been on colloidal particles in an aqueous medium. These systems are dependent on the surface charge of the particle and are limited to low voltages. Planar electrodes separated by a distance in the micron scale are used in these studies. AC electrokinetic techniques have been used in controlled manipulation of nanoparticles; for example, dielectrophoretic and electrohydrodynamic forces acting on sub-micrometer particles are discussed in detail by Green [97] and Castellanos[98]. Velev and Bhatt [99] have written a detailed review on the behavior of nano size colloidal particles suspended in water under the influence of AC and DC electric fields. A variety of nanoparticles dispersed in aqueous solutions can be assembled into microwires, nanowires, connections, chains, dendrites and 1D, 2D crystals by dielectrophoresis [100-109].

AC electric field was used to assemble colloidal gold microstructures [100, 101, 107-109]. Assembly of gold nanoparticles in all these studies was highly influenced by the electric field frequency. In one such study by Bahukudumbi et al, [108] different microstructures were assembled in between planar electrodes as a function of AC voltage of 0.5 V to 2.5

V and a frequency of 10 Hz to 1 MHz. Microstructures were mainly dependent on AC electric field frequency due to the various electrokinetic forces acting on the particles. Electrokinetic forces acting on the gold nanoparticles resulted in mainly three dominant transport regimes; First, between ω=0.01 kHz and 1 kHz, electrophoresis produced oscillatory colloidal motion between the electrodes resulting in structures shown in Figure 1.17. Second, between ω =1 kHz and 100 kHz, AC electroosmosis produced three dimensional periodic, recirculating flows on the electrodes, resulting in the gold colloids being ejected from the electrode gaps and, along with sedimentation, the colloids are reconcentrated on top of the electrodes. Third, at ω > 100 kHz, linear wire

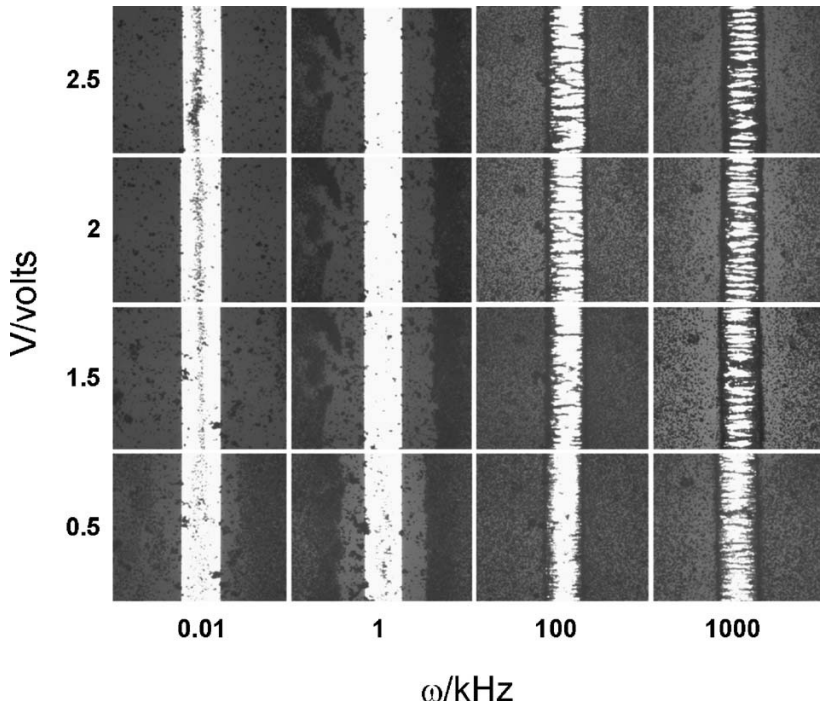

Figure 1.17. Optical microscopy images of gold nanoparticles between gold electrodes as a function of applied AC electric field frequency and amplitude. Gap between electrodes is 30 μm. [108]

structures were formed due to dielectrophoresis. Increasing the applied voltage increased the number of chains, rate of formation and chain bundling. In a similar study by Lumsdon et al[109], microwires were assembled from colloidal gold nanoparticles, carbon black and MWNTs by AC dielectrophoresis. Voltage of 5 V to 7 V was applied at a frequency of 100 Hz to 1 kHz. Experiments indicate a threshold voltage exists below which there is no microwire formation, as shown in Figure 1.18. This is because of a minimum dielectrophoretic force is required to overcome other forces like repulsive interparticle potential. The small frequency range did not affect the microwire formation. The type of particle affected the microwire formation, where thick wires were formed from 30 nm carbon black particles compared to the microwires formed from the 25 nm gold particles as shown in Figure 1.19. The size and the conductivity of the particle affected the wire formation.

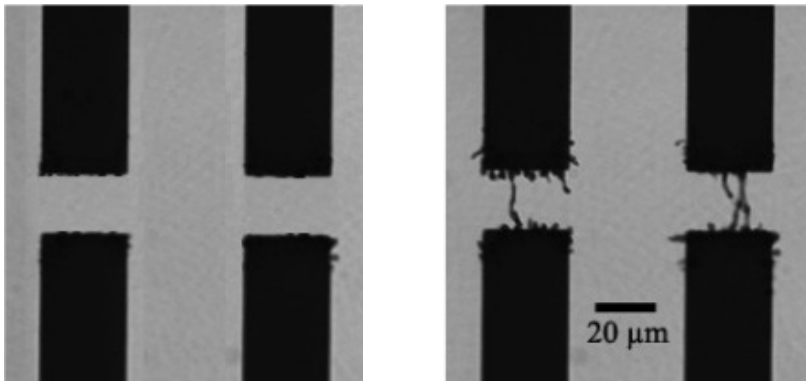

(a) (b)

Figure 1.18. Gold wires grown in a 20 mm electrode gap. (a) No wire formation before the threshold voltage is reached and (b) Increasing the voltage to 7 V RMS at 250 Hz results in the formation of wires. [109]

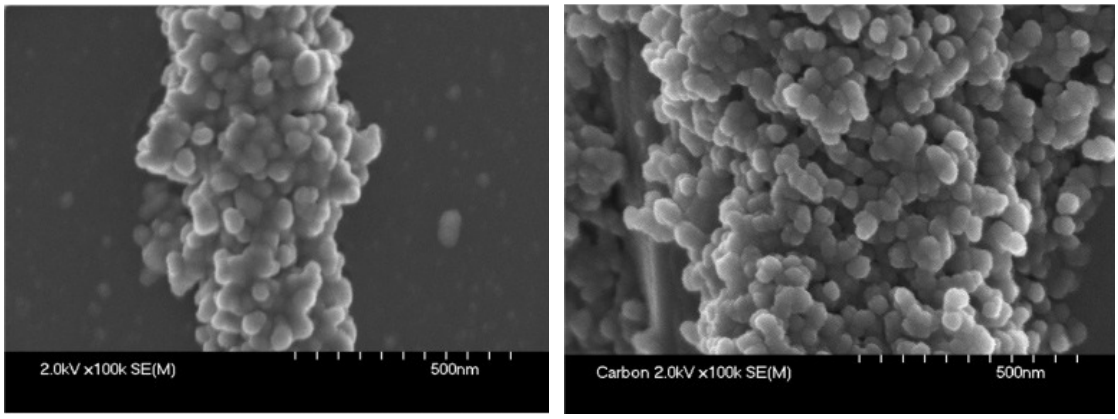

(a) (b)

Figure 1.19. SEM images of microwires. (a) Wire grown from 25 nm diameter gold particles and (b) a wire grown from 30 nm diameter carbon black. [109]

Other studies have focussed on electric field-manipulation of micron and nano particles in non-aqueous media like solvents [110-118] and polymers[24-27, 119-123]. SWNTs suspended in isopropyl alcohol were subjected to an AC electric field [111]. A voltage of 6 V_{pp} at 10 MHz frequency was applied. SWNTs bridge the gap between the electrodes in the direction of electric field, as shown in Figure 1.20. This behavior was analyzed in terms of induced torque acting on SWNTs to align in the direction of electric field and in terms of dielectrophoresis that causes translation of SWNTs. A simulation also analyzes the time for rotation and translation for metallic and semiconducting SWNTs. The effect of frequency on the behavior of metallic and semiconducting SWNTs is also studied [112].

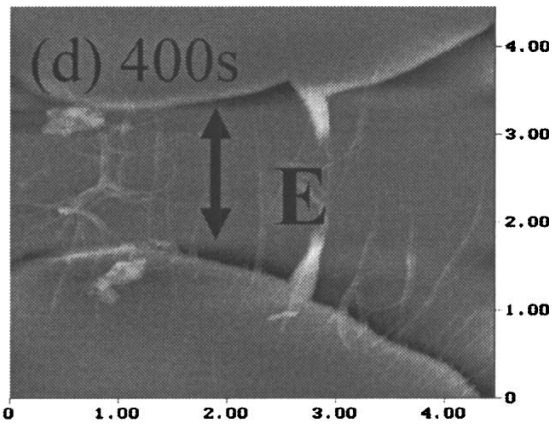

Figure 1.20. AFM image of SWNTs in between the electrodes, bridge the gap between electrodes. [111].

SWNTs dispersed in dimethylformamide (DMF) solvent were subjected to both AC (0 to 9 V at 10 Hz to 10 MHz frequency) and DC electric fields (0 to 5 V) [116]. Orientation of SWNTs between the electrodes was seen for both DC and AC electric fields as shown in Figure 1.21. The density of SWNTs aligned by DC electric field was lower compared to the density of SWNTs aligned by AC electric field. Most of the SWNTs moved towards the anode under the influence of DC electric field indicating negative charge on SWNTs. In the case of AC electric field the frequency showed a great influence on the SWNT alignment, where the SWNTs are better aligned at higher frequencies. The mechanism was explained in terms of induced electric dipoles in the SWNTs, that result in strong attractive electrostatic forces.

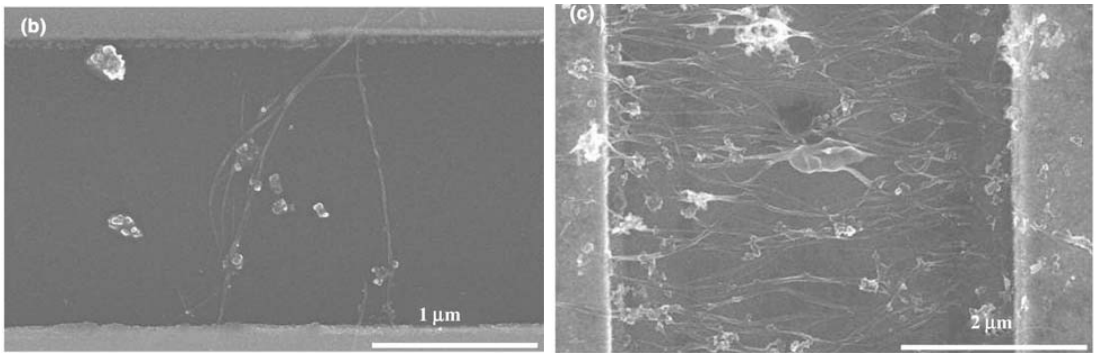

(a) (b)

Figure 1.21. SWNTs aligned in between electrodes by applying (a) DC voltage of 4 V and (b) AC voltage of 3 V with a frequency of 6.5 kHz. [116].

CNFs were aligned in polydimethylsiloxane (PDMS) using DC electric field [121]. An aligned network structure was formed in between the electrodes. The network formation was dependent on the duration of applied electric field. Increasing the time from 0 minutes to 10 minutes improved the network formation as shown in Figure 1.22. Combination of three forces, rotational force, Coulombic and electrophoresis forces, causes the formation of the network. This study was conducted on different viscosity silicone oils and it was concluded that the time required to form a network structure was proportional to the matrix viscosity. In all these studies the electric field aligned microstructure of nanoparticles can not be retained after the removal of electric field.

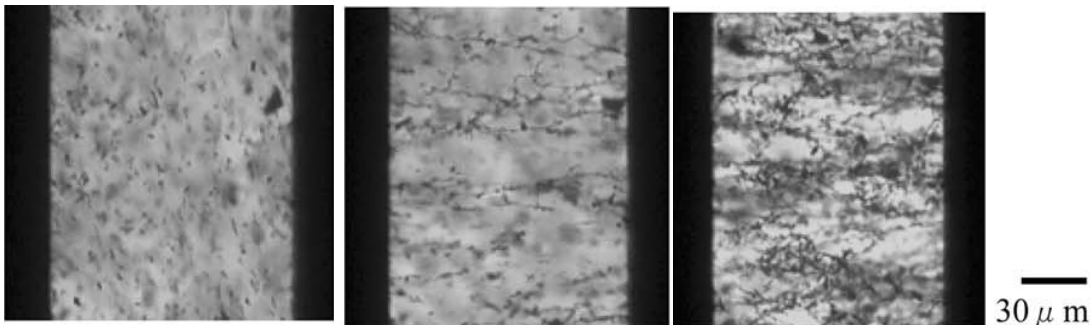

(a) (b) (c)

Figure 1.22. CNF network formation in PDMS using an DC electric field. OMs after (a) 0 min, (b) 1 min and (c) 10 min. [121]

There have been relatively few studies that have taken the extra step of curing the polymer to retain the electric field manipulated microstructure resulting in solid polymer composites [24-26, 119, 120, 122]. Both AC and DC electric fields were applied to align CNFs in epoxy matrix [26]. Applying a DC electric field resulted in CNF getting attracted towards the anode as shown in Figure 1.23a. Applying an AC electric field of 400 V/cm, 1 kHz frequency resulted in a web-like structure as shown in Figure 1.23b. Polymer curing was initiated immediately after the electric field was applied. Curing the polymer immobilized the aligned structure. Resistance of these composites was measured parallel and perpendicular to the applied electric field. At 0.2 wt% CNF there was no percolation, at a higher fraction of 0.5 wt% the network percolated only in the direction parallel to the applied electric field. Dielectric constant measured parallel and perpendicular to the applied electric field was similar at 0.2 wt% CNF, but as the CNF concentration increased dielectric constant in the parallel direction was greater than the

dielectric constant in the perpendicular direction. This study lacks the details on the effect of electric field magnitude and frequency on CNF network formation.

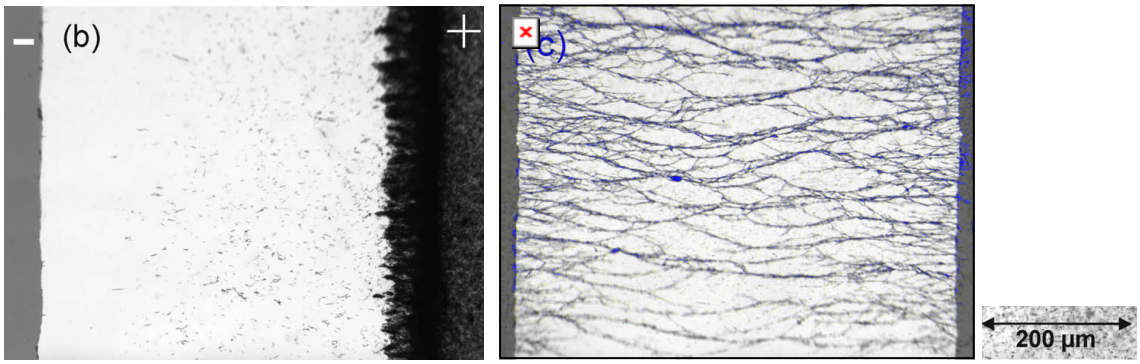

(a) (b)

Figure 1.23. CNF web-like structure formed from a suspension of CNFs in curing agent. (b) An AC electric field of 400 V/cm at 1 kHz frequency was applied [26].

MWNTs were aligned in epoxy composites by applying both AC and DC electric fields[24]. Applying a DC electric field of 100 V/cm caused the MWNTs to move towards the anode due to electrophoresis indicating that the MWNTs are negatively charged. A network structure starts to grow from the anode towards the cathode. Thermal cure of epoxy is initiated when the electric field is applied. The viscosity of epoxy increases due to curing and eventually at the end of the curing process a denser MWNT network is formed near the anode and the volume close to the cathode is bridged by a small number of thin MWNT network, as shown in Figure 1.24a. A more uniform aligned MWNT network was assembled by the application of 100 V/cm AC electric field at 1 kHz frequency, as shown in Figure 1.24b. Conductivity of composite in the direction of alignment increased as the electric field increased from 50 V/cm to 200 V/cm.

Conductivity of samples subjected to AC electric field was greater than when subjected to DC electric field. This was due to the better network formation for AC electric fields. A combination of particle rotation and dielectrophoresis resulted in MWNT network formation.

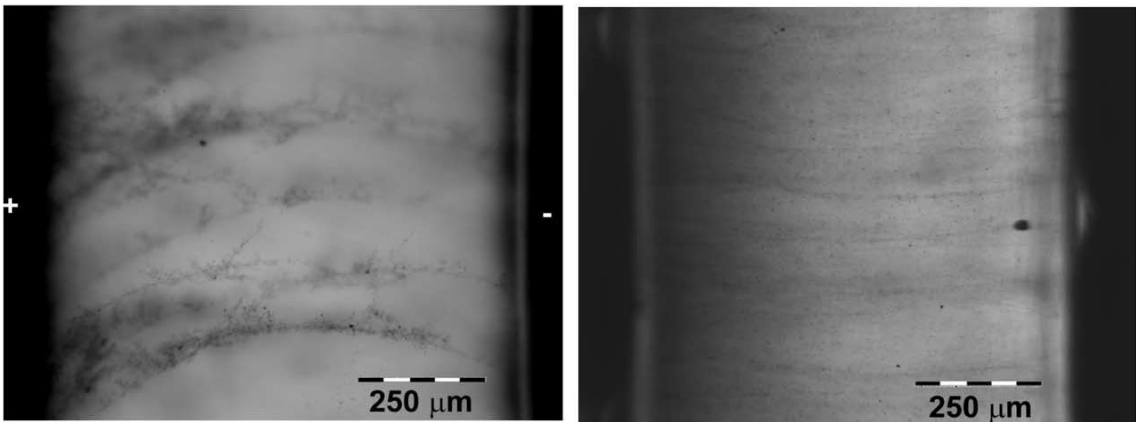

(a) (b)

Figure 1.24. OMs of MWNT network in epoxy composites by applying (a) DC electric field of 100 V/mm and (b) AC electric field of 100 V/mm at 1 kHz frequency. [24]

AC electric field was used to align SWNTs in an acrylate polymer [25]. SWNT network was formed in between the electrodes as shown in Figure 1.25a and b. Network formation was dependent on electric field magnitude and frequency. The polymer curing was initiated by using a blue light gun after applying the electric field for 10 minutes. The acrylate polymer cured immediately after blue light exposure and the aligned SWNTs were immobilized. Electrical conductivity and dielectric constant was measured to quantify SWNT alignment in the acrylate polymer. Increase in electric field

magnitude from 10 V_{pp} to 250 V_{pp} resulted in a 5 orders magnitude increase in the conductivity and a 2 orders increase in dielectric constant. Increasing the electric field frequency from 0.01 Hz to 100 kHz also resulted in a 5 orders magnitude increase in conductivity and a 2 orders magnitude increase in dielectric constant. In all these cases the dielectric constant and conductivity in the parallel direction was greater than the values in the perpendicular direction.

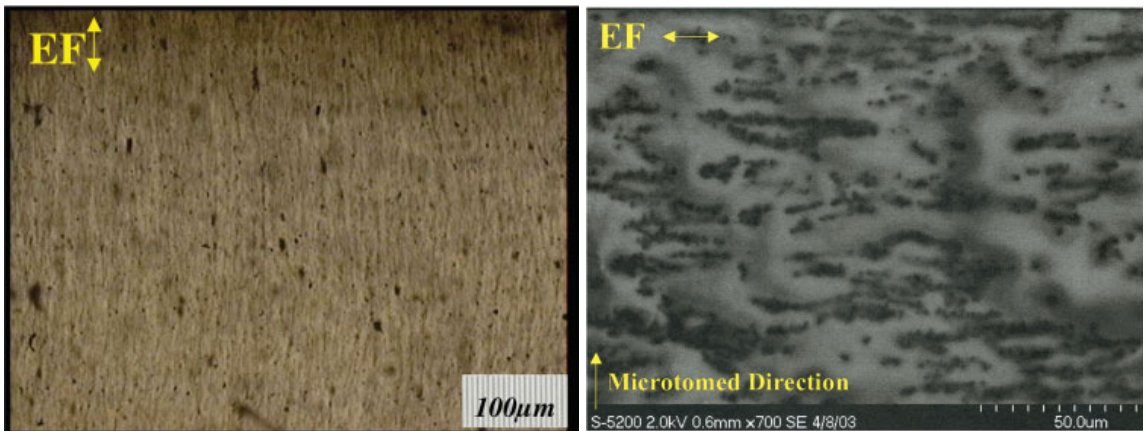

(a) (b)

Figure 1.25. SWNT network formation by the application of an AC electric field. (a) Optical microscope micrograph and (b) SEM micrograph.

There has been some theoretical and experimental analysis of electric field manipulation of nano and micro particles in the colloids community where planar electrodes are used. In contrast in electric field manipulation of nanoparticles in polymers using parallel electrodes, there are a very few studies with little details on mechanisms. Therefore, there is a need for a comprehensive description of the effect of different electric field

parameters on aligning and network formation, and the role of different mechanisms that drive the network formation. Also, study of the limitations of electric field to manipulate different size nanoparticles and the relationship between the physical properties and the resulting microstructure is lacking.

1.3 Organization of dissertation

This dissertation consists of six sections. Section 1 introduces the problem statement, gives a background on SWNTs and CNFs, and presents a critical review of the current literature on dispersion of SWNTs and manipulation and alignment of nanoparticles. Section 2 is the experimental section, describing the details of processing and characterization of the polymer nanocomposites in this study. Processing techniques consist of solvent-based and solvent-free processing of polymer solutions and electric field manipulation of nanoparticles. The remaining sections focus on the characterization of the resulting nanocomposites through optical microscopy, scanning electron microscopy, in-situ electrical and dielectric measurements, and dielectric spectroscopy of the solid nanocomposites, Raman spectroscopy and dynamic mechanical analysis. Section 3 presents the results on dispersion of nanoparticles in polymers obtained from optical microscopy, scanning electron microscopy, electrical conductivity measurements, dielectric measurements, mechanical properties of nanocomposites and Raman spectroscopy. Section 4 presents the results on effect of electric field magnitude, frequency and time on alignment of nanoparticles in polymer solutions. Experimental results from optical microscopy, polarized Raman spectroscopy, in-situ electrical and

dielectric properties are discussed. Different forces acting on nanoparticles under applied electric field are analyzed and the experimental findings are validated. Section 5 presents the physical properties of electric field-manipulated polymer nanocomposites. Physical properties such as electrical conductivity, dielectric constant and storage modulus are measured parallel and perpendicular to the electric field direction. Section 6 offers conclusions and recommendations for future work.

2. EXPERIMENTAL

The first part of this section introduces different techniques on processing homogenously dispersed random polymer nanocomposites and electric field manipulated polymer nanocomposites. The experimental conditions and the description of different characterization tools like optical microscopy, scanning electron microscopy, electrical conductivity and dielectric spectroscopy, Raman spectroscopy, and dynamic mechanical analysis are described in the later part of this section.

2.1 Solvent free processing of polymer nanocomposites

In this method nanoparticles are directly dispersed in the polymer. SWNT-acrylate and CNF-epoxy nanocomposites are processed by this method.

2.1.1 Processing of acrylate nanocomposites

Acrylate polymer is a photopolymerizable monomer, which is a blend of urethane dimethacrylate (UDMA) and 1,6-hexanediol dimethacrylate (HDDMA) at the ratio of 9:1. The mixture instantaneously polymerizes by blue light (λ=475 nm) when 0.2 wt% camphorquinone and 0.3 wt% N,N-dimethylaminoethyl methacrylate are used as the photoinitiator and accelerator respectively. LE Demtron blue light gun is used for the curing process. UDMA was obtained from Esschem Co, HDDMA, photoinitiator and accelerator was purchased from Sigma Aldrich. Pristine Hipco processed SWNTs were obtained from CNI® and 0.03 wt% SWNTs is predispersed in HDDMA, which has a lower viscosity compared to UDMA. The mixture is subjected to simultaneous

mechanical stirring at 150 rpm and sonication for 3 hours. Fisher scientific mechanical stirrer and an ultrasonic bath FS 20 sonicator from Fisher Scientific, operating at 40 kHz are used. UDMA is added to the predispersed solution and the mixture is further stirred and sonicated for 5 hours to obtain the acrylate polymer solution. Initiator and accelerator are added to this solution and stirred for 10 minutes and the beaker is covered with aluminum foil to prevent exposure to light. SWNT-acrylate solution is poured into cuvet cells, which is cured with a blue light gun for 3 minutes. Pure and 0.03 wt% SWNT-acrylate polymer composites are prepared in the manner described.

2.1.2 Processing of epoxy nanocomposites

CNFs from Pyrograf® are purified in our laboratory. The purification process consists of refluxing the CNFs in dichloromethane, followed by several deionized H_2O washes. CNFs were rinsed again, vacuum filtered for 24 hrs and dried at 110 °C for at least 24 hrs. Epon 862 epoxy and curing agent 'W' were purchased from Miller Stephenson. Chemical structures of Epon 862 and curing agent 'W' are shown in Figure 2.1. Epon 862 and 'W' are mixed in the ratio 100/26.4. The mixture is stirred in a round neck flask with a Fisher scientific mechanical stirrer operating at 150 rpm for 1 hour. The solution is thermally cured at 125ºC for 2 hours and 177ºC for 2 hours.

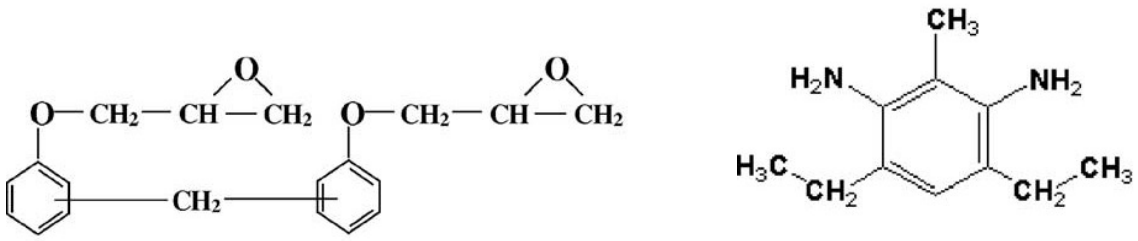

(a) (b)

Figure 2.1. Chemical structures of (a) Epon 862 epoxy and (b) curing agent 'W'. [124]

CNFs are weighed in a Metler Toledo microbalance and added to round neck flask along with the curing agent, 'W'. The flask along with the mechanical stirrer is setup in a sonication bath. The mixture is subjected to simultaneous mechanical stirring and sonication for 3 hours. Epon 862 epoxy is then added to this pre-dispersed solution where the ratio of Epon 862 to 'W' is 100/26.4 and is further subjected to sonication and mechanical stirring for 3 hours. This solution is then degassed at 60ºC in a Fisher Scientific® vacuum oven for about 30 minutes until all the air bubbles disappear. The solution is then poured into a metal mold with dimensions 10mm x 5 mm x 2mm, with silicone release agent sprayed onto the metal molds. The metal molds are then placed in a Sun environmental oven for 2 hours at 122ºC and for an additional 2 hours at 177ºC to complete the curing cycle of the epoxy polymer. In this procedure, the solution viscosity starts to increase after adding the epoxy to the predispersed nanoparticle-curing agent mixture.

2.2 Solvent based processing of polymer nanocomposites

Solvent is used as an aid to disperse CNFs and SWNTs in polymers like epoxy and polyimides. Nanoparticles are predispersed in a solvent along with sonication and mechanical shear. Mechanical shear on the low viscosity solvent along with sonication reduces the nanoparticle agglomerates. Polymer is then added to this predispersed solution to obtain a stable well dispersed polymer solution.

2.2.1 Processing of epoxy nanocomposites

Purified CNFs are weighed and added to round neck flask along with 5 grams of solvent. N,N-dimethylacetamide (DMAc) is chosen as the solvent as it is a polar solvent and its polar nature interacts with the nanoparticles leading to better dispersion. The mixture is subjected to simultaneous mechanical stirring and sonication for 1 hour. Epoxy is then added to this pre-dispersed solution and is further subjected to sonication and mechnical stirring for 3 hours. The flask is then placed in a vacuum oven operating at a temperature of 80ºC to evaporate the DMAc solvent from the nanoparticle-epoxy mixture. The solvent is completely eliminated after about 6 hours. Curing agent 'W' is then added to the solvent free mixture and is again subjected to sonication and mechanical stirring at 150 rpm for 1 hour. The viscosity of the solution increases after mixing the curing agent. This solution is then degassed at 60ºC in a vacuum oven for about 30 minutes until all the air bubbles disappear. The solution is then poured into a metal mold, which is then placed in a Sun environmental oven for 2 hours at 122ºC and for 2 hours at 177ºC to

complete the curing cycle of the epoxy polymer. Different concentrations of CNF-epoxy nanocomposites are prepared ranging from 0 wt% to 3 wt% CNFs.

2.2.2 Processing of polyimide nanocomposites

To prepare a SWNT polyimide nanocomposite, SWNTs are dispersed in polyimide matrix using in-situ polymerization under sonication, which is a technique developed by Park et al [56]. A dilute SWNT solution in DMAC is prepared in a three neck round bottom flask equipped with a mechanical stirrer, nitrogen gas inlet, and drying tube outlet. The solution is prepared by homogenizing for 10 min. Then the diamine 2,6 Bis (3-amino phenoxybenzo nitrile) (βCN-APB) is added into the SWNT solution. The SWNT solution and diamine mixture is continuously stirred for 15 min before adding the dianhydride 4,4 Oxydiphthalic anhydride (ODPA). The entire reaction is carried out in an ultrasonic bath (40 kHZ) until the solution viscosity increases and is stabilized indicating completion of polymerization. Additional stirring is continued overnight without sonication to obtain polyamic acid solution. Solid content for SWNT-polyamic acid is 15 wt% in DMF. A series of SWNT-polyamic acid solutions with SWNT concentrations ranging from 0.01wt% to 5wt% are prepared. The SWNT polyamic acid solution is cast on a glass plate using a doctor blade, and dried in a dry-box until it is tack-free. After drying, the cast film is thermally cured at 110°C, 170°C, 210°C and 250°C for 1 hour each in a nitrogen circulating oven to obtain solvent free SWNT polyimide films. The method of film casting produces randomly oriented SWNT

polyimide composite films. Different concentrations of SWNT-polyimide nanocomposites are prepared ranging from 0 wt% to 2 wt% SWNTs.

2.3 Electric field manipulation of nanoparticles in polymers

2.3.1 Experimental set up

AC electric field is used to manipulate SWNTs and CNFs in acrylate and epoxy polymer solution. An HP 33120A function generator is used to apply AC voltages and this is integrated with a TREK 609D-6 high voltage amplifier to obtain high voltages in the range of 1 kV to 8 kV. Copper electrodes with dimensions of L = 10 mm, w = 2 mm, h = 2 mm are placed parallel to each other. Two different electrode distances are prepared, 1 mm and 10 mm. The first setup, with a distance of 1 mm is for use on a microscope slide as shown in Figure 2.2a and the second setup is on a silicone mold as shown in Figure 2.2b. First setup is for optical microscopy, where the behavior of nanoparticles is observed under the microscope when AC electric field is applied; the polymer solution is not cured using this set up. Second setup is to prepare solid aligned polymer nanocomposites. AC electric field is applied to the polymer solution in between parallel electrodes and then polymer solution is cured. Curing the polymer while the electric field is ON immobilizes nanoparticles, thus retaining microstructure even after the electric field is turned OFF.

(a) (b)

Figure 2.2. Electrode set up for electric field manipulation of SWNTs and CNFs. (a) Distance between electrodes is d=1mm, used for optical microscopy and (b) distance between electrodes is d=10mm, used for preparing solid polymer nanocomposites.

SWNT-acrylate polymer solution with 0.03 wt% SWNT concentration was used for electric field manipulation. AC electric field of 100 V/mm and 300 V/mm was applied at varying frequencies of 1 Hz, 10 Hz, 100 Hz, 1 kHz, 10 kHz and 25 kHz to the SWNT-acrylate polymer solution. AC electric field was applied for 10 minutes, 20 minutes and 30 minutes. Blue light curing cycle started after electric field was applied for 30 minutes. CNF-epoxy polymer solution with 0.1 wt% CNF concentration processed by the solvent based method was used for electric field manipulation. AC electric field of 100 V/mm was applied at varying frequencies of 0.1 Hz, 1 Hz, 10 Hz, 100 Hz, 500 Hz, and 1 kHz. In the case of the CNF-epoxy system drastic increase in viscosity is seen after 90 minutes of starting the thermal curing cycle. The cure cycle is started at the same time as the AC electric field. The electric field is applied for a total of 90 minutes.

2.3.2 Theoretical analysis

There are different forces acting when a particle is suspended in a fluid medium and subjected to an electric field. The forces can be divided into two kinds, first is a random or stochastic force, which arise in the thermal energy or temperature of the system. The particles bump into each other and this type of motion is known as Brownian motion where the resultant force does not lead to movement of the particle in a particular direction. Second are deterministic forces like gravity, viscosity of the medium and the electrical forces, which can be controlled. When the size of the particle is sub micrometer, gravity is of little importance and Brownian motion is highly dominant. Viscous and electrical forces are dominant depending on viscosity of the polymer and the electric field parameters respectively. The forces produced by electrical forces on particles in a fluid are known as the electrokinetic forces. Different electrokinetic forces are electrophoresis, electroosmosis, dielectrophoresis and electrorotation. A charged particle in a uniform electric field experiences electrophoresis or electroosmosis; a non-uniform electric field gives rise to dielectrophoresis; and an electric field with rotating field vector gives rise to a torque on a particle resulting in electrorotation. [125]

Electrophoretic force is given by[126]

$$F_{electrophoresis} = qE \qquad 2.1$$

where q is the charge of the particle and E is applied electric field. The properties of the suspending liquid can also affect the behavior of the particle under the influence of electric field. When a charged particle is in an electrolyte, opposite charge ions are

attracted and like charges are repelled. The region around the particle has a high density of counterions, which is known as the double layer. The presence of a double layer affects the electrophoretic mobility of the particle. In electroosmosis the fluid is pulled generating a flow to the surface. When the applied electric field is tangential to the surface and the electrolyte, the charge in the double layer between the surface and electrolyte experiences electroosmotic force. Dielectrophoresis refers to the force exerted on a charged or uncharged particle by a non uniform electric field[127]. Dielectrophoretic (DEP) force is given by

$$F_{DEP} = V\varepsilon_m \,\mathrm{Re}\left|K\right|\nabla E^2 \qquad 2.2$$

where V is the volume of the particle, ε_m is the dielectric permittivity of the suspending medium, E is the electric field and $\mathrm{Re}\left|K\right|$ is the real part of the Clausius Mossoti factor, which is dependent on the shape of the particle. Clausius Mossoti factor, for a sphere is $K_{Sphere} = (\varepsilon_p^* - \varepsilon_m^*)/(\varepsilon_p^* + 2\varepsilon_m^*)$ and for an anisotropic particle like prollate ellipsoid $K_{Ellipsoid} = (\varepsilon_p^* - \varepsilon_m^*)/\varepsilon_m^*$, where $\varepsilon_{p,m}^* = \varepsilon_{p,m} - i\frac{\sigma_{p,m}}{w}$, ε_p and ε_m are the permittivity of the particle and medium respectively and σ_p and σ_m are the conductivities of the particle and medium respectively and w is the frequency. Depending on the conductivity and permittivity of the particle and the medium, the particle undergoes either positive or negative dielectrophoretic force depending on frequencies. In positive dielectrophoresis the particle moves towards the high electric field strength region and in negative dielectrophoresis, the particle moves towards the low electric field strength region.

The forces that oppose the electrokinetic forces are Brownian and gravitational forces. Nanoparticles in a solution experience a force due to thermal energy, which causes them to move in random direction known as Brownian motion. This is due to the collision between the vibrating molecules of the solution and the particles. After a certain time (t) the average displacement of the particle is zero and the rms displacement of the particle is given by[126]

$$\Delta d = \sqrt{6DT} \tag{2.3}$$

where D is diffusion constant of particle given by $\frac{kT}{f}$, f is the friction factor, K is the Boltzman's constant and T is the absolute temperature. There will always be gravity and buoyancy forces acting in opposite direction on a particle suspended in a fluid medium. The net force will result in sedimentation or creaming (floating) of the particle, which is dependent on the densities of the particle and medium. When the density of the particle is greater than the medium sedimentation force is given by

$$F_{\text{sedimentation}} = V(\rho_p - \rho_m)g \tag{2.4}$$

where V is the volume of particle, ρ_p and ρ_m are density of particle and medium respectively and g is acceleration due to gravity.

Electrorotation is the behavior where anisotropic particle rotates under the influence of electric field. Particle either rotates parallel or perpendicular to the applied electric field; this behavior is highly dependent on frequency. Applying an electric field polarizes the anisotropic nanoparticle, which acts as an induced dipole that rotates either parallel or

perpendicular to the direction of electric field. Polarizability along the long axis is greater due to the anisotropy of the nanoparticle, which induces a torque (τ). The general equation of torque is $\tau = |\mu \times E|$, where μ is the dipole moment and E is the electric field. The dipole moment is given by $\mu = V\varepsilon_m \beta_{\perp/ll} E$, where V is the volume of the particle, ε_m is the permittivity of the medium and $\beta_{\perp/ll}$ is the shape factor, perpendicular and parallel to the particle axis, β for a prollate ellipsoid or cylinder is [119] $\beta_{\perp} = \frac{2(\varepsilon_p^* - \varepsilon_m^*)}{(\varepsilon_p^* + \varepsilon_m^*)}$ and $\beta_{ll} = \frac{\varepsilon_p^* - \varepsilon_m^*}{\varepsilon_m^*}$. Resultant electrical torque is given by

$$\tau^{(E)} = \left(\mathrm{Re}|\beta_{ll}| - \mathrm{Re}|\beta_{\perp}|\right) V\varepsilon_m E^2 \sin\theta\cos\theta \qquad 2.5$$

and the force acting on the particle is

$$F_{rotation} = \frac{\tau}{L} = \frac{\beta V \varepsilon_m E^2 \sin\theta\cos\theta}{L} \qquad 2.6$$

where, θ is the angle between the particle axis and the applied electric field ($0^\circ < \theta < 90^\circ$), L is the length of the particle.

2.4 Optical microscopy and scanning electron microscopy

Inverted Zeiss® transmission optical microscope is used to assess the uniform dispersion and alignment of SWNTs and CNFs in acrylate and epoxy polymers. In addition, the resulting microstructure of electric field manipulated polymer nanocomposites can be studied through optical microscopy. In a transmission optical microscope (OM), light is transmitted through the sample and this allows us to probe dispersion and alignment

inside the sample. Zeiss® 1530 high resolution scanning electron microscope (SEM) is used to further probe dispersion, SWNT bundle sizes and interaction with the polymer matrix. In this study polymer nanocomposite samples are placed in liquid nitrogen for around 2 hrs and then fractured to characterize by SEM. SEM has resolving powers of about 2 nm – 10 nm and magnifications up to 200,000x. SEM can be used to study three dimensional features of the nanoinclusions [128].

2.5. Impedance spectroscopy

Novocontrol® broadband high impedance analyzer and Quadtech LCR meter are used to measure the dielectric constant and electrical conductivity of the polymer nanocomposites. The measurement frequency range of the Novocontrol® is 10^{-2} Hz to 10^{7} Hz. Circular silver electrodes are vapor deposited onto polymer nanocomposite samples. High purity SPI® silver paint is used as an electrode for electric field manipulated polymer nanocomposites, which are tested in two different directions

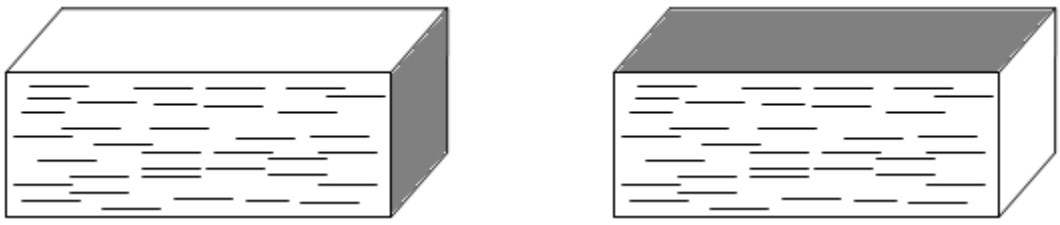

(a) (b)

Figure 2.3. Silver paint is used as an electrode for aligned polymer nanocomposites. Shaded region indicates the electrodes in the (a) parallel and (b) perpendicular directions.

parallel and perpendicular to alignment, as shown in Figure 2.3. Electrical conductivity and dielectric constant are measured at different frequencies.

2.5.1 Electrical conductivity

The electrical conductivity of a material is described by complex conductivity (σ^*)

$$\sigma^* = \sigma' + i\sigma'' \tag{2.7}$$

where, σ' and σ'' are the conductivity and loss components. Conductivity is given by

$$\sigma' = \frac{g * t}{A} \tag{2.8}$$

where g is the conductance, t is the thickness and A is the area. At critical volume content, nanoinclusions form a conductive path in the polymer resulting in percolation. DC conductivity near the percolation threshold is given by the power law [21, 129].

$$\sigma_{DC}(\nu) \propto (\nu_c - \nu)^{-s} \tag{2.9}$$

where ν_c is the percolation threshold, and ν is the nanoinclusions concentration, s is the critical exponent. Equation 2.9 is valid below the percolation point (i.e. $\nu < \nu_c$). The DC conductivity for nanoinclusions concentration above the percolation threshold is given [130] by:

$$\sigma_{DC}(\nu) \propto (\nu - \nu_c)^t \tag{2.10}$$

where t is the critical exponent. These two expressions give two regions; one region before the percolation threshold concentration and the other region after the percolation threshold.

2.5.2 Dielectric spectroscopy

Dielectric spectroscopy is a technique capable of probing the molecular motion and electrical properties of polymeric materials. A dielectric material must contain a charge that can be displaced by applying an electric field and store a part of the applied field. The displacement of the charge by applying the electric field is called "polarization". The dielectric properties of a material are defined by a complex dielectric permittivity, ε^*,

$$\varepsilon^* = \varepsilon' + i\varepsilon'' \qquad 2.11$$

where ε' is the relative dielectric permittivity also known as the dielectric constant of the material and ε" is the imaginary part which is a measure of the heat related loss of the material known as the dielectric loss. The dielectric constant (ε') is used to define the ability of an insulator to store electrical charge,

$$\varepsilon' = \frac{C * t}{\varepsilon_0 * A}$$

where C is the value of capacitance of a material when placed between parallel plates held in vacuum, ε_0 is the dielectric constant in vacuum ($\varepsilon_0 = 8.85 \times 10^{-12}$ F/m), t is the thickness of the material and A is the area of the parallel plates. The complex dielectric permittivity of the material depends on the polarizability of the molecules; the higher the polarizability of the molecules the higher the permittivity of the material. For an insulator, below percolation, dielectric constant is fairly constant with frequency and above percolation, dielectric constant is highly dependent on frequency. Polarization arises from a range of mechanism, where each occurs with a different strength, response

time and frequency. Understanding the polarization mechanisms in the dielectric materials is very important, as they affect the dielectric constant and the dielectric loss of the material. There are different types of polarization mechanisms: electronic polarization, atomic polarization, orientation polarization and interfacial polarization. In a given dielectric material, the total polarization is a sum of all the polarizations resulting from each one of them. For the polymers and composites studied in the range of 10^{-2} Hz to 10^{6} Hz interfacial polarization plays a more dominant role. Interfacial polarization arises for electrically heterogeneous materials such as a nanoparticle-polymer composite in which the conductivity of the polymer matrix and the conductivity of the inclusion are different. A schematic of interfacial polarization is shown in Figure 2.4. In these materials the motion of charge carriers may occur more easily through one phase and therefore are constricted at phase boundaries. Interfacial polarization results in an increase in the dielectric constant due to the motion of virtual charge which gets trapped at the interface of components of a multiphase material with different conductivity.

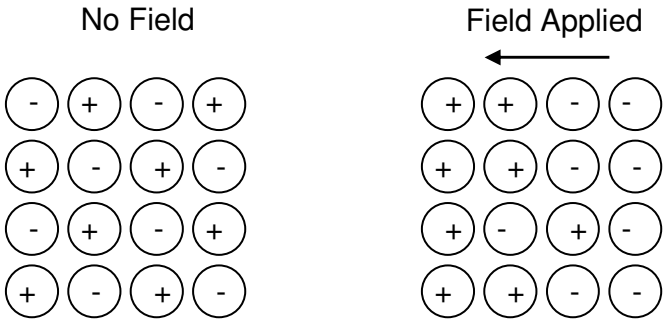

Figure 2.4. Effect of electric field on interfacial polarization.

2.5.3 In-situ electrical conductivity and dielectric constant

Quadtech® LCR meter is used to measure the electrical conductivity and dielectric constant of the liquid polymer solution placed in a sample cell as shown in Figure 2.2a. Electrical conductivity and dielectric constant of 0.03 wt% SWNT-acrylate solution are measured as a function of frequency (50 Hz to 1 MHz). An electric field of 300 V/mm is applied for 10 minutes and 30 minutes at 10 Hz, 100 Hz, 1 kHz, 10 Hz and 25 kHz frequency. LCR meter is connected to the sample cell after 10 minutes and 30 minutes of applying electric field to measure the electrical conductivity and dielectric constant of the microstructure. The change in microstructure can be related to the measured properties.

2.6 Raman spectroscopy

A JY Horiba LabRam IR system is used to probe SWNTs in polymer composites. The spectrometer operates at a constant wavelength of 785 nm with a laser power of 10%, a 50x objective lens, and a 25μm aperture slit. Raman spectra are obtained by measuring the vibrational modes of a material. SWNTs consist of two major vibrational modes that are sensitive to Raman spectroscopy: one is radial breathing of the tube, and the other is longitudinal, referred to as tangential. The spectra are recorded on electric field manipulated 0.03 wt% SWNT-acrylate nanocomposites. Spectrometer in conjunction with a rotating stage is used for polarized Raman spectroscopy to characterize SWNT alignment in polymers. Aligned SWNT-acrylate nanocomposites are placed on the rotating stage. SWNT-acrylate nanocomposites aligned by applying an electric field of

300 V/mm for 30 minutes at various frequencies of 10 Hz, 100 Hz, 1 kHz, 10 kHz and 25 kHz are tested. Setting the rotating stage to 0° aligns the polarization parallel to the alignment axis and 90° is perpendicular to the alignment axis of the aligned nanocomposite. Alignment axis of the sample is same as the direction in which electric field was applied during processing. Tangential peak of SWNT is inspected to assess degree of SWNT orientation. Tangential peak intensity is maximum when the polarization of incident light is parallel to nanotube axis. Same tangential mode intensity is suppressed when the polarization of incident light is perpendicular to nanotube axis [131, 132]. The stage is rotated by 15º, which sets the polarization of Raman laser at an angle of 15º to the direction of alignment. Raman spectra is obtained at 15º intervals starting from 0º to 90º. By comparing signal intensity of tangential SWNT peak at 1590 cm^{-1} for each polarization angle, degree of alignment of SWNT is qualitatively assessed. An orientation distribution function (ODF) is established at different angles to quantify SWNT alignment in acrylate polymer at different frequencies [133].

2.7 Dynamic mechanical analysis

TA® instruments RSA 3 dynamic mechanical analyzer is used to measure mechanical properties. Storage modulus, loss modulus and tan δ are measured using a 3-point bending clamp and a tensile clamp, at 1 Hz frequency. Storage modulus is measured at different nanoparticle loadings. In the aligned nanocomposites, storage modulus is measured in parallel and perpendicular directions.

SWNTs are added to the polymer matrix to enhance the physical properties of the composite. The properties of the individual components and the interfaces between the components affect the properties of the composite. Factors that influence the mechanical properties of the composite include inclusion concentration, inclusion geometry and packing, and the relative modulus of each component. Utilizing dynamic mechanical analysis (DMA), the relaxation in polymers under stress and temperature is studied. DMA can give information about the influence of inclusions on the relationships between structure and properties of a composite and hence, can reveal the modifications to mechanical properties of the polymer created by the inclusions. E' is the storage modulus, which is a measure of stiffness, and E" is loss modulus, which is a damping or energy dissipation factor. The angle that reflects the time lag between the applied stress and strain is δ, and it is defined by a ratio called the loss tangent (tan δ).

$$\tan\delta = \frac{E''}{E'} \qquad 2.12$$

tan δ, a damping term, is a measure of the ratio of energy dissipated as heat to the maximum energy stored in the material during one cycle of oscillation. The storage modulus (E') and the loss modulus (E'') in terms of stress (σ) and strain (γ) are $E' = \frac{\sigma}{\gamma}\cos\delta$ and $E'' = \frac{\sigma}{\gamma}\sin\delta$.

3. DISPERSION OF NANOPARTICLES IN POLYMERS

We have used the dispersion approach of non-covalent functionalization along with mechanical shear and sonication. Two methods were used, solvent free and solvent based methods to disperse SWNTs and CNFs in polyimides, acrylate and epoxy polymers. In this section, dispersion of SWNTs and CNFs will be analyzed by optical microscopy, scanning electron microscopy, electrical conductivity, dielectric spectroscopy and dynamic mechanical analysis.

3.1 Solvent free processing of polymer nanocomposites

A solvent free method is used to disperse 0.03 wt% SWNTs in acrylate polymer and 0.1 wt% CNFs in epoxy polymer as described in section 2.1. Flow chart describing the various steps is shown in Figure 3.1. Nanoparticles are easier to disperse in low viscosity medium compared to high viscosity medium. Acrylate polymer consists of two parts UDMA and HDDMA. SWNTs are predispersed in HDDMA as it has a much lower viscosity compared to UDMA. Predispersion of SWNTs reduces the initial size of SWNT agglomerates, which results in better distribution after the addition of high viscosity UDMA. Mechanical shear along with sonication is used during predispersion and final dispersion.

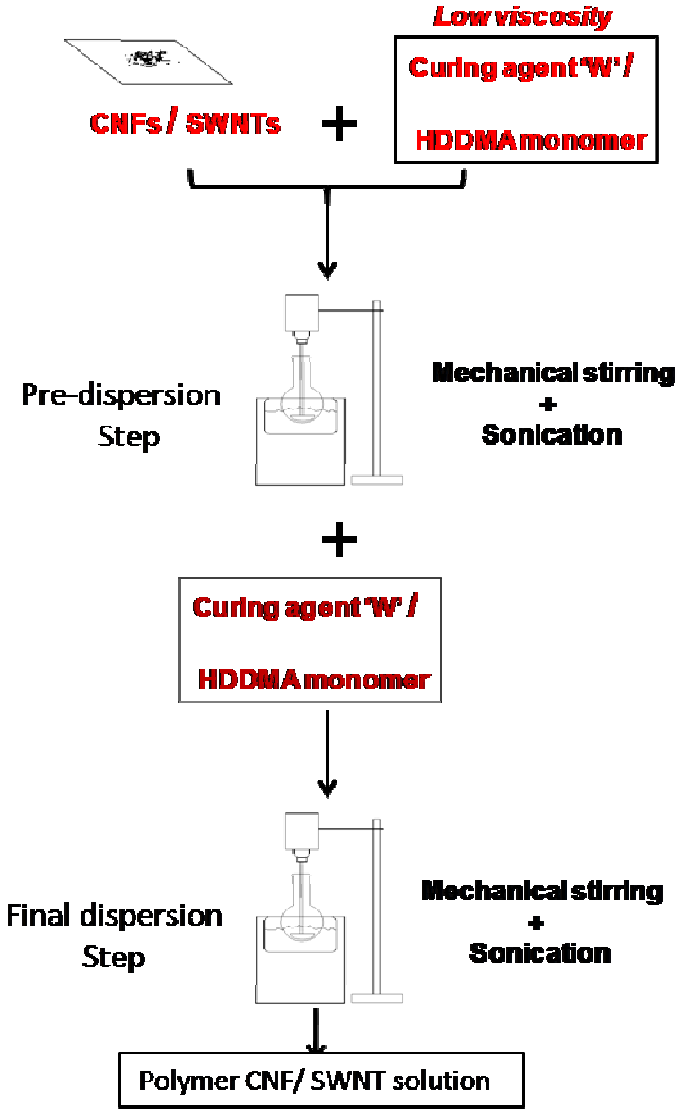

Figure 3.1. Flow chart showing various steps in solvent free processing of acrylate and epoxy polymer nanocomposites.

Inspection of OMs of 0.03 wt% SWNT-acrylate solution (Figure 3.2a and b) indicate presence of SWNT bundles, in the shape of spheres that are mostly ~1μm with a few that are ~ 3μm. The remaining are in the shape of ellipsoids with a length of ~8μm and radius of ~1μm. Increasing the sonication and stirring time for this reduces the SWNT

bundle sizes. Solution of SWNTs and HDDMA is sonicated (at 40 kHz) and stirred (at 150 rpm) for 3 hours. Solution of UDMA is mixed in and the mixture is further sonicated and stirred for 5 hours. These conditions gave the best homogenous distribution.

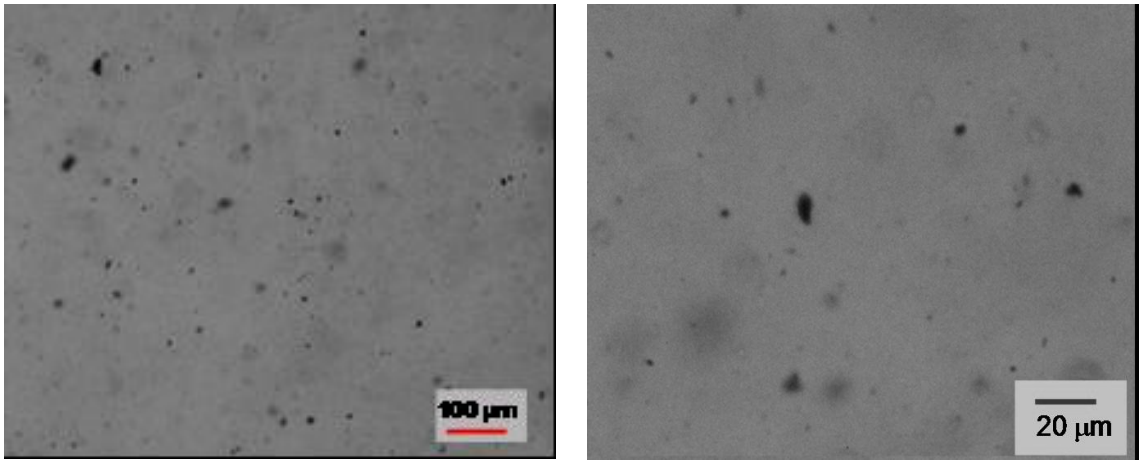

(a) (b)

Figure 3.2. OM images of 0.03 wt% SWNT – acrylate polymer composite processed by solvent free method (a) 10x magnification and (b) 50x magnification, presence of spherical and ellipsoidal SWNT bundles is seen.

Similarly solvent free method is used to disperse CNFs in EPON 862 epoxy polymer. Epoxy has a high viscosity (3000 cP) and it is difficult to directly disperse CNFs in it. CNFs are predispersed in a low viscosity curing agent 'W' along with mechanical stirring and sonication. This reduces the CNF agglomerates. Epoxy is then added to the CNF-curing agent solution; this mixture is subjected to mechanical stirring and sonication to complete the dispersion process. OM images in Figure 3.3 shows the final dispersion state of 0.1 wt% CNFs in epoxy. There is homogenous distribution of CNFs

with many large agglomerates present. Figure 3.3b shows individually dispersed CNFs but a few large CNF agglomerates are present.

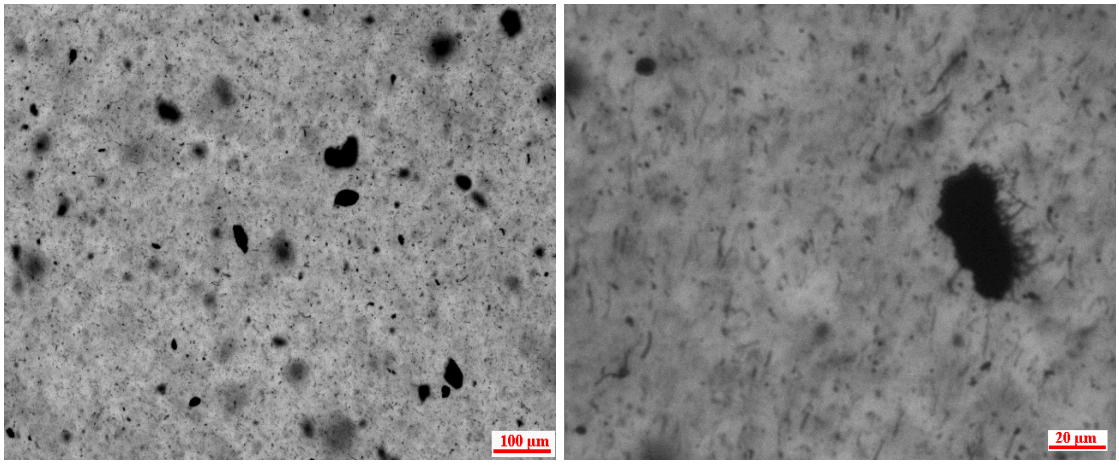

(a) (b)

Figure 3.3. OM images of 0.1 wt% CNF-epoxy polymer composite processed by solvent free method (a) 10x magnification and (b) 50x magnification.

Although the solvent-free method resulted in a homogenous dispersion of CNF bundles, there was still some large bundles present. The predispersion of CNFs in the curing agent was not very effective to reduce the CNF agglomerates. Once epoxy was added to the CNF-curing agent mixture there was an increase in viscosity due to the initiation of partial curing of epoxy. Increase in viscosity inhibited CNF dispersion resulting in large CNF agglomerates. SWNTs bundles were homogenously dispersed in acrylate polymer solution with no large agglomerates by the solvent-free method. SWNT agglomerates were reduced in the predispersion step. After adding UDMA monomer to the predispersed SWNT mixture, the solution was mechanically stirred and sonicated to

achieve homogenous distribution. The monomer was in the uncured state which resulted in better distribution. To improve the CNF in epoxy, a second method is explained next.

3.2 Solvent based processing of polymer nanocomposite

CNFs formed large agglomerates in epoxy polymer by the solvent free dispersion method. In order to improve the dispersion of CNFs and SWNTs, solvent based method is used, where nanoparticles are predispersed in a very low viscosity polar solvent.

3.2.1 CNF-epoxy nanocomposites

Solvent based method to disperse CNFs in epoxy polymer is described in section 2.2.1. Flow chart of solvent based processing of polymer nanocomposites is shown in Figure 3.4. First CNFs are predispersed in DMAc along with mechanical stirring and sonication, which reduces the CNF agglomerates. The duration of mechanical stirring and sonication influences the size of CNF agglomerates. OM images of CNFs predispersed in DMAc for 2 hours and 3 hours are shown in Figure 3.5a respectively. After 2 hours of sonication, CNFs are uniformly distributed, but there are a few very large agglomerates. Further mechanical stirring and sonication for 1 hour reduced the size of large agglomerates. Epoxy polymer is added to the predispersed CNF-solvent solution and the mixture is subjected to further sonication and stirring. Solvent is evaporated before adding the curing agent into the mixture. Optical micrographs of 0.1 wt% CNF-epoxy nanocomposites are shown in Figure 3.6. CNFs are homogenously

distributed in the epoxy matrix with no large agglomerates (Figure 3.6a) and at a higher magnification we see individual CNFs (Figure 3.6b). This indicates CNF dispersion in epoxy has improved when solvent based method is used; there are more uniformly dispersed individual CNFs and absence of large CNF agglomerates. The length of CNFs is ~12 µm. CNF concentration up to 3 wt% are dispersed in epoxy polymer by the same method. OMs of 1 wt% CNF- epoxy and 3 wt% CNF-epoxy are shown in Figure 3.7.

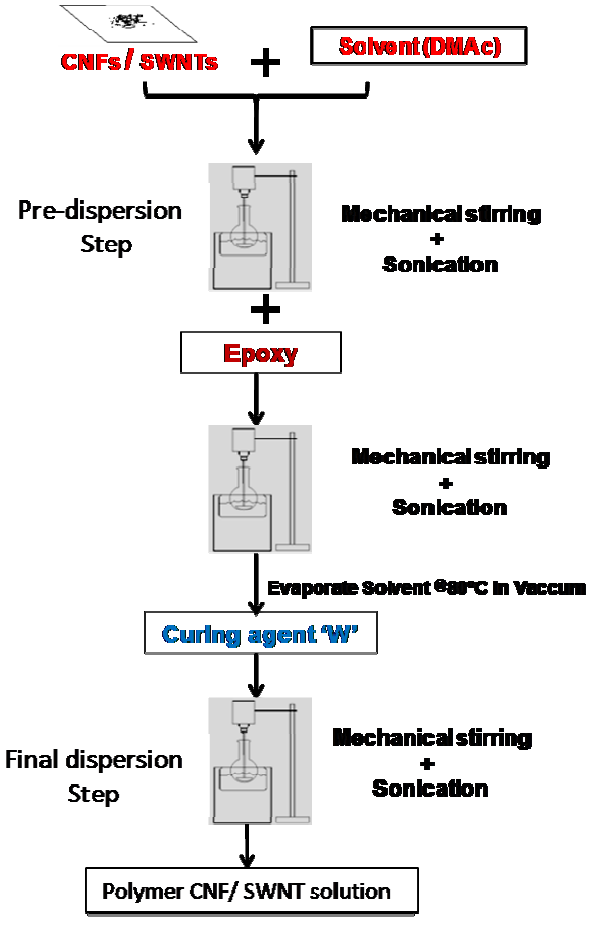

Figure 3.4. Flow chart showing various steps of solvent based processing of epoxy polymer nanocomposites.

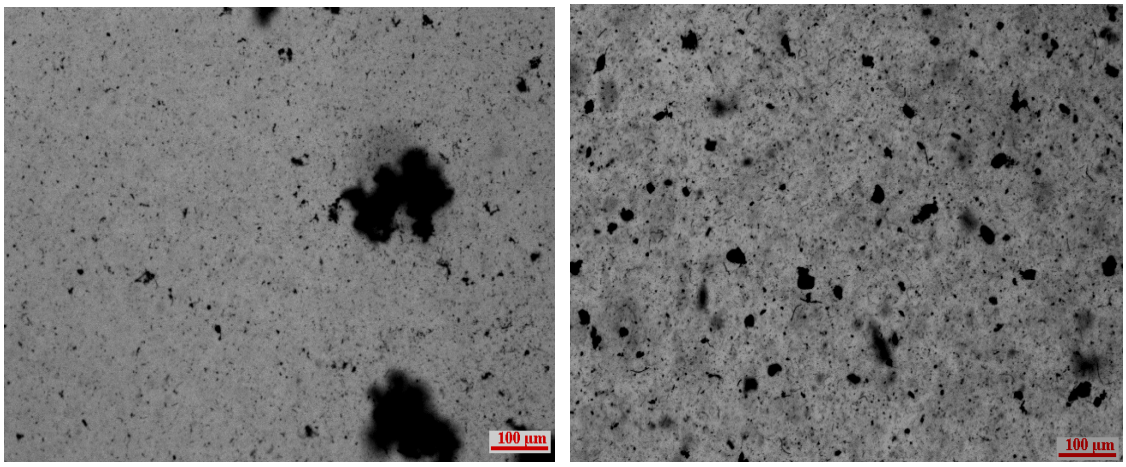

(a) (b)

Figure 3.5. OMs images of CNFs dispersed in DMAc solvent. (a) 2 hours (b) 3 hours of sonication and mechanical stirring

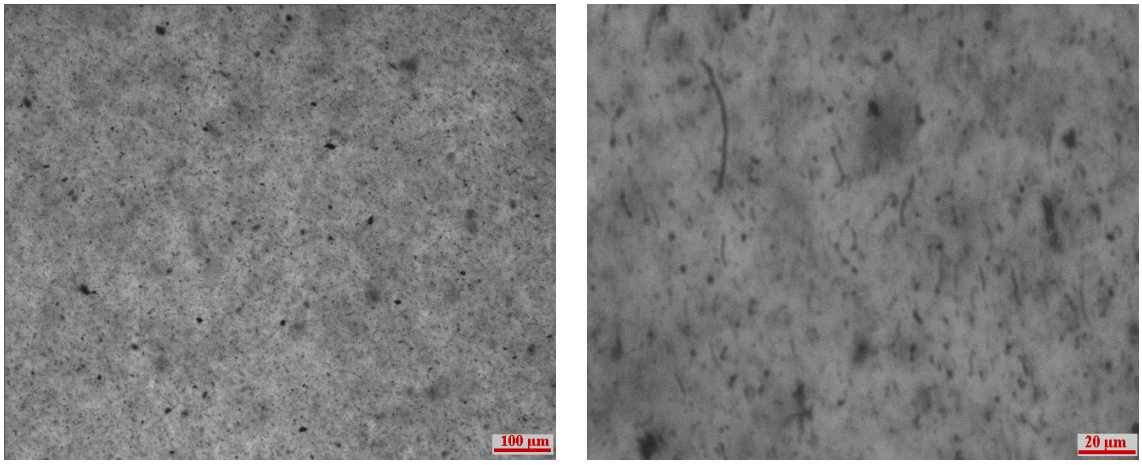

(a) (b)

Figure 3.6. OMs images of 0.1 wt% CNF-epoxy polymer composite processed by solvent based method (a) 10x magnification and (b) 50x magnification.

There are a few large agglomerates at 1 wt% CNF loading but the size and number of agglomerates increase at 3 wt% CNF loadings. As the CNF concentration increases it is

difficult to separate the CNF agglomerates and it is difficult to obtain uniform homogenous distribution at higher concentrations.

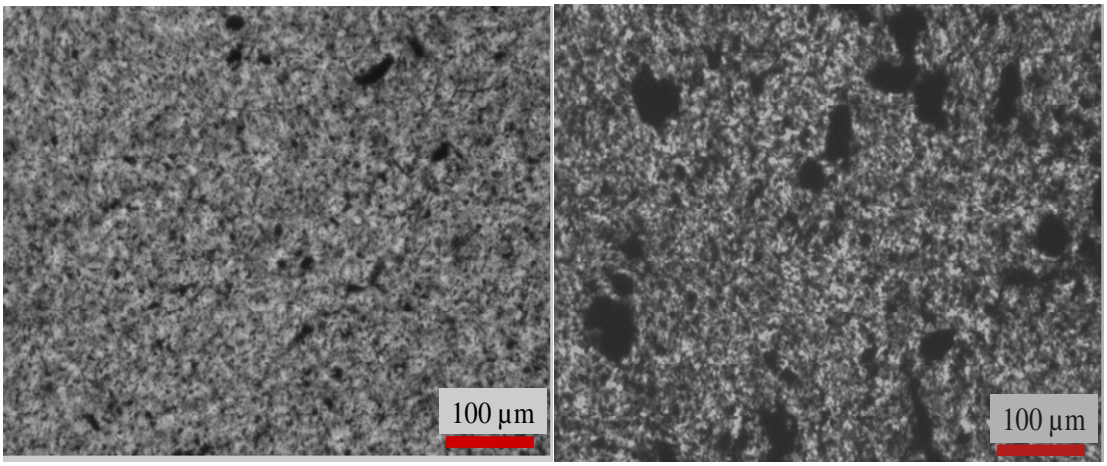

(a) (b)

Figure 3.7. OMs of CNF-epoxy polymer solutions (a) 1 wt% CNFs and (b) 3 wt% CNFs.

Electrical conductivity of CNF-epoxy nanocomposites is measured as a function of frequency at different CNF concentrations, as shown in Figure 3.8. There are three different regions, one where conductivity is dependent on frequency, a second one where it is constant at low frequencies increases with frequency in the kHz range, and a third where conductivity is fairly constant at all frequencies. Conductivity of pure epoxy is highly dependent on frequency, where it increases from 10^{-15} S/cm at 0.01 Hz to 10^{-5} S/cm at 10^{6} Hz. This large dependence on frequency is typical of an insulator. By the addition of 0.1 wt% CNFs there is no change in the conductivity and its behavior with frequency. There is a small increase in conductivity to 10^{-14} S/cm at 0.01 Hz by the addition of 1 wt% CNFs, but still no change in behavior. At 1.5 wt% CNF loading,

conductivity of the epoxy nanocomposite increases to 10^{-8} S/cm at 0.01 Hz. There is also a change in behavior; conductivity is constant up to 10 kHz frequency and then increases to 10^{-5} S/cm at 10^{6} Hz. This behavior indicates the nanocomposite is in the percolation transition region where it is changing from an insulator to a conductor. Further increasing the CNF concentration to 2.25 wt% and 3 wt% loading, conductivity reaches values of 10^{-6} S/cm and 10^{-4} S/cm respectively, and is fairly constant with frequency, which is a behavior typical of a conductor. Figure 3.9, shows electrical conductivity as a function of different CNF wt%. There is a sharp rise in electrical conductivity at 1.5 wt%, which indicates a percolation transition in CNF-epoxy nanocomposites.

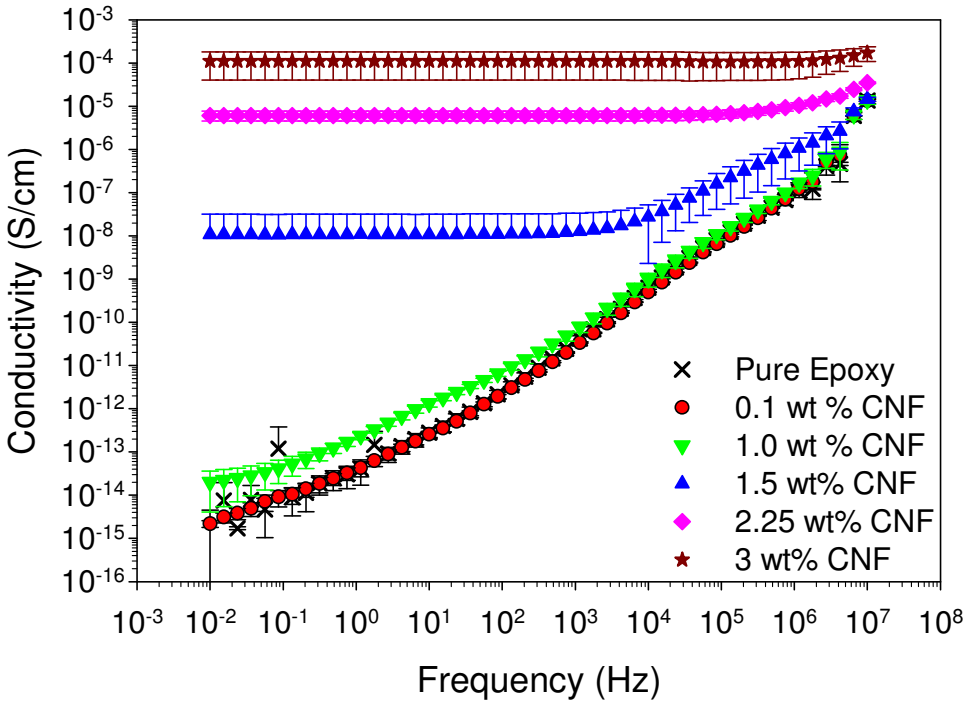

Figure 3.8. Electrical conductivity of CNF-epoxy polymer nanocomposites as a function of frequency.

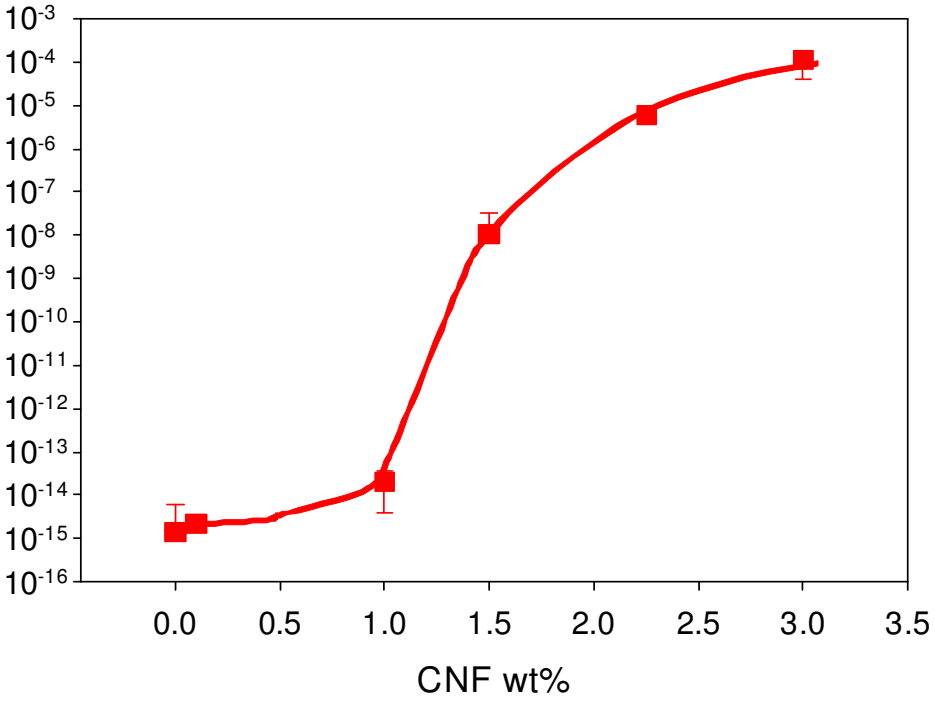

Figure 3.9. Electrical conductivity of CNF-epoxy nanocomposite as a function of different CNF concentrations. Solid line is a trend line.

Figure 3.8 and Figure 3.9, show error bars for every CNF concentration. The standard deviation is very small for all samples, which is an indication of good repeatability in the measurements, and is possibly due to the homogenous distribution of CNFs through out the epoxy nanocomposite processed by solvent-based method.

The dielectric constant of CNF-epoxy nanocomposites is measured to further study the dispersion of CNFs in epoxy polymer. In Figure 3.10, the dielectric constant at different CNF concentrations is measured as a function of frequency. There are two different

regions, one where dielectric constant is fairly constant with frequency and the other where dielectric constant is dependent on frequency. For the pure epoxy, 0.1 wt% and 1 wt% CNF-epoxy nanocomposites, the dielectric constant is fairly constant with frequency. This behavior is typical of an insulator. At higher CNF concentration of 1.5 wt%, 2.25 wt% and 3 wt% CNF-epoxy nanocomposite the dielectric constant decreases with frequency. This behavior is typical of a conductor. This change in behavior at 1.5 wt% CNF loading is indicative of a percolation transition where the epoxy nanocomposite is now above percolation. Similar behavior was also seen with the conductivity measurements. Achieving similar percolation behavior for both conductivity and dielectric constant is a strong indication of very good homogenous dispersion of CNFs in epoxy polymer. At frequencies below 10 Hz, the dielectric constant of epoxy nanocomposites with CNF loadings greater than 1.5 wt% could not be measured as the nanocomposite has a very high conductivity and large dielectric losses.

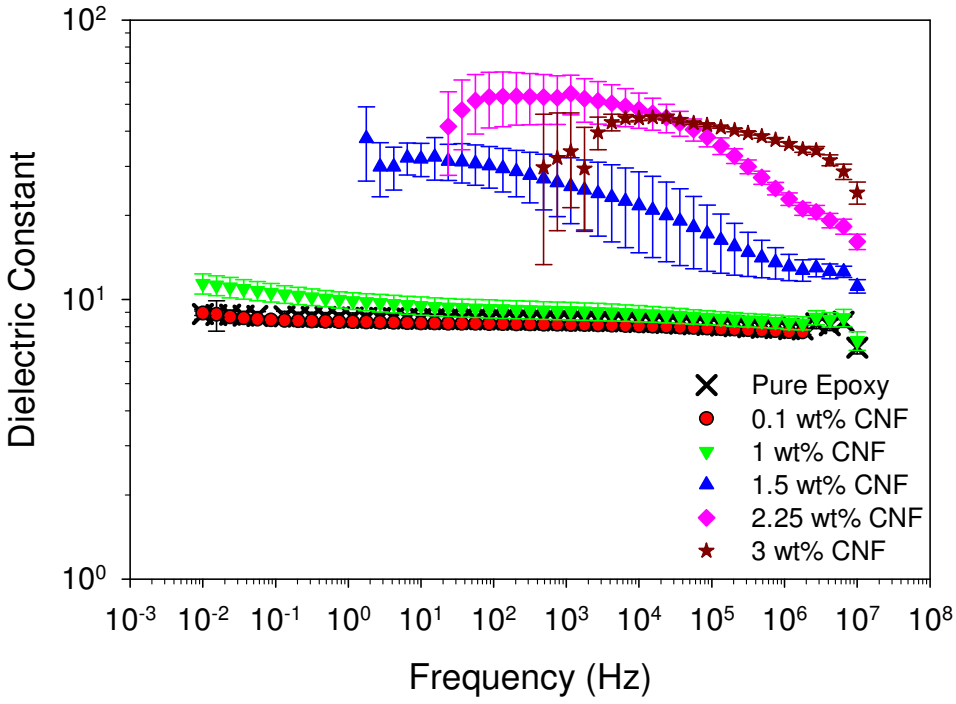

Figure 3.10. Dielectric constant of CNF-epoxy polymer nanocomposites as a function of frequency.

3.2.2 SWNT-polyimide nanocomposites

Solvent based method is used to disperse SWNTs in polyimide polymer as described in Section 2.2.2. Flow chart describing various steps in solvent free processing method is shown in Figure 3.11. Optical micrographs of a low concentration SWNT polyimide composite (0.05 wt%) and a high concentration of SWNT polyimide composite (0.2 wt%) are shown in Figure 3.12a and b respectively. It is seen that the SWNTs are homogenously dispersed in the polymer matrix and there are no large agglomerates present. The polyimide, ((β-CN)-APB)/ODPA, is believed to stabilize the dispersion of SWNTs by way of an electron donor acceptor interaction between the SWNTs and the

nitrile dipole present in the polymer[4]. This type of interaction leads to the formation of non-covalent bonds between the SWNTs and the polyimide, which may result in homogenous dispersion and strong adhesion in the composite.

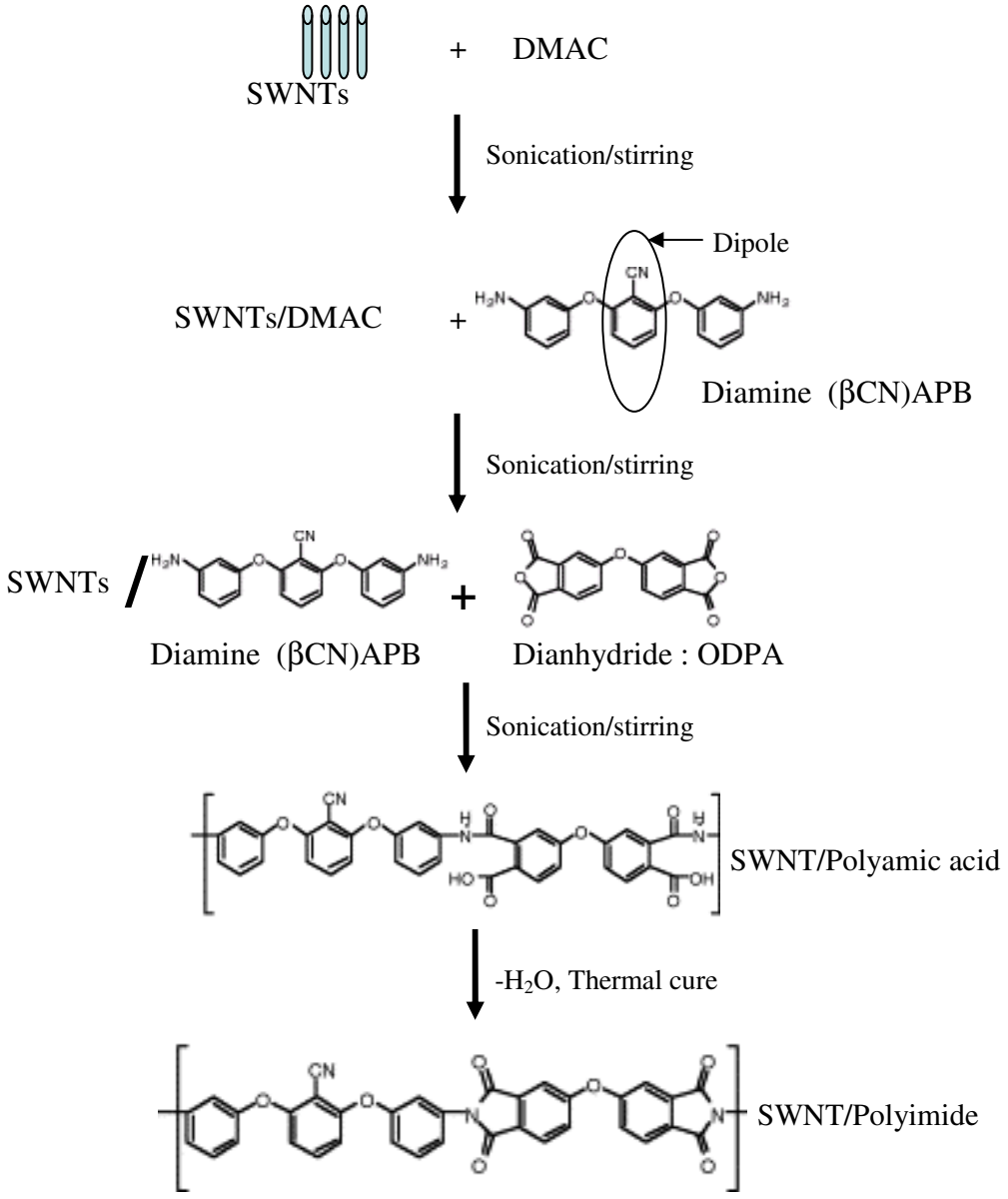

Figure 3.11. The synthesis procedure of SWNT polyimide composite.

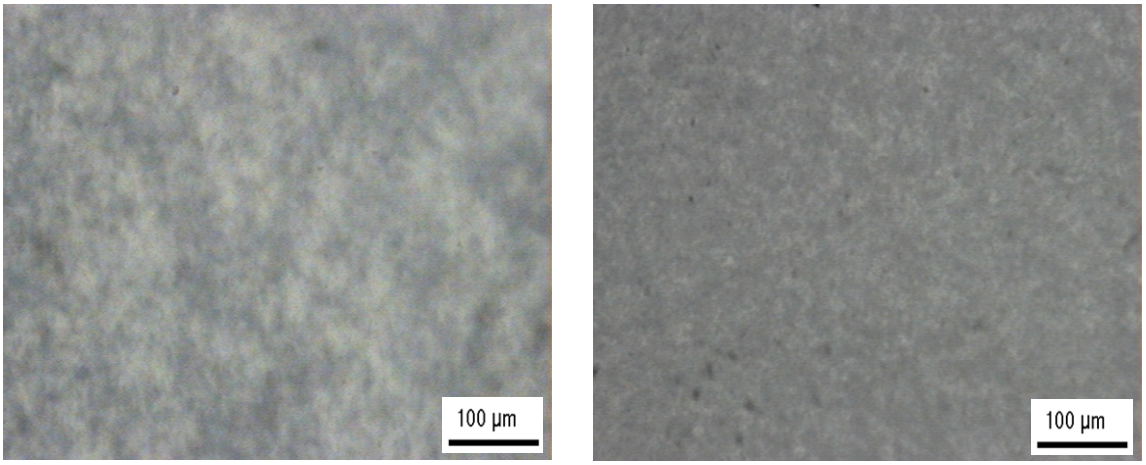

(a) (b)

Figure 3.12. OMs images of SWNT-polyimide polymer nanocomposites (a) low concentration of 0.05 wt% SWNTs and (b) high concentration 0.2 wt% SWNTs.

SEM micrograph on the fracture surface of a 0.5 wt% SWNT-polyimide nanocomposite is shown in Figure 3.13a. This micrograph shows uniform distribution of SWNT bundles with no large agglomerates of SWNTs present in the polyimide. SWNT bundles are completely embedded into the polymer matrix and Figure 3.13b shows polymer matrix around the SWNT bundle, which indicates there is wrapping of polymer chains around the SWNTs.

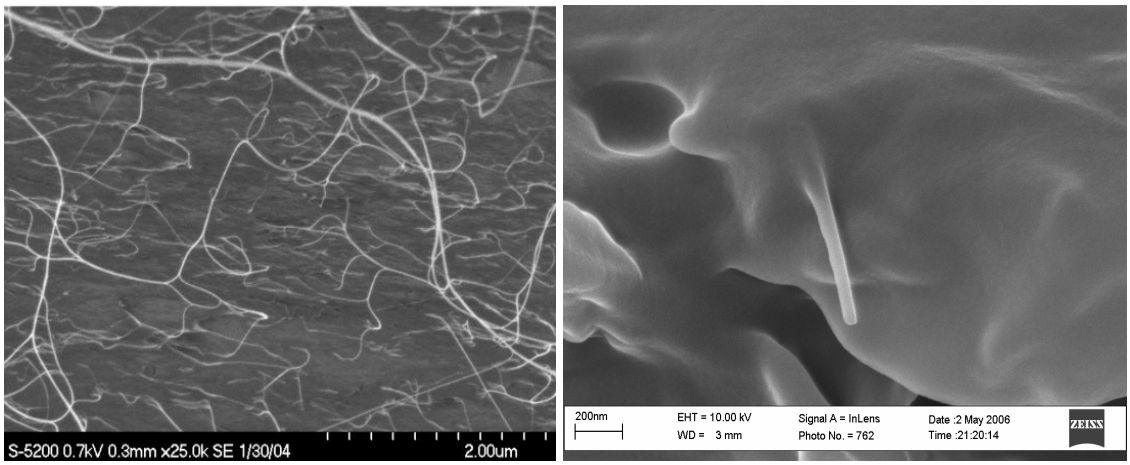

(a) (b)

Figure 3.13. SEM micrograph of 0.5 wt% SWNT polyimide. (a) uniformly distributed SWNTs, scale bar is 2 μm, (b) SWNT wrapped with polymer matrix, scale bar is 200 nm.

Figure 3.14 shows the electrical conductivity of SWNT-polyimide nanocomposites as a function of frequency for different SWNT concentrations. There are two different regions, one where conductivity is highly dependent on frequency and one where it is fairly constant with frequency. At 0 wt% SWNTs and 0.02 wt% SWNTs conductivity is highly dependent on frequency, which is indicative of an insulator behavior. These nanocomposites are below percolation. The second region that is fairly constant with frequency extends from 0.075 wt% SWNTs up to 2 wt% SWNTs and is indicative of a conductive behavior. In this region there is a continuous path of nanotubes, making the composite conductive and these nanocomposites are above percolation.

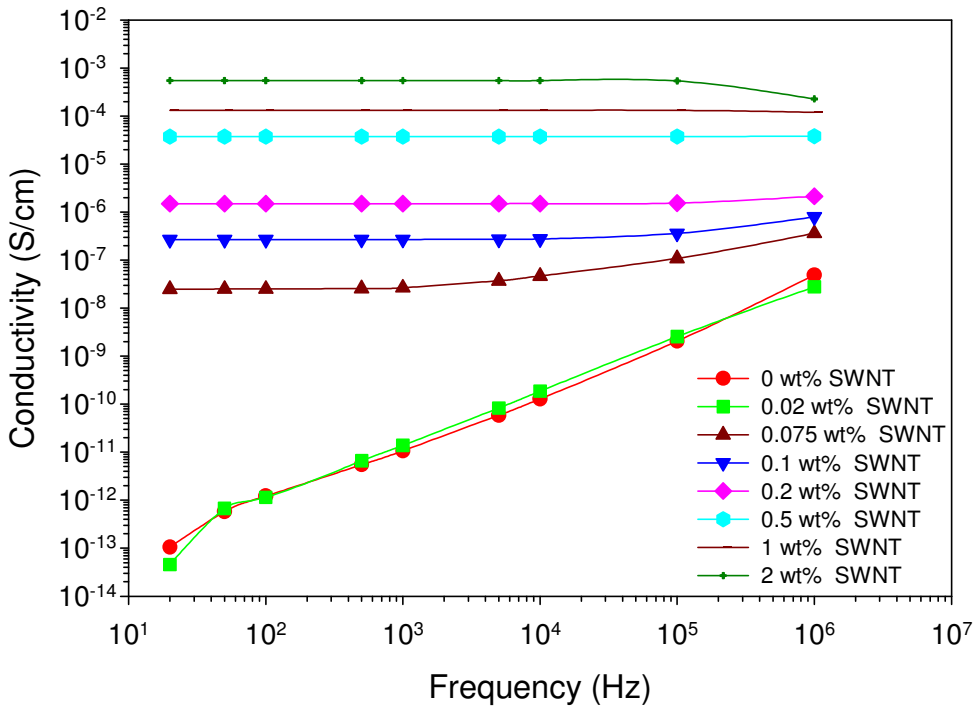

Figure 3.14. Electrical conductivity of SWNT-polyimide polymer nanocomposites as a function of frequency at different SWNT concentrations.

To study the percolation transition and percolation threshold, DC electrical conductivity is plotted as a function of SWNT weight fraction in Figure 3.15 . The DC electrical conductivity data is extrapolated to 0 Hz from the AC electrical conductivity measured at 20 Hz. Electrical conductivity increases as the SWNT concentration increases, where there is a sharp rise in conductivity from 10^{-13} S/cm at 0.02 wt% SWNTs to 10^{-8} S/cm at 0.075 wt% SWNTs. This sharp rise in conductivity indicates percolation transition. Conductivity further increases to 10^{-4} S/cm with 0.5 wt% SWNT concentration, as seen in Figure 3.15. The conductivity data can be fitted to a power law in terms of volume fraction of SWNT, to determine the critical volume concentration. The conductivity is

linear with (v-v_c) in a logarithmic scale and the relationship is described by Equation 2.10. A critical volume fraction of 0.06 wt% is obtained for the SWNT polyimide composite [134]. This indicates that the composite behaves as a conductor above 0.06 wt% and behaves as an insulator below 0.06 wt% of SWNT concentrations. The low critical volume fraction of 0.06 wt% is indicative of uniform dispersion of SWNTs in the polyimide matrix.

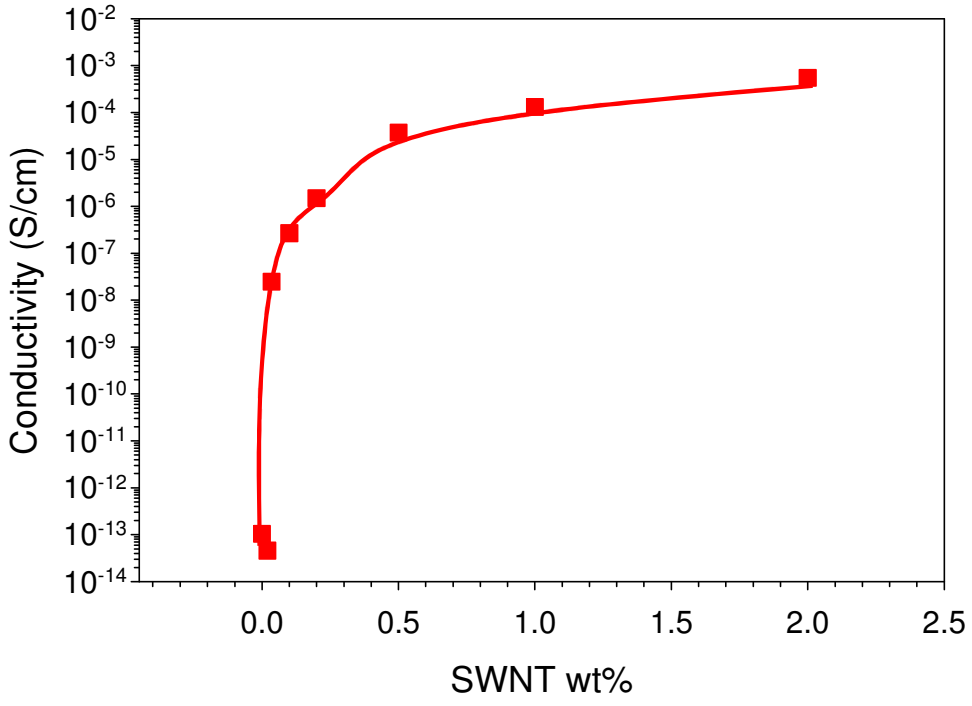

Figure 3.15. Electrical conductivity of SWNT-polyimide nanocomposites as a function of different SWNT concentrations. Solid line is a trend line.

The storage modulus of SWNT-polyimide nanocomposites was measured to study the effect of SWNTs on the polyimide matrix. Figure 3.16 summarizes the results of storage

modulus as a function of temperature for SWNT-polyimide nanocomposites. Pure polyimide and SWNT-polyimide nanocomposites display the typical behavior of an amorphous thermoset polymer. Below T_g, polymer is in a glassy state with a high storage modulus, as shown in Figure 3.16. The storage modulus of pristine polyimide below T_g, drops from 1450 MPa at 30°C to 950 MPa at 200°C. Above T_g at 240°C, the polymer is in a rubbery state where there is a sharp drop in modulus to 10 MPa. SWNT polyimide composites also follow a similar trend.

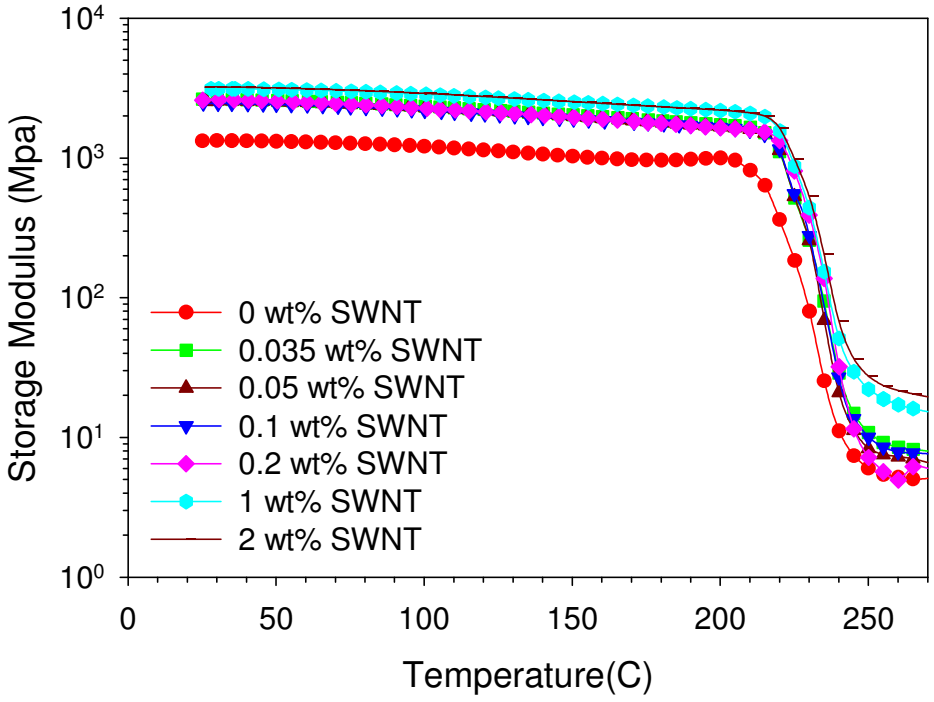

Figure 3.16. Storage modulus of SWNT-polyimide nanocomposite as a function of temperature at different SWNT concentrations.

Figure 3.17 displays the increase in storage modulus of the pristine polyimide with increase in SWNT concentration. The storage modulus of the pristine polyimide at 30ºC

increases from 1450 MPa to 3200 MPa with the addition of 2 wt% SWNTs, corresponding to a 120% increase in storage modulus. The storage modulus of the pristine polyimide at 240ºC, increased from 10 MPa to 58 MPa with the addition of 2 wt% SWNTs, corresponding to a 480% increase in storage modulus. The significant increase in the storage modulus of SWNT polyimide composite below and above T_g confirms the reinforcing effect of SWNTs on polyimide matrix. Uniform dispersion of SWNTs in polyimide leads to good interfacial interaction, due to the large surface area of SWNTs. The interfacial interaction between the SWNTs and the polyimide matrix reduces the mobility of the polymer chains around the SWNTs, which leads to an increase in the storage modulus.

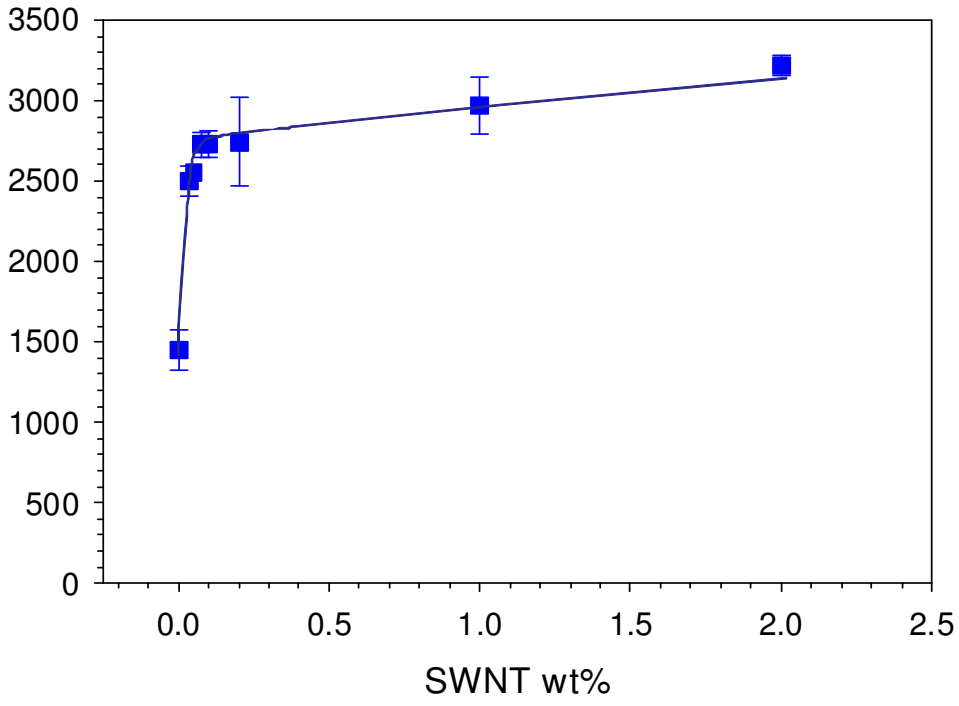

Figure 3.17. Storage modulus of SWNT-polyimide nanocomposite as a function of SWNT concentration.

We have achieved good dispersion of CNFs in epoxy polymer and SWNTs in polyimide. Predispersion of CNFs and SWNTs in a polar solvent along with a combination of mechanical stirring and sonication was very effective to reduce the large agglomerates. Adding the monomer to this well dispersed nanoparticle mixture along with sonication and mechanical stirring prevented reagglomeration of CNFs and SWNTs. A very low percolation threshold has been obtained for the nanocomposites processed by solvent based method as seen by the electrical conductivity and dielectric spectroscopy. There has also been a significant increase in storage modulus due to the good dispersion and interaction with the polymer matrix. Results have shown that this method is very effective in dispersion of CNFs and SWNTs.

4. EFFECT OF ELECTRIC FIELD MAGNITUDE, FREQUENCY AND TIME ON NANOPARTICLES IN POLYMERS

Electric field was applied to nanoparticles dispersed in polymer solution by the method described in Section 2.3. AC electric field magnitude, frequency and duration are varied and their effects on the behavior of CNFs and SWNTs are studied. In this section we will first study the experimental observations from optical microscopy, Raman spectroscopy, and in-situ electrical and dielectric properties at different AC electric field conditions. Finally, the possible electrokinetic forces that drive electric field manipulation of nanoparticles will be examined.

4.1 Experimental observations

When an AC electric field is applied to a nanoparticle polymer suspension, firstly, anisotropic particles rotate and align in the direction of electric field and secondly, particles attract towards each other to form long chains between the electrodes, in the direction of electric field.

4.1.1 Rotation of nanoparticles

4.1.1.1 Optical microscopy

Dilute suspensions of randomly oriented CNFs were dispersed in silicone oil. When an AC electric field is applied, CNFs rotate in the direction of the electric field (i.e, perpendicular to the electrodes). Figure 4.1 shows the rotation of a CNF at different intervals of time after applying an electric field of 300 V/mm; the length of the CNF is

25 μm. CNFs are randomly dispersed when E=0 and t=0 (Figure 4.1a). Applying an electric field of 300 V/mm, causes the CNF to rotate in the direction of electric field and it takes 4 seconds to completely rotate in this particular case (Figure 4.1c).

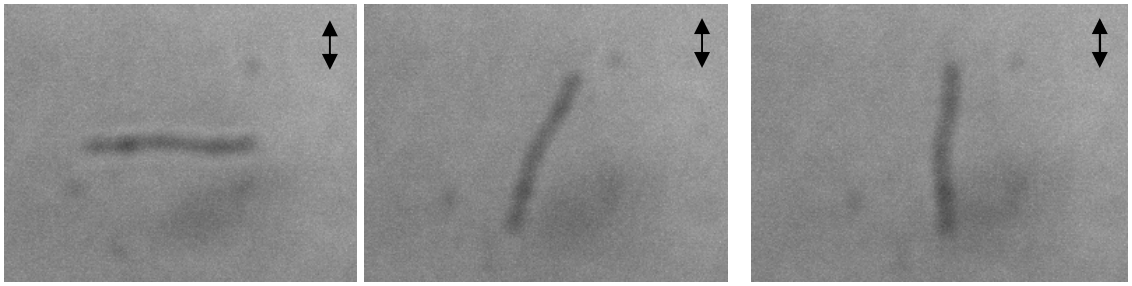

(a) (b) (c)

Figure 4.1. Different stages of a CNF after the electric field is applied. Length of CNF is 25 μm. Applied voltage and time is (a) E=0, t= 0sec, (b) E=300 V/mm, t=2sec and (c) E=300 V/mm, t=4sec. Arrow indicates direction of applied electric field.

Similar behavior is also seen for anisotropic SWNT bundles dispersed in acrylate polymer solution (η = 1600 cP), epoxy polymer solution (η = 3000 cP) and silicone oil solution (η = 50 cP). Rotation of a SWNT bundle in acrylate polymer solution when E=300 V/mm is shown in Figure 4.2, the length of the SWNT bundle is ~8μm. It takes 12 sec for the SWNT bundle to rotate from its initial position before reaching a stable state.

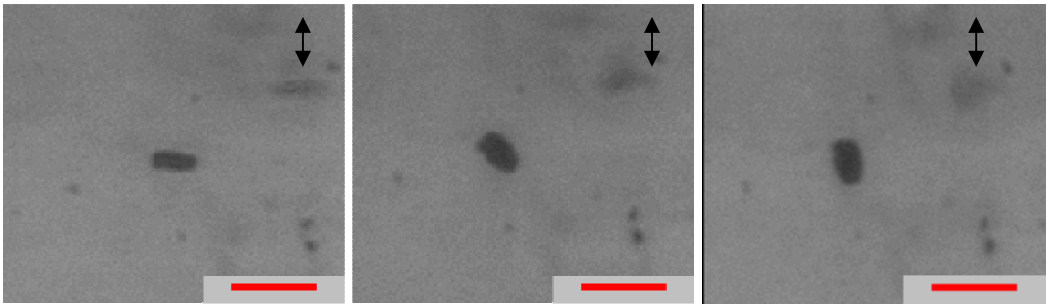

(a) (b) (c)

Figure 4.2. Rotation of an ellipsoidal SWNT bundle, arrow indicates direction of electric field. Magnitude of the applied electric field is 300 V/mm and the frequency is 10 Hz (a) t=0, (b) t=3 sec (c) t=5 sec. Scale bar is 20 µm.

Various electric fields, from 50 V/mm to 350 V/mm, were applied to all three polymer solutions at 10 Hz frequency and the time taken for rotation is recorded. Figure 4.3 shows the time taken for SWNT bundles to rotate as a function of applied electric field magnitudes. In all three solutions, the time for SWNT rotation decreases as the applied electric field increases. The time for rotation in epoxy and acrylate polymer solution is similar because of similar viscosities, but the time for rotation in silicone oil is much less because it has the lowest viscosity (50 cP). Based on these initial observations, it is seen that the time for rotation is a function of viscosity and electric field. It is also important to note that the starting dispersion of SWNTs in acrylate, epoxy and silicone oil is different.

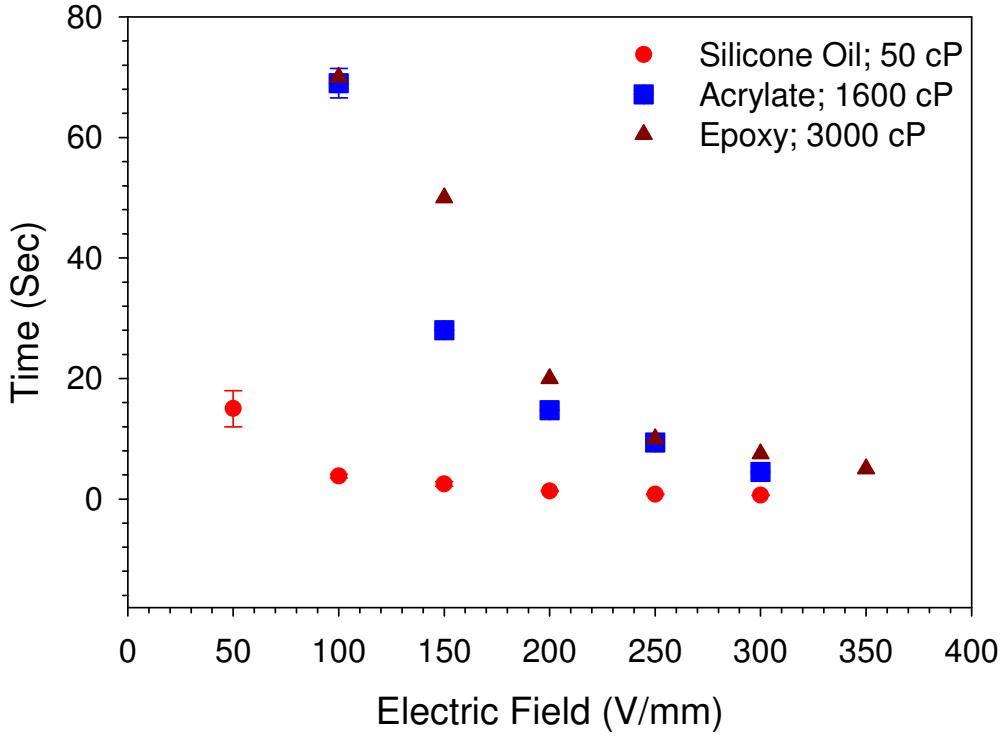

Figure 4.3. Time taken for an anisotropic SWNT bundle to rotate from horizontal to vertical position as a function of different electric fields in different viscosity polymers, silicone oil (50 cP), acrylate (1600 cP) and epoxy (3000 cP). The frequency of the applied electric fields was 10 Hz.

4.1.1.2 Polarized Raman spectroscopy

The SWNT tangential peak was examined to detect alignment of SWNTs in the acrylate polymer nanocomposite. An electric field of 300 V/mm was applied for 30 minutes at a frequency of 10 Hz, 100 Hz, 1 kHz, 10 kHz and 25 kHz. Samples were aligned and cured as described in Section 2.7. Figure 4.4 shows the SWNT tangential peak intensity at 1590 cm^{-1} for the SWNT-acrylate polymer nancomposite aligned at 300 V/mm, 1 kHz and 30 minutes. Raman intensity of the tangential peak reduces as the polarizer angle increases from 0º to 90º, which indicates SWNT alignment. Similar behavior is obtained

for other SWNT-acrylate samples aligned at different frequencies of 10 Hz, 100 Hz, 10 kHz and 25 kHz. Setting the polarizer to 0º it is parallel to the direction of SWNT alignment, which results in a maximum intensity. Changing the polarizer from 0º to 90º changes it from being parallel to being perpendicular to the direction of SWNT alignment, which results in decreasing the intensity. This change in intensity indicates preferential SWNT alignment. In a randomly aligned sample, changing the polarizer angle does not decrease the peak intensity as the SWNTs are randomly oriented at different angles. Although these results tell us that SWNTs are preferentially aligned, we do not know how well they are aligned with respect to the electric field.

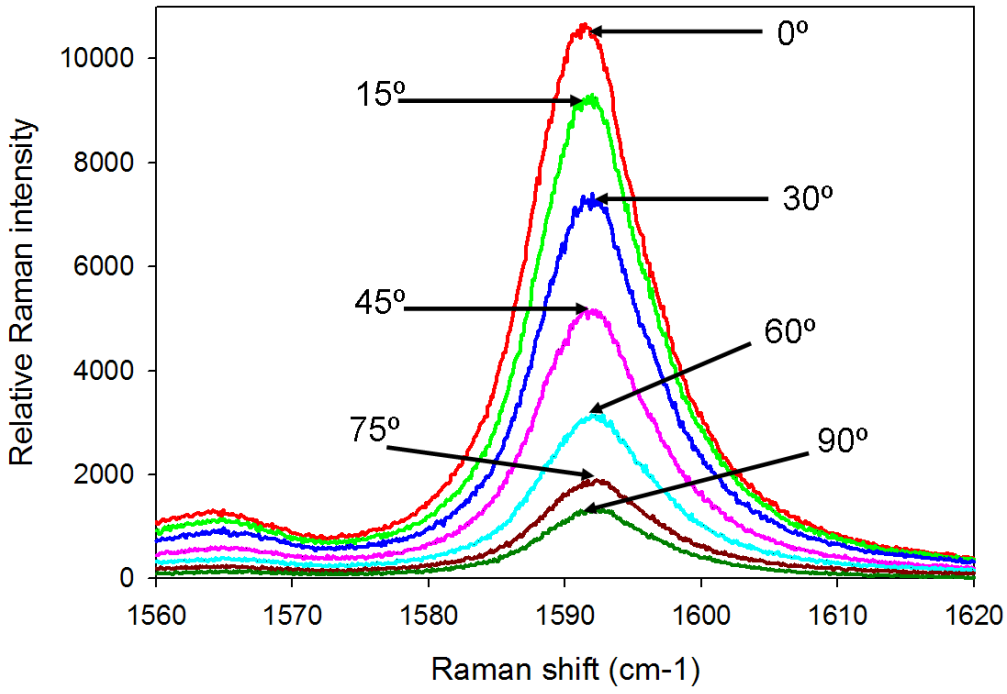

Figure 4.4. Raman spectra of SWNT-acrylate aligned at 300 V/mm, 1kHz, 30 minutes. Raman spectra is obtained at different polarizer angles (0º to 90º).

To further quantify SWNT alignment at different frequencies, an orientation distribution function (ODF) is used.[133] Two different 0.03 wt% SWNT-acrylate solutions are aligned. It is noted that different batches of SWNTs were used to prepare the solutions, which resulted in different SWNT dispersion. The first solution was used to prepare three samples, which were aligned by applying an electric field of 300 V/mm for 30 min at 10 Hz, 100 Hz and 1 kHz. The second solution was used to prepare three samples, which were aligned by applying an electric field of 300 V/mm for 30 min at 1 kHz, 10 kHz and 25 kHz. ODF of each set of samples is developed separately. ODF of SWNT-acrylate samples aligned by applying 300 V/mm for 30 min at 10 Hz, 100 Hz and 1 kHz is shown in Figure 4.5, which indicates that SWNT alignment at 1 kHz is better than 100 Hz, which is better than 10 Hz. This is evidenced by the larger ODF value and by the narrow peak of the ODF centered at 0º. ODF of SWNT-acrylate samples aligned by applying 300 V/mm for 30 min at 1 kHz, 10 kHz and 25 kHz is shown in Figure 4.6, which indicates that SWNT alignment at 25 kHz is better than 10 kHz, which is better than 1 kHz. The evidence is again the larger ODF value and by the narrow peak of the ODF centered at 0º.

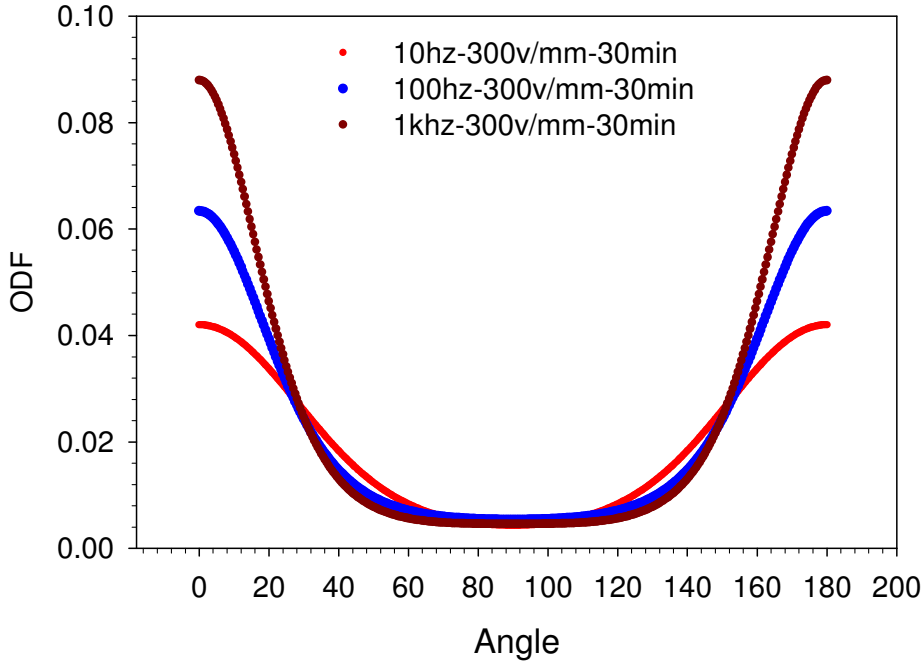

Figure 4.5. Orientation distribution function for SWNTs aligned at 300 V/mm, 30min at 10 Hz, 100 Hz and 1 kHz in acrylate polymer nanocomposite.

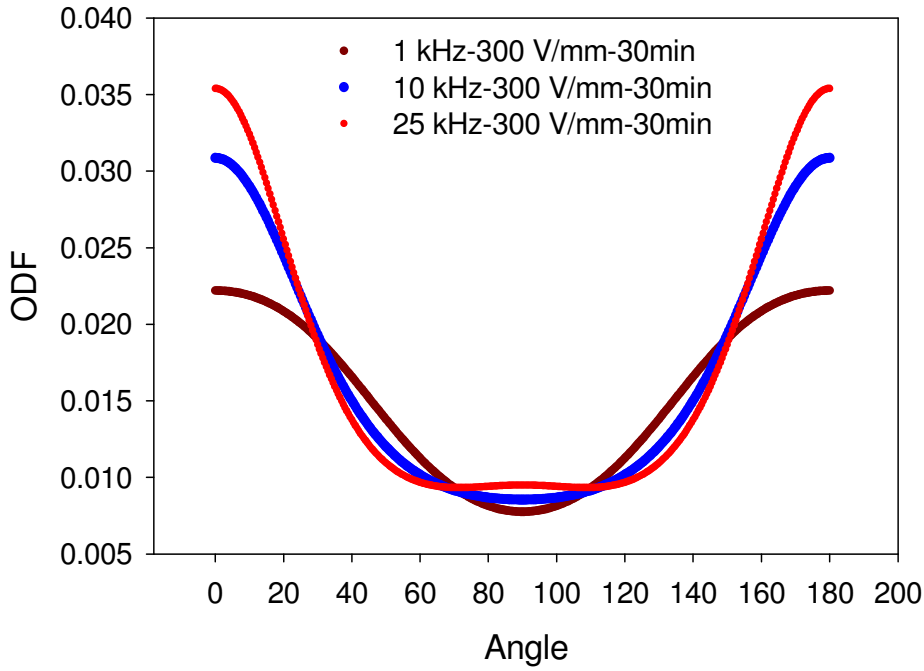

Figure 4.6. Orientation distribution function for SWNTs aligned at 300 V/mm, 30min at 1 kHz, 10 kHz and 25 kHz in acrylate polymer nanocomposite.

These results indicate that the degree of SWNT alignment is dependent on the alignment frequency. SWNT alignment increases as the frequency is increased from 10 Hz to 25 kHz. It is possible to further analyze the ODF data in Figure 4.5 and Figure 4.6 to quantify the probability of finding aligned SWNTs at different angles to the applied electric field. Figure shows the probability histogram per angle interval of 15^{o}. Results indicate that the probability of finding SWNTs in the 0^{o} to 15^{o} angle range increases from 10 Hz to 1 kHz (Figurea) and from 1 kHz to 25 kHz (Figureb). This signifies that more SWNTs are aligned at higher frequency (25 kHz) as compared to lower frequency (10 Hz).

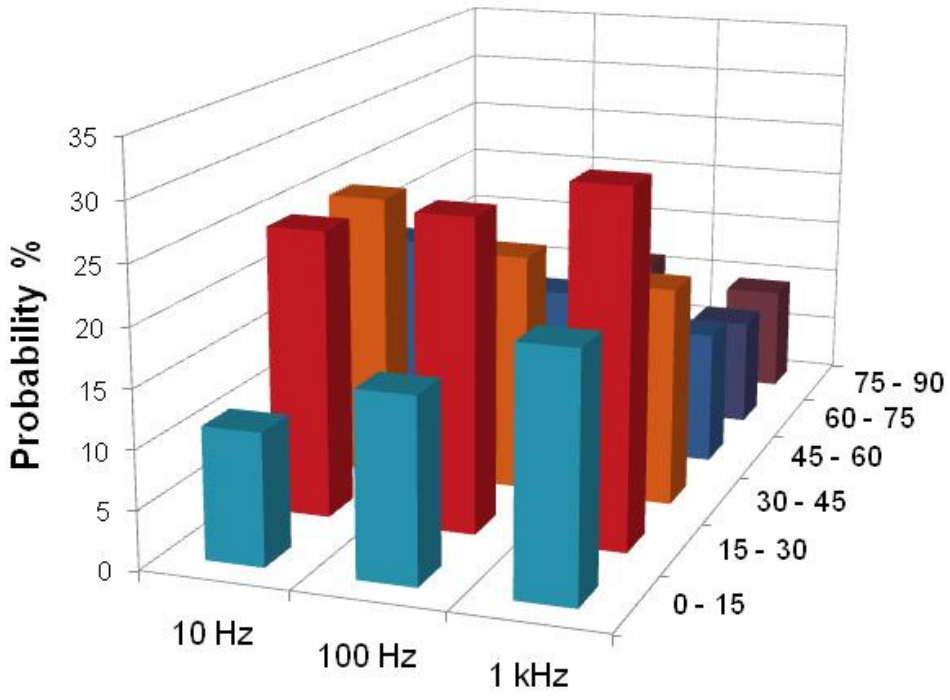

(a)

Figure 4.7. Histogram of probability from the ODF data (a) for 10 Hz, 100 Hz and 1 kHz case and (b) for 1 kHz, 10 kHz and 25 kHz case.

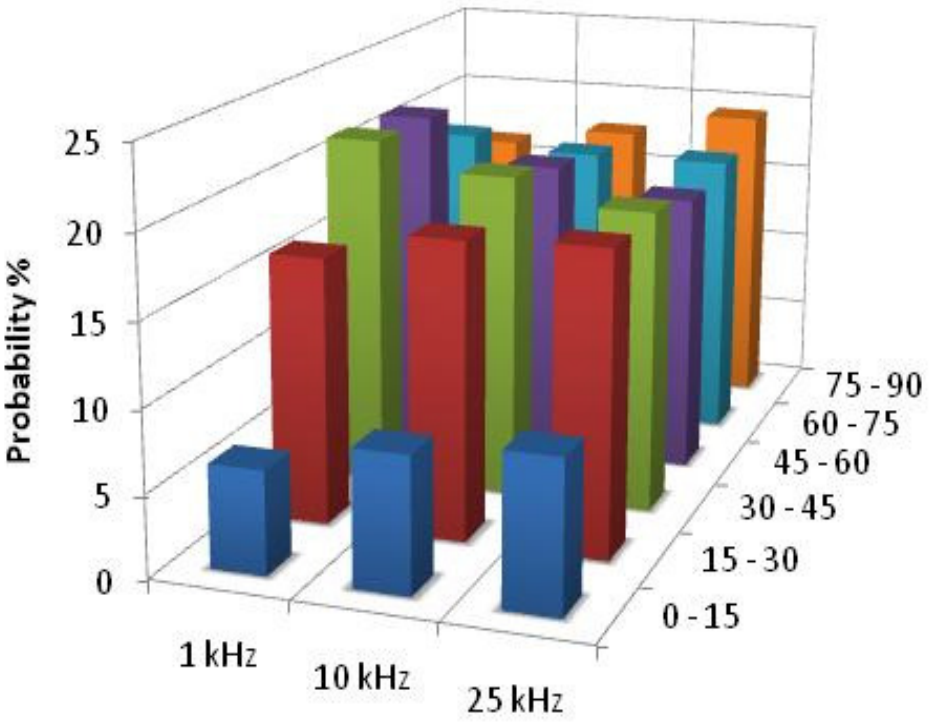

(b)

Figure 4.7. Continued.

4.1.2 Chaining of nanoparticles

Upon application of an electric field, both CNFs and SWNT bundles rotate and align in the direction of electric field. When 100 V/mm external electric field is applied to 0.03 wt% SWNT-acrylate polymer solution, SWNT bundles rotate in the direction of electric field. Figure 4.8a shows the microstructure before the electric field was applied here, SWNT bundles are random with no preferred orientation direction. Figure 4.8b and Figure 4.8c show the microstructure after applying an electric field magnitude of 100 V/mm at a frequency of 100 Hz and 25 kHz respectively for 30 minutes. Applying the

electric field up to 30 minutes showed no visible change in the microstructure in addition to rotation.

.

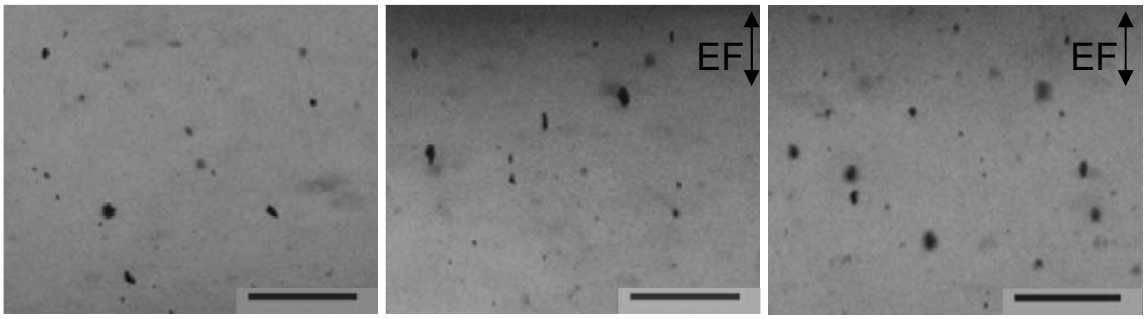

(a) (b) (c)

Figure 4.8. OM images of 0.03 wt% SWNT-acrylate polymer solution. (a) E=0, (b) 100 V/mm, 100 Hz, 30 minutes and (c) 100 V/mm, 25 kHz, 30 minutes. Scale bar in all the images is 100 μm.

Increasing the applied electric field to 300 V/mm, SWNT bundles rotate in the direction of applied electric field followed by attraction of SWNT bundles towards each other forming long chains in the direction of electric field and perpendicular to the electrodes. A summary of OM images are shown in Figure 4.9Figure 4. At frequencies between 1 Hz and 100 Hz, no visible chains are formed at 10 minutes. Very thin chains are formed at 20 minutes and 30 minutes. As the frequency is increased to 1 kHz, visible thin chains are formed at 10 minutes, which are very closely spaced. At the end of 20 minutes and 30 minutes the chains became thicker and the gap between the chains also increased. At higher frequencies of 10 kHz and 25 kHz, closely-spaced thin chains start to form immediately after the electric field is applied. After 10 minutes the chains become thicker and the distance between the chains also is increased. At the end of 30 minutes very thick and highly dense chains are formed, which are comprised of many thin

chains. In summary, the chain formation is dependent on electric field magnitude, frequency and duration. Further, chain thickness increased measurably as electric field duration is increased.

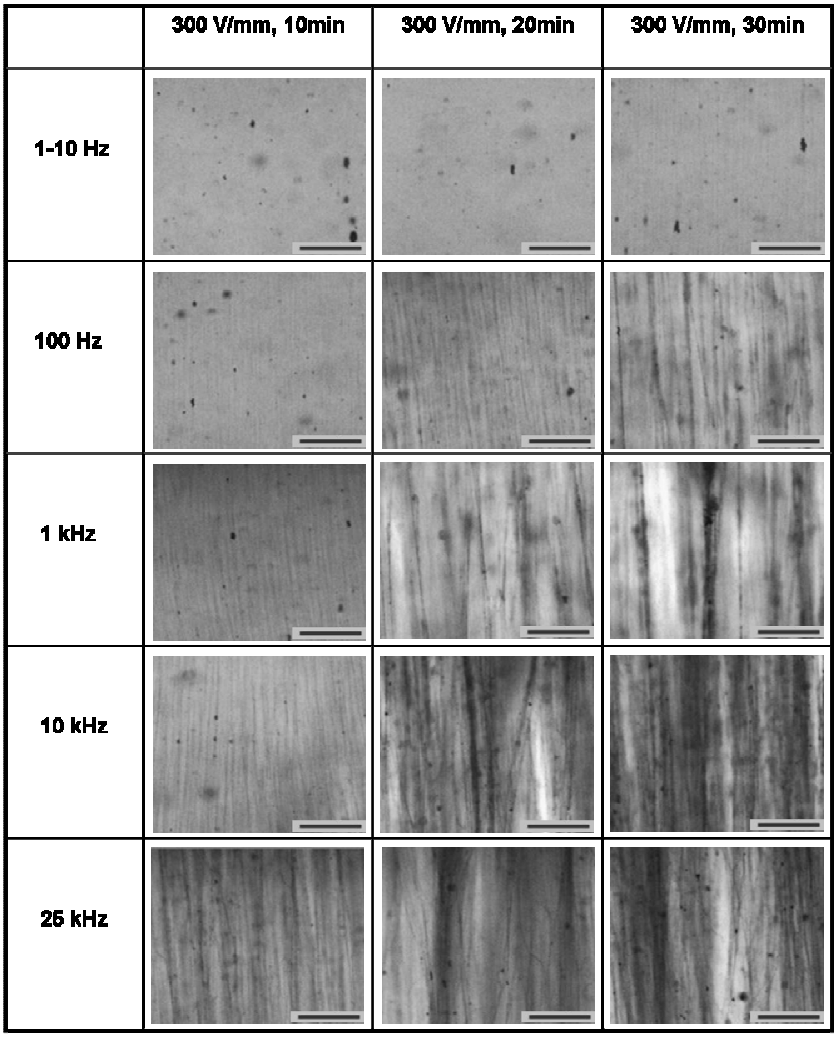

Figure 4.9. Optical microscopy images of 0.03 wt% SWNT-acrylate system at an applied electric field of 300 V/mm, different frequencies (1 Hz to 25 MHz) and different time intervals (0-30min).

To assess how long it takes for chains to achieve a steady state configuration an electric field of 300 V/mm at a frequency of 1 kHz is applied for a duration of 62 hours. The microstructure continuously changes with lateral interaction between the chains, as the duration of applied electric field increases, as shown in Figure 4.10. After 45 hours no

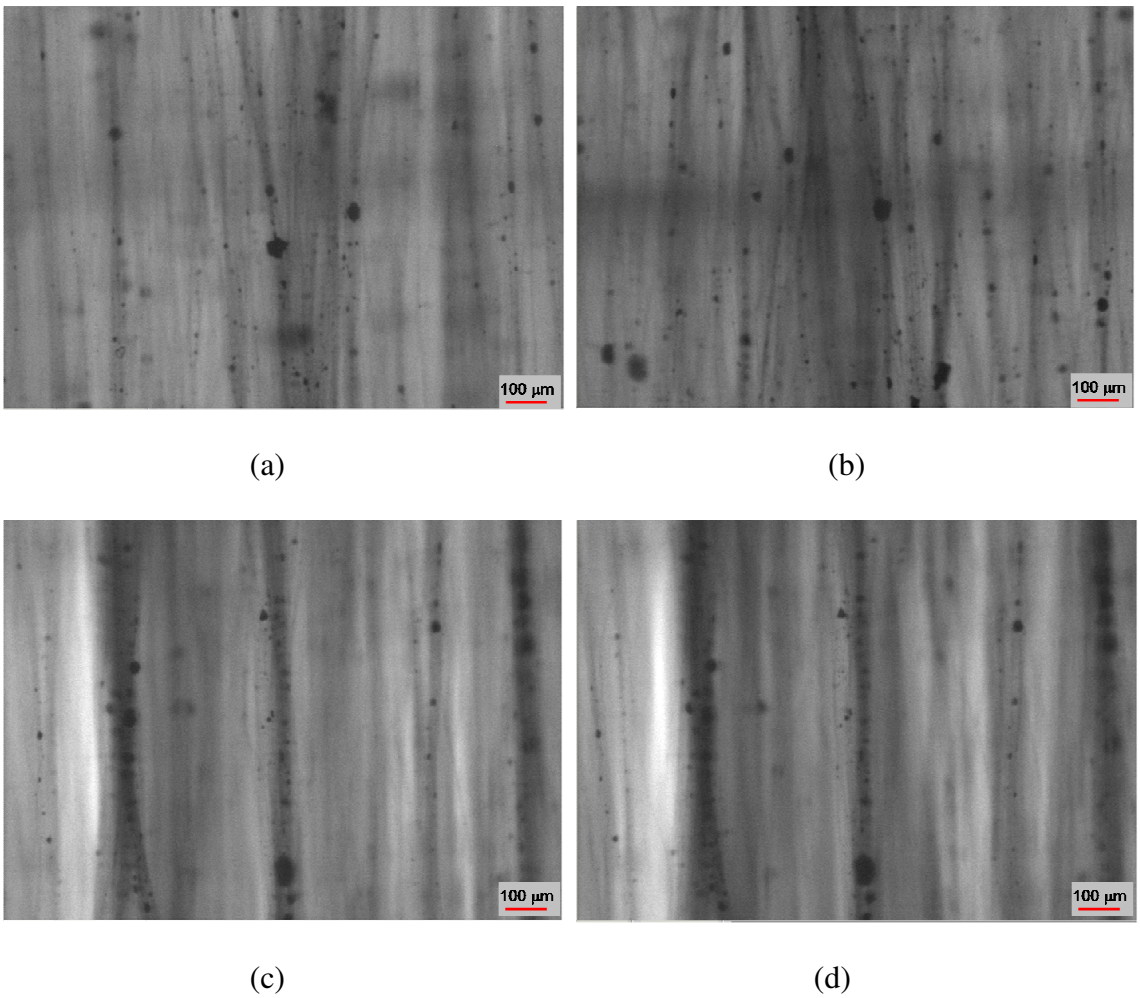

Figure 4.10. OMs images of electric field manipulated 0.03 wt% SWNT-acrylate polymer solution. Applied electric field was 300 V/mm at 1 kHz frequency for a duration of (a) 6 hours, (b) 15 hours, (c) 45 hours, and (d) 62 hours.

visible change in microstructure is observed up to 62 hours. This indicates that the system attains an equilibrium state with no change in microstructure after 45 hours at this field magnitude and frequency.

4.1.3 In-situ electrical conductivity and dielectric constant

Dielectric constant and electrical conductivity is measured in the liquid state after alignment of nanoparticles. These in-situ electrical measurements will quantify the alignment and also will determine the aligning conditions that will result in a significant increase in electrical properties. Figure 4.11**Figure 4**a and b show the electrical conductivity and dielectric constant of 0.03 wt% SWNT-acrylate polymer solution when an electric field of 300 V/mm, 10 Hz-25 kHz is applied for 10 minutes. Electrical conductivity for the random case (E=0) and the aligned cases (E≠0) shows frequency dependence as a function of the input measurement frequency (50 Hz to 10^6 Hz), as shown in Figure 4.11a. The value increases from 9.2×10^{-10} S/cm at low frequency (50 Hz) to 1.8×10^{-8} S/cm at the high frequency (10^6 Hz). Conductivity dependence on input measurement frequency indicates the solution is below the percolation threshold. E=0 (random case), the electrical conductivity value of the solution was 9×10^{-10} S/cm. There was no increase in the electrical conductivity after 10 minutes of applying an AC electric field of 300 V/mm, at 10 Hz, 100 Hz and 1 kHz. There was an increase in conductivity to 1.2×10^{-9} S/cm when the applied AC electric field frequency was 10 kHz and 25 kHz. Dielectric constant for the random case (E=0) and the aligned samples (E≠0) was fairly constant as a function of the input measurement frequency (50 Hz to 10^6 Hz), shown in

Figure 4.11**Figure 4**b. The dielectric constant at E≠0 was 22. There was no increase after 10 minutes of applying 10 Hz, 100 Hz and 1 kHz frequencies. An increase in dielectric constant to a value of 37 is seen when 10 kHz and 25 kHz frequencies were applied. To explain the absence of increase in values after applying 300 V/mm at 10 Hz, 100 Hz and 1 kHz, for 10 minutes, we need to inspect Figure 4.9. The Figure shows that at those conditions only rotation of SWNT bundles occurs and no visible chain form. This indicates that only rotation of SWNTs is not sufficient to increase the electrical conductivity and dielectric constant values. A small increase in electrical conductivity and dielectric constant is seen after applying 300 V/mm, at 10 kHz and 25 kHz for 10 minutes. At these conditions, Figure 4.9Figure 4 shows rotation of SWNT bundles and also thin chain formation. This indicates that the thin chains contribute to the small increase in electrical conductivity and dielectric constant. Electrical conductivity and dielectric constant after 30 minutes of applying AC electric field is shown in Figure 4.11c and Figure 4.11d respectively. Electrical conductivity was dependent on the input measurement frequency (50 Hz to 10^6 Hz) and there are two trends: random, 10 Hz, 100 Hz and 1 kHz conductivity is highly dependent on frequency. For example, for the random case, it increases from $4.4x10^{-10}$ S/cm at low frequency to $3.7x10^{-8}$ S/cm at high frequency. In contrast solutions aligned at 10 kHz and 25 kHz have conductivity values that do not sharply depend on frequency. For example, for 25 kHz case, it increases from $9x10^{-8}$ S/cm at low frequency to $6x10^{-7}$ S/cm at high frequency. The conductivity also increased from $4x10^{-10}$ S/cm to $9x10^{-8}$ S/cm as the electric field alignment frequency increased from 10 Hz to 25 kHz, which was two orders of magnitude increase. There

were two trends for dielectric constant: random, 10 Hz, 100 Hz and 1 kHz dielectric was fairly constant as a function of input measurement frequency. For example, for the random case, it was 14 at low frequency and 10 at high frequency. In contrast dielectric constant of solutions aligned at 10 kHz and 25 kHz were highly dependent on frequency. For

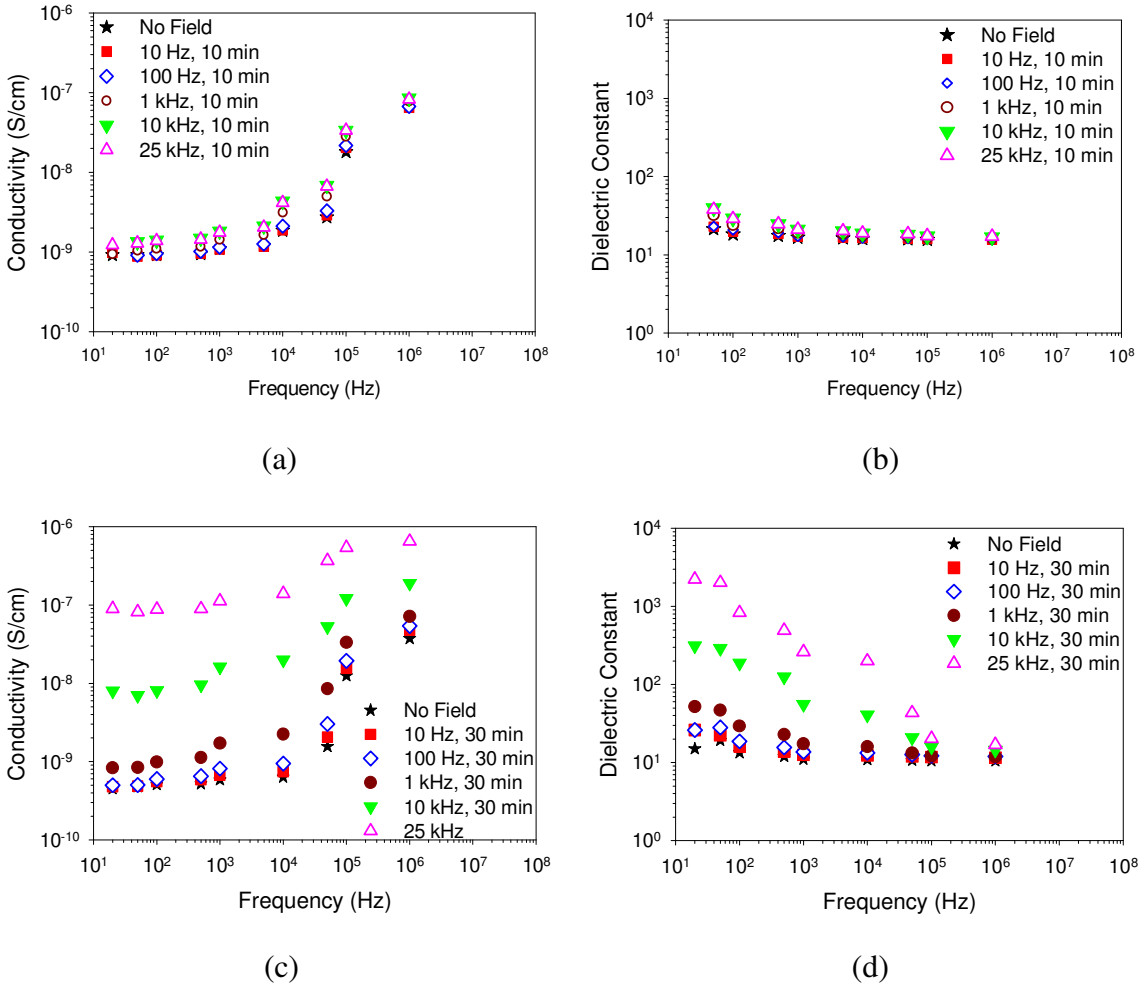

Figure 4.11. In-situ electrical conductivity and dielectric constant of 0.03 wt% SWNT-acrylate solution (before cure) as a function of input measurement frequency 50 Hz to 1 MHz. The applied AC electric field magnitude is 300 V/mm and the frequency is 10 Hz, 100 Hz, 1 kHz, 10 kHz and 25 kHz. (a) electrical conductivity and (b) dielectric constant after 10 minutes of applying the electric field, (c) electrical conductivity and (d) dielectric constant after 30 minutes of applying the electric field.

example, for the 25 kHz case, it decreased from 2300 at low frequency to 16 at high frequency, as shown in Figure 4.11**Figure 4**d. Dielectric constant also increased from 24 to 2300 as applied electric field frequency changed from 10 Hz to 25 kHz, which was an two orders of magnitude increase.

As seen in Figure 4.9, after 30 minutes of applying an AC electric field, the thickness of the chains increase as the AC electric field frequency is increased from 10 Hz to 25 kHz. At 25 kHz there are thick chains, which are ~70 μm, which result in increasing conductivity and dielectric constant by 2 orders. As seen in Figure 4.9, at low frequencies like 10 Hz and 100 Hz there are very thin chains, which are ~10 μm, which do not increase the conductivity and dielectric constant.

Figure 4.12a and b shows the dielectric constant and electrical conductivity respectively as a function of measurement frequency at different time intervals. Dielectric constant is fairly constant with frequency before the electric field is applied. This behavior starts to change once the electric field is applied, where dielectric constant decreases with increase in frequency (25 Hz to 1 MHz). Dielectric constant measured at 25 Hz in Figure 4.12a are compared next. When no electric field is applied, the dielectric constant is 25, which increases to 76 after 3 hours of applying the electric field and further increases to 448 after 6 hours. There is an increase as the duration of applied electric field increases due to the increase in chain formation as seen in Figure 4.10. After 15 hours dielectric

constant value is 4300, which increases to 5100 after 45 hours. After 45 hours there is no change in the dielectric constant, which remains at 5100 even after 62 hours. Again, this correlates to the no change in the microstructure as seen in Figure 4.10. Electrical conductivity increases with increase in frequency before the electric field is applied. This behavior starts to change once the electric field is applied for a longer time. At low frequencies electrical conductivity is fairly constant and increases at high frequencies (> 10 kHz). The following discussion concerns the electrical conductivity values measured at 25 Hz. When no electric field is applied electrical conductivity is in the order of 10^{-10} S/cm, which increases to 10^{-9} S/cm after 3 hours of applying the electric field and further increases to 10^{-8} S/cm after 6 hours. This increase as the duration of applied electric field increases is the result of the increase in chain formation as seen in Figure 4.10. After 15 hours electrical conductivity value is 10^{-6} S/cm, which does not change after 45 hours and 62 hours, as there is no change in the microstructure as seen in Figure 4.10. In addition to the OM images in Figure 4.10, these in-situ results confirm that an equilibrium state is obtained where the SWNT bundles stop interacting and there is no change in the microstructure when the alignment electrical field has been applied for 45 hours. These results indicate that a measurable contrast in the electrical conductivity and dielectric constant is observed only when the chained network reaches a certain dimension.

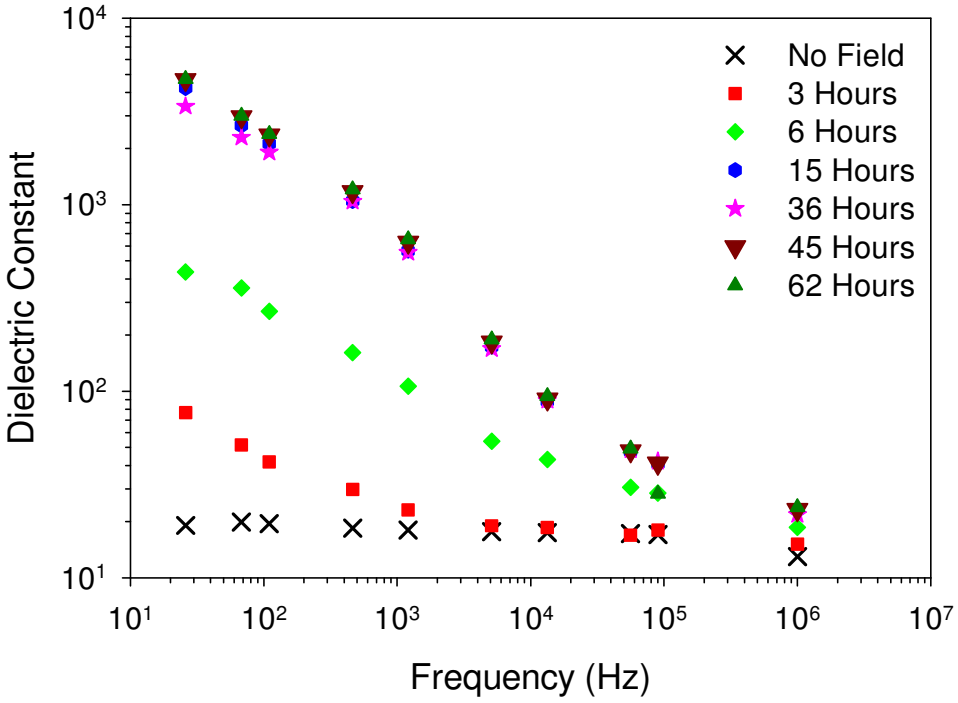

(a)

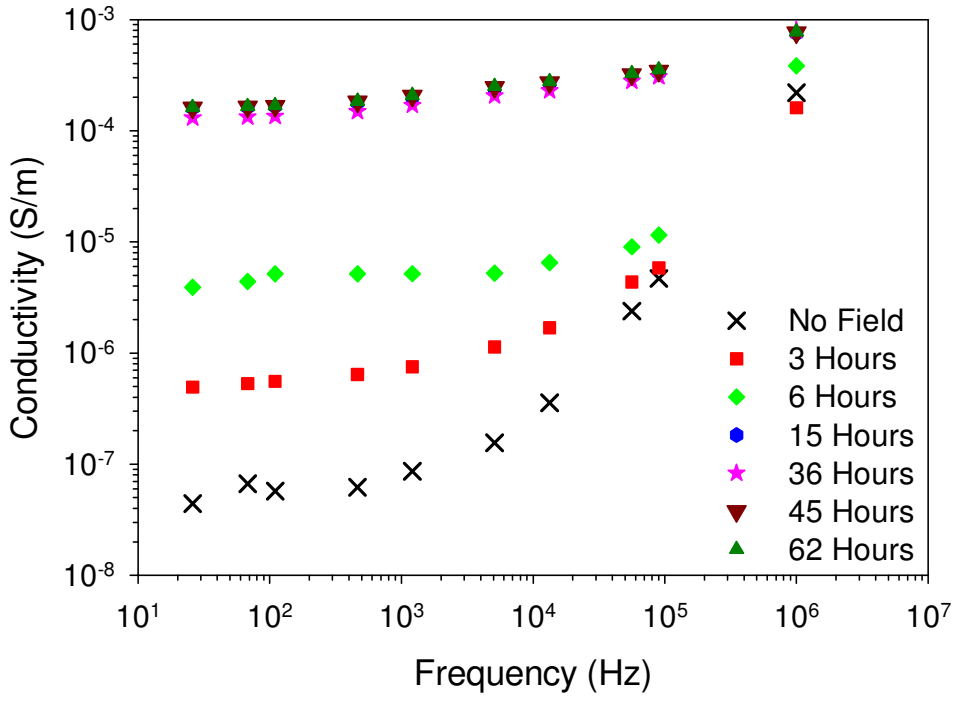

(b)

Figure 4.12. (a) In-situ dielectric constant and (b) in-situ electrical conductivity of 0.03 wt% SWNT-acrylate solution (before cure) as a function of input measurement frequency. AC electric field magnitude is 300 V/mm and the frequency is 1 kHz.

4.2 Discussion on rotation and chaining of nanoparticles

The different kind of forces acting on a particle dispersed in a fluid under an external electric field are summarized in Section 2.3. It is seen in Section 4.1 that alignment and chain formation of CNFs and SWNT bundles is dependent on electric field magnitude, frequency and time. A certain threshold voltage and frequency is required for the nanoparticles to form chains. In this section we discuss the possible forces that might be driving alignment and chain formation of CNFs and SWNT bundles under the influence of an external AC electric field.

4.2.1 Rotation of nanoparticles: Effect of electric field magnitude, frequency and time

Applying an electric field polarizes the anisotropic CNF and SWNT bundles, resulting in a torque acting on the CNF and SWNT bundles, aligning them in the direction of electric field as described in Section 2.3.2. Rotation is highly dependent on the magnitude of electric field and viscosity of the medium. Time for nanoparticle rotation is quicker at high electric field magnitude and in low viscosity medium. The electrical torque acting on the particle is counteracted by the viscous torque, which arises from the medium. The viscous torque is given by [126]:

$$\tau^{(v)} = 8\pi\eta V \frac{d\theta}{dt} \qquad 4.1$$

where η is the viscosity of the polymer medium, V is the volume of the particle and θ is the initial angle of the particle axis. The nanoparticle rotates and aligns in the direction

of electric field when the electrical torque overcomes the viscous torque. The time required to rotate the CNF or SWNT bundle in the direction of electric field is obtained by balancing the electrical torque and the viscous torque, $\tau^{(E)} + \tau^{(v)} = 0$. The time estimate for rotation of particle is given by

$$t = \frac{(3.2)\pi}{\varepsilon_m(\mathrm{Re}|\beta_{ll}| - \mathrm{Re}|\beta_{\perp}|)} \frac{\eta}{E^2} \qquad 4.2$$

which varies with angle θ (Equation 4.2 is for θ=89º).

Equation 4.2 is used to estimate the theoretical time for rotation of SWNT bundles. SWNTs are considered to behave as lossy dielectric particles. The electric field was applied at a frequency of *w*=10 Hz. The experimentally determined values are viscosity of the acrylate polymer solution, η= 1600 cP, permittivity of the acrylate polymer solution, $\varepsilon_m = 8.3\varepsilon_0$, and conductivity of the medium $\sigma_m=10^{-10}$ S/cm. A range of SWNT permittivity and conductivity have been reported in the literature, ranging from $5\varepsilon_0$ to $2000\varepsilon_0$ for the permittivity [111, 112, 135] and 10 S/cm to 10^6 S/cm for the electrical conductivity [136, 137]. The unknown variables are determined by using a least square method to fit the experimental data with Equation 3, as shown in Figure 4.13. Dielectric permittivity and electrical conductivity values of the SWNTs are obtained from the least square fit as $\varepsilon_p = 2053\varepsilon_0$, and conductivity of SWNTs as $\sigma_p=10^3$ S/cm, which are close to those reported in the literature.

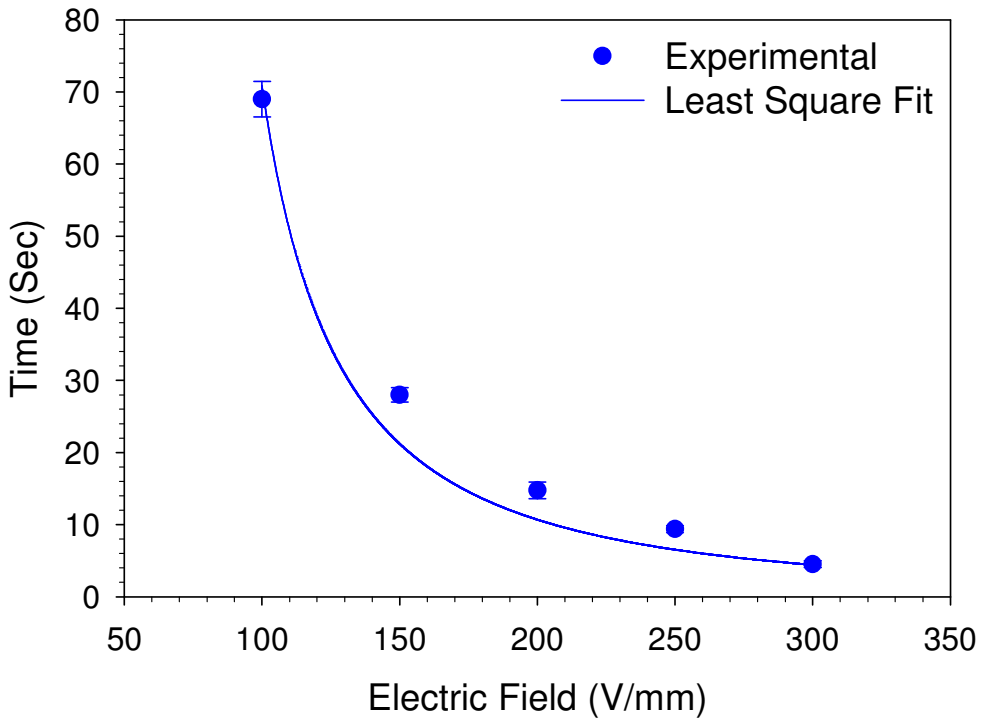

Figure 4.13. Time taken for a SWNT bundle to rotate in the direction of electric field in acrylate polymer solution as a function of applied electric field at a frequency of 10 Hz. Solid line is the least square fit with equation 4.2.

The SWNT alignment increases with increasing frequency as seen in Section 4.1.2. SWNT bundles were better aligned at high frequency of 25 kHz compared to low frequency of 10 Hz. Orientation and alignment of SWNTs is due to the torque acting on the bundles: a large torque results in better orientation of SWNTs. From the experiments, we can conclude that the torque acting on SWNT bundles at higher frequency is greater than the torque at low frequency, indicating an increase in torque with frequency. Inspection of equation 2.5 reveals that the frequency dependent term is $\left(\mathrm{Re}|\beta_{//}| - \mathrm{Re}|\beta_{\perp}|\right)$, which is comprised of dielectric permittivity and conductivity of the medium and SWNT. Dielectric permittivity and conductivity of the medium are

determined experimentally at low (10 Hz) and high (25 kHz) frequency. Dielectric permittivity and conductivity of SWNT at low frequency are determined from the rotation-time experiment, but these values are unknown at high frequency.

As the frequency increases, dielectric permittivity and conductivity increases, decreases or stays constant depending on the type of material, which can be an insulator, conductor or intermediate, such as a semiconductor. To find out the behavior of conductivity and dielectric constant with frequency, we take a look at the data from pure polymer (insulator) and polymer composite with different SWNT concentrations (semiconductor or conductor), as shown in Figure 4.14. Conductivity of an insulator increases with increase in frequency; this behavior changes as the material start to conduct, where it becomes fairly constant at low frequency and increases at high frequency. In the intermediate range, there is 0 to 1 order increase in conductivity from 10 Hz to 25 kHz. Dielectric constant of an insulator is fairly constant with increase in frequency, but decreases with increase in frequency as the material becomes conductive. There is 1 to 2 orders decrease in conductivity from 10 Hz to 25 kHz. We assume the dielectric permittivity of SWNT to reduce by 2 orders, from $2053\varepsilon_0$ at 10 Hz to $100\varepsilon_0$ at 25 kHz. Similarly we also assume the conductivity of SWNT to increase by 1 order, from 10^3 S/cm at 10 Hz to 10^4 S/cm at 25 kHz.

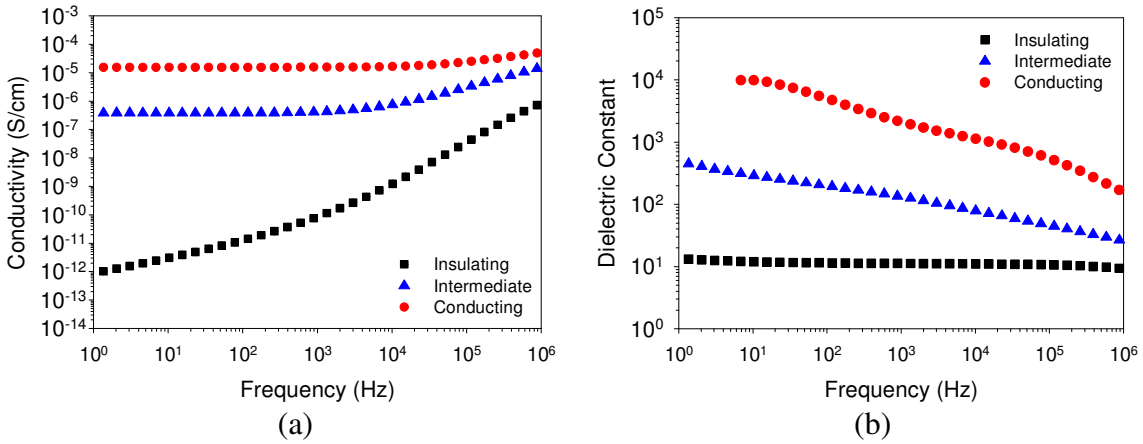

Figure 4.14. (a) Electrical conductivity and (b) dielectric constant behavior of insulating and conducting polymer nanocomposites as a function of frequency.

Torque was calculated at low (10Hz) and high (25 kHz) frequency from Equation 2.5 by considering the following input values. A SWNT bundle is considered to have a length of L = 5 μm, radius of 0.1 μm, applied electric field E = 300 V/mm, initial angle θ=89º. Figure 4.15 shows the torque as a function of frequency. There is a decrease in torque with increase in frequency, which is contrary to the experimental observation where there is an increase in torque with increase in frequency from 10 Hz to 25 kHz. We have done a sensitivity analysis of both dielectric permittivity and conductivity of SWNT on the value of torque, which shows that dielectric permittivity of SWNT does not have a major influence on variation of torque at different frequencies. SWNT conductivity plays a major role in varying the torque. Torque is calculated by increasing SWNT conductivity at 25 kHz from 10^7 S/cm to 10^{11} S/cm and SWNT conductivity at 10 Hz is kept constant at 10^5 S/cm, as shown in Figure 4.15. Torque acting on SWNT bundle increases when SWNT conductivity at 25 kHz is 10^{11} S/cm, as shown in Figure 4.15.

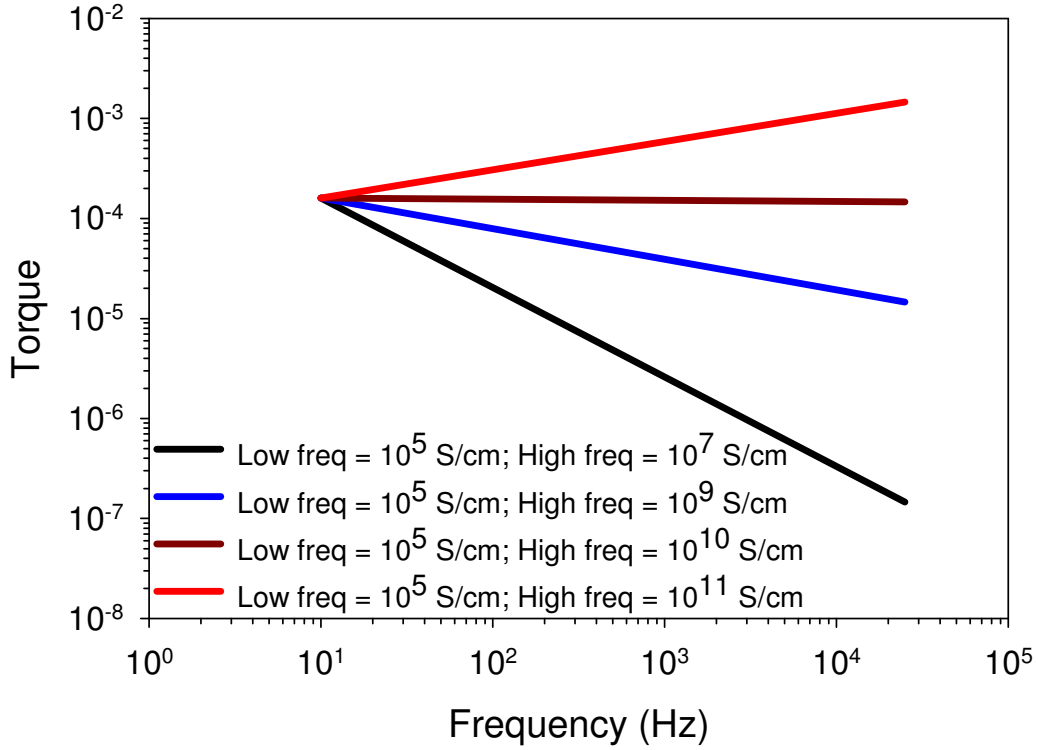

Figure 4.15. Torque on SWNT bundle as a function of frequency. SWNT conductivity at 25 kHz is varied from 10^7 S/cm to 10^{11} S/cm, which changes the behavior of torque with frequency.

Table 4.1 lists the dielectric permittivity and conductivity of SWNT and acrylate medium at low and high frequency obtained from the above analysis.

Table 4.1. Permittivity and conductivity of SWNT bundles and acrylate polymer solution at 10 Hz and 25 kHz.

	Permittivity of SWNT (ε_p)	Conductivity of SWNT (σ_p)	Permittivity of acrylate (ε_m)	Conductivity of acrylate (σ_m)
Low frequency (10 Hz)	$2053\varepsilon_0$	10^3 S/cm	$8.3\varepsilon_0$	10^{-10} S/cm
High frequency (25 kHz)	$100\varepsilon_0$	10^9 S/cm	$8.3\varepsilon_0$	10^{-9} S/cm

4.2.2 Chaining of nanoparticles

Increasing the applied electric field to 300 V/mm causes rotation and chaining of SWNTs in a 0.03 wt% SWNT-acrylate polymer solution. Figure 4.9 indicates, that the chain formation is frequency dependent and points to dielectrophoresis as a possible driving force for chain formation. Dielectrophoresis arises from the non uniform electric field. In this work, a uniform electric field is applied with parallel electrodes separated by a distance of 1 mm. The difference in the dielectric permittivity of SWNTs and acrylate polymer solution distorts the uniform electric field lines resulting in a local non uniform electric field, as shown in Figure 4.16 [127]. This results in a local gradient in the electric field, thus the SWNT bundles that behave as induced dipoles experience a DEP force. DEP force acts on the polarized SWNT bundles and due to their polarization the SWNT bundles are attracted to the regions of higher electric field intensity. This leads to chain formation also known as mutual dielectrophoresis [127, 138].

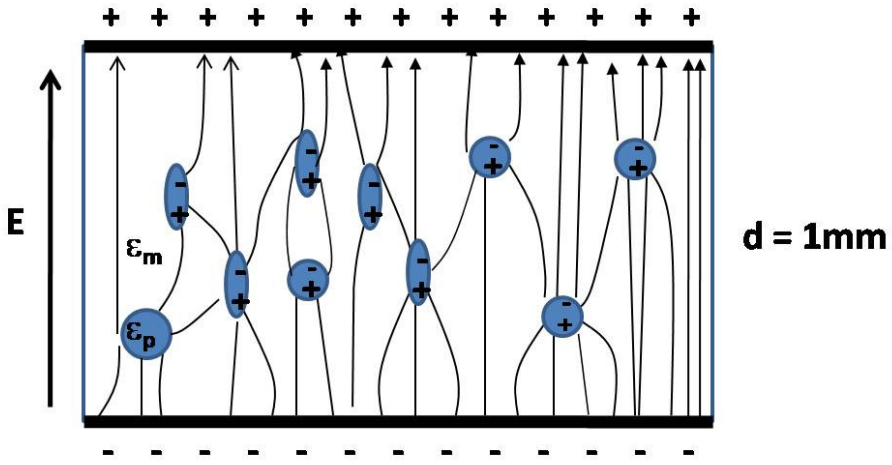

Figure 4.16. Distorted electric field lines due to the presence of particles.

As seen in Section 4.1.2 the chain formation was mainly dependent on three factors (a) electric field magnitude, (b) electric field frequency and (c) duration of electric field (time). DEP force is dependent on electric field as shown in Equation 2.2 and increasing electric field increases DEP force, thus resulting in thicker chain formation. The Clausius Mossoti factor is the only frequency dependent term in Equation 2.2 and this changes the DEP force as the frequency is varied. This value increases or decreases with frequency, depending on the conductivity and permittivity of the particle and medium [110], thus DEP force is also frequency dependent. Figure 4.17 shows the Clausius Mossoti factor as a function of frequency from 10 Hz to 25 kHz for a spherical SWNT bundle and an ellipsoidal SWNT bundle. From the previous sections, we established that the SWNT bundles act as lossy dielectric particles. Dielectric permittivity and conductivity of SWNTs and acrylate polymer are taken from Table 4.1. Clausius Mossoti factor of the spherical SWNT bundle does not change with frequency. For an ellipsoidal SWNT bundle, the Clausius Mossoti factor increases as the frequency increases from 10 Hz to 25 kHz, which implies the DEP force also increases. This explains the experimental results where we see thicker chain formation as the frequency increases from 10 Hz to 25 kHz. The change in microstructure with frequency is influenced by the ellipsoidal SWNT bundles, as the spherical SWNT bundles do not contribute to the change with frequency. DEP force is dependent on the size of the particle (Equation 2.2), the greater the size the greater the DEP force. When the electric field is applied, the particles are under the influence of dielectrophoresis and they attract towards each other, which results in increasing the initial particle size. As time increases,

the size of the particles continuously increases, resulting in an increase in DEP force. This explains the experimental results of thicker chain formation at longer durations of applied electric fields. Steady state is obtained when the chains are far apart from each other and DEP force no longer influences the SWNT bundles. This behavior is seen in the experiments (Figure 4.10) where there is no change in microstructure after applying the electric field for 45 hours.

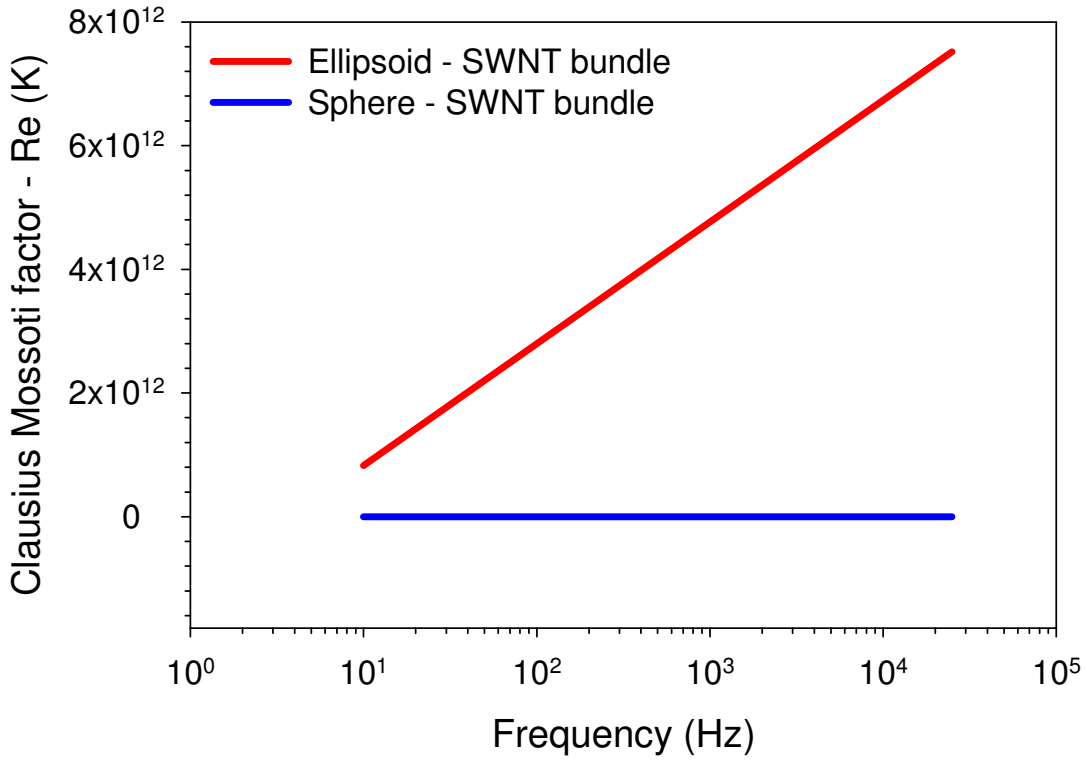

Figure 4.17. Clausius Mossoti factor of an ellipsoidal and spherical SWNT bundle in acrylate polymer as a function of frequency (10 Hz to 25 kHz).

We have seen that the dielectrophoretic force is dependent on volume of the particle, dielectric constant of the particle and medium; this indicates that changing the initial

state of dispersion, type of nanoparticle and type of medium will change the DEP force. The density of the chains formed in CNF-epoxy system are different from those formed for the SWNT-acrylate system. The dimension of CNFs in epoxy are much greater than the SWNTs in acrylate, which led to the formation of thicker chains. In the CNF-epoxy composite, alignment and chain formation was obtained by applying an electric field of 100 V/mm. Chain formation was not observed in the SWNT-acrylate polymer composite until a field of 300 V/mm. The optimum dielectrophoretic force to align and form chains is attained at a lower electric field due to the large CNF dimension.

5. PHYSICAL PROPERTIES OF ELECTRIC FIELD MANIPULATED POLYMER NANOCOMPOSITES

Parameters identified in the in-situ study were used to prepare solid aligned polymer nanocomposites; a summary on type of polymer nanocomposites and aligning conditions is shown in Figure 5.1. SWNT and CNF alignment was retained in the polymer composite after curing. Electrical conductivity, dielectric constant and storage modulus were measured parallel and perpendicular to the direction of applied electric field to assess the effect of AC electric field frequencies on alignment of SWNTs and CNFs.

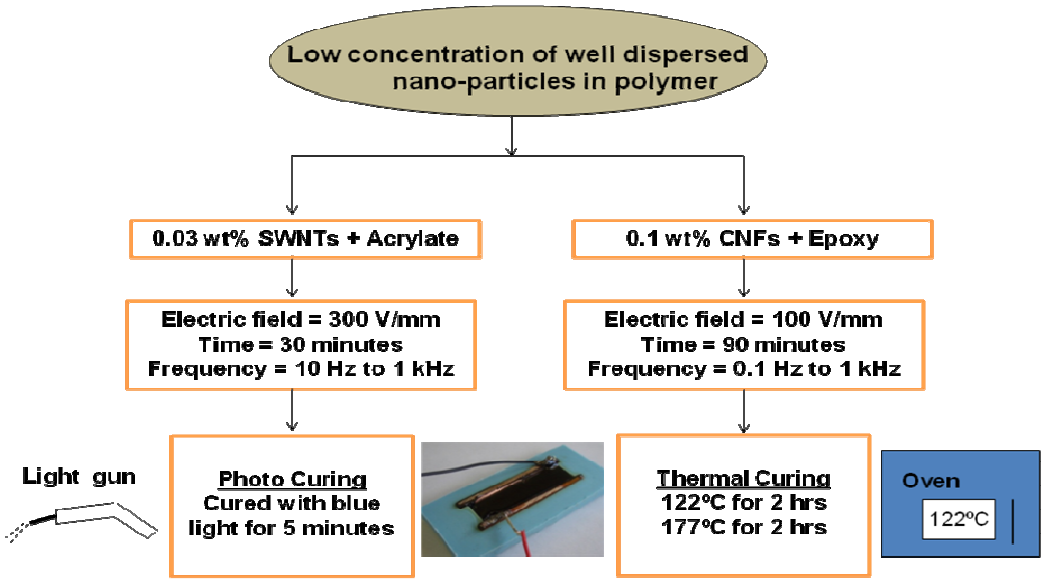

Figure 5.1. Summary on the types of polymer nanocomposites along with their aligning electric field conditions and curing conditions.

5.1 Electrical conductivity of electric field manipulated polymer nanocomposites

Electrical conductivity measured as a function of frequency can show three types of behaviors. One that is dependent on frequency, one is constant with frequency, and an intermediate behavior. Pure polymer is an insulator, with a low conductivity which increases as the measurement frequency is increased from 10^{-2} Hz to 10^{-7} Hz, see Figure 4.15 for trends. Electrical conductivity of a nanocomposite depends on the nanoparticle loading and dispersion. When the electrical conductivity increases by orders of magnitude with respect to that of pure polymer and is constant with frequency, the composite is above percolation.

5.1.1 SWNT-acrylate polymer nanocomposites

Electrical conductivity of electric field manipulated 0.03 wt% SWNT-acrylate polymer nanocomposites measured in parallel and perpendicular directions is shown in Figure 5.2a and b respectively. SWNT-acrylate nanocomposites are manipulated by applying an AC electric field of 300 V/mm for a duration of 30 minutes at 10 Hz, 100 Hz and 1 kHz frequency and were cured as described in Section 2.3.1. Conductivity of pure acrylate polymer is dependent on frequency, which is typical of insulators. When no electric field is applied the nanocomposite is termed as a random sample. The random sample also shows a large frequency dependence; its conductivity increases from 4.5×10^{-12} S/cm at a frequency of 0.01 Hz to a value of 1.8×10^{-6} S/cm at a frequency of 10^{6} Hz. Such frequency dependence is typical for nanocomposites below the percolation threshold where the conductivity remains strongly influenced by the polymer matrix properties. In

this case, the presence of the 0.03 wt% nanotubes is thus observed in Figure 5.2 to have increased the magnitude of the conductivity by three orders over the neat polymer value of 3×10^{-15} S/cm, but not to have altered the frequency dependence of the conductivity, therefore indicating that the nanocomposite remains an insulator. The nanocomposite samples processed under the 10 Hz electric field are observed to behave much like the random sample, having nearly equivalent conductivities in the parallel and perpendicular directions which are also nearly equal to the no field case at each measured frequency. This indicates that the changes in the microstructure introduced by processing under a 10 Hz electric field are not yet significant enough to be detected in macroscale conductivity measurements. In contrast, the nanocomposites processed under a 100 Hz electric field are observed to have differing electrical conductivity behavior in the parallel direction compared to the perpendicular. In the parallel direction, the measurements at low frequency are observed to have increased relative to the random sample by an order of magnitude, while in the perpendicular direction, the electrical conductivity remained unchanged relative to the random sample. Parallel conductivity of the nanocomposite processed at 1 kHz increased by three orders at low frequency relative to the random sample, with no change in perpendicular conductivity. As the concentration of nanotubes has not changed, this indicates that the microstructure consists of a sufficient quantity of aligned nanotubes so as to affect the macroscale conductivity, resulting in anisotropic nanocomposite conductivity. The results are consistent with the OMs shown in Figure ; processing the nanocomposites under a 1 kHz electric field results in larger quantities of

aligned SWNT bundles forming longer, thicker chains compared to nanocomposites processed under a 10 Hz or 100 Hz.

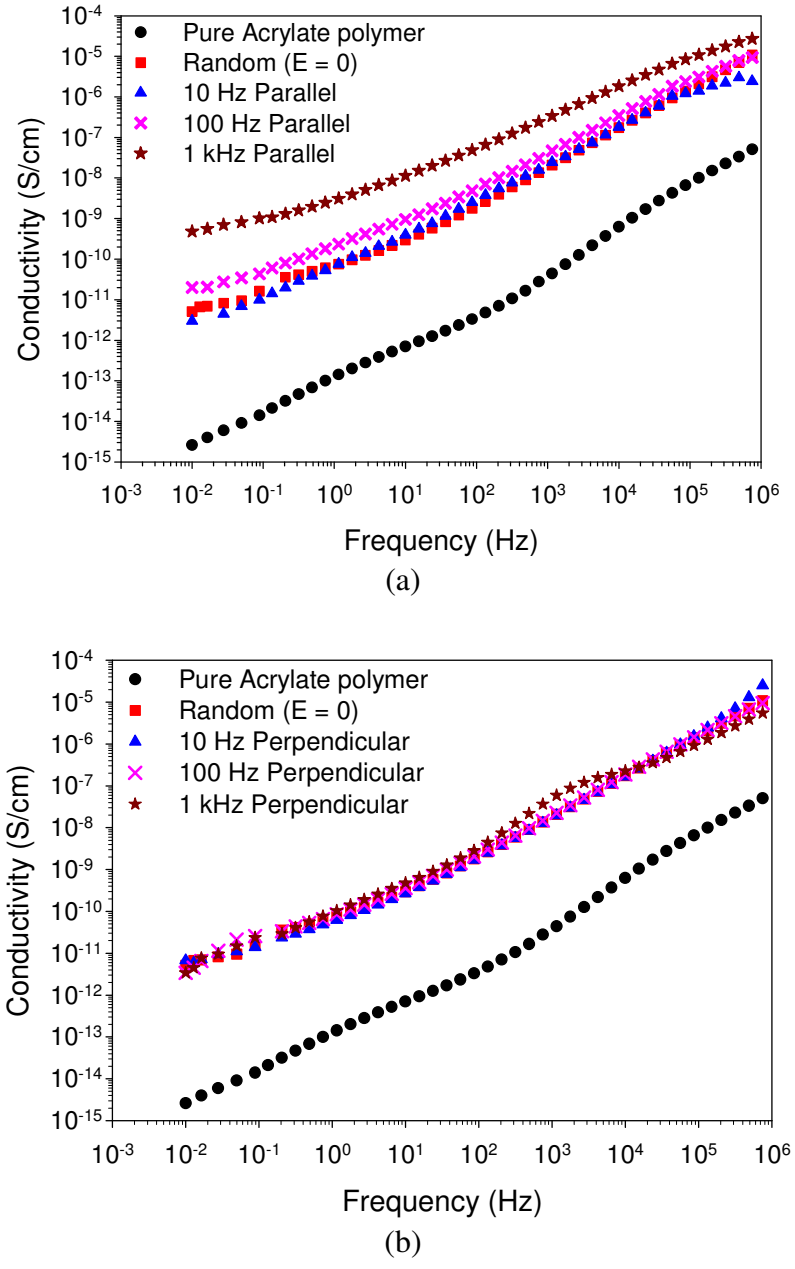

Figure 5.2. Electrical conductivity of electric field manipulated 0.03 wt% SWNT-acrylate polymer nanocomposite as a function of frequency (a) parallel and (b) perpendicular to the electric field. Applied AC electric field was 300 V/mm, which was applied for 30 min.

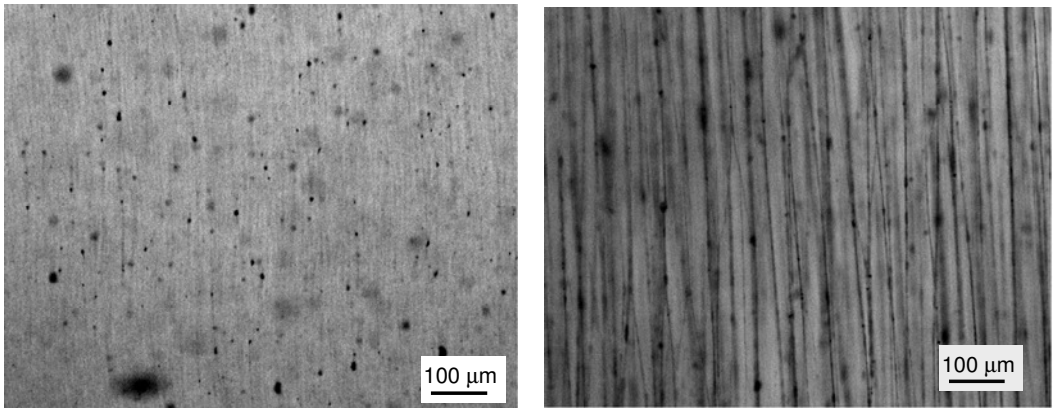

(a) (b)

Figure 5.3. OM images of electric field manipulated SWNT-acrylate polymer nanocomposites. Applied electric field E = 300 V/mm, t = 30 minutes, frequency of (a) 100 Hz and (b) 1 kHz.

The behavior of electric field manipulated 0.03 wt% SWNT-acrylate nanocomposites is below percolation. There is a percolation transition that starts to occur in the parallel direction for the nanocomposite processed at 1 kHz electric field. Thicker chains in the microstructure are required to further increase conductivity, which can be attained by either increasing the applied electric field or by increasing the SWNT concentration. In this study we were limited by the voltage and frequency that could be amplified using the Trek voltage amplifier. We were also limited by the SWNT concentration in acrylate polymer system as concentrations greater than 0.03 wt% could not be cured with blue light.

5.1.2 CNF-epoxy polymer nanocomposites

Electrical conductivity of electric field manipulated CNF-epoxy nanocomposite measured in parallel and perpendicular directions is shown in Figure 5.4a and b, respectively. CNF-epoxy nanocomposites are manipulated by applying an AC electric field of 100 V/mm for a duration of 90 minutes at 0.1 Hz, 1 Hz, 10 Hz, 100 Hz, 500 Hz and 1 kHz frequency and were processed as described in Section 2.3.1. Upon measuring the electrical conductivity for these cases, the following observations are made. The pure epoxy sample shows a large frequency dependence where its conductivity increases from 10^{-16} S/cm at a frequency of 0.01 Hz to a value of 10^{-7} S/cm at a frequency of 10^{6} Hz, as shown in Figure 5.4. The random sample with 0.1 wt% CNFs also shows large frequency dependence, its conductivity increases from 10^{-15} S/cm at a frequency of 0.01 Hz to a value of 10^{-7} S/cm at a frequency of 10^{6} Hz. In this case the presence of 0.1 wt% CNFs increases the electrical conductivity by one order over the pure epoxy but does not alter the frequency dependence of the conductivity and therefore indicates that the nanocomposite remains an insulator.

The electrical conductivity in the parallel direction increases when processed under a 0.1 Hz electric field where its conductivity increases from 10^{-12} S/cm at low frequency (0.01 Hz) to 10^{-7} S/cm at high frequency (10^{6} Hz). There is a three orders increase in conductivity with reference to the random sample but the nanocomposite still behaves as an insulator. There is a further increase in electrical conductivity in the parallel direction when processed under a 1 Hz electric field. Its conductivity is 10^{-10} S/cm at low

frequency and there is also a change in behavior with frequency. Conductivity increases from 10^{-10} S/cm at 0.01 Hz to 10^{-7} S/cm at 10^{6} Hz but it is fairly constant up to 100 Hz before it starts to increase. The change in nanocomposite behavior indicates a percolation transition in the parallel direction when processed at 1 Hz electric field. There is a nine orders increase in parallel conductivity of the nanocomposite when processed at 10 Hz electric field. Its conductivity is not dependent on frequency and is 10^{-6} S/cm at both 0.01 Hz and 10^{6} Hz. This behavior indicates the nanocomposite is above percolation and behaves as a conductor in the parallel direction when processed at 10 Hz electric field. There is a further increase in the parallel conductivity value when the nanocomposite is processed at 100 Hz, 500 Hz and 1 kHz, while its behavior reamians constant with frequency. Parallel conductivity of nanocomposites processed at 1 kHz is 10^{-5} S/cm at 0.01 Hz and 10^{6} Hz. Electrical conductivity in the perpendicular direction increases by two orders with respect to the random sample when processed under a 0.1 Hz electric field. Its behavior is dependent on frequency and increases from 10^{-13} S/cm at low frequency (0.01 Hz) to 10^{-7} S/cm at high frequency (10^{6} Hz), as shown in Figure 5.4b (i.e., nancomposite behaves as an insulator). This system shows similar behavior when processed at 1 Hz electric field. There is three orders increase in conductivity in the perpendicular direction with reference to the random sample when processed at 10 Hz electric field, but the composite still behaves as an insulator. There is a further increase in perpendicular electrical conductivity by eight orders when the nanocomposites are processed at 100 Hz, 500 Hz and 1 kHz electric field. Conductivity is 10^{-7} S/cm at 0.001 Hz and it increases to 10^{-6} S/cm at 10^{6} Hz. Conductivity is constant

at 10^{-7} S/cm up to 10 kHz and then increases at higher frequency. This behavior indicates that the nanocomposite is in the percolation transition. In summary, processing the nanocomposites at low frequency (0.1 Hz and 10 Hz) resulted in increasing the conductivity, but the CNF network formation was not sufficient to achieve percolation. Increasing the frequency to 10 Hz and higher resulted in an improved CNF network, thus achieving percolation in the direction of alignment, although keeping the CNF concentration constant.

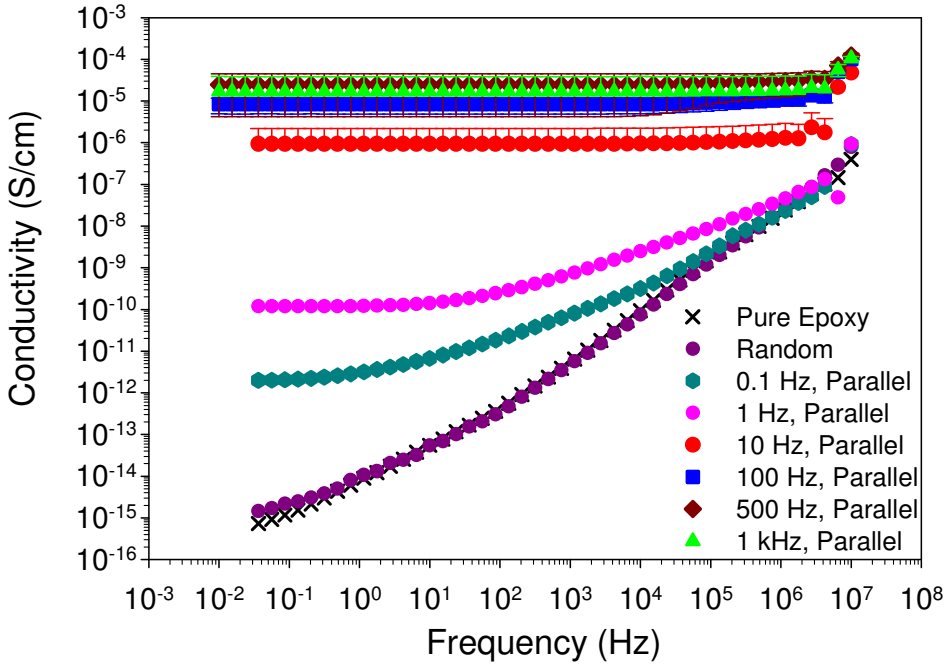

(a)

Figure 5.4. Electrical conductivity of electric field manipulated 0.1 wt% CNF-epoxy polymer nanocomposite as a function of frequency (a) parallel and (b) perpendicular to the electric field. Applied AC electric field was 100 V/mm, which was applied for 90 min.

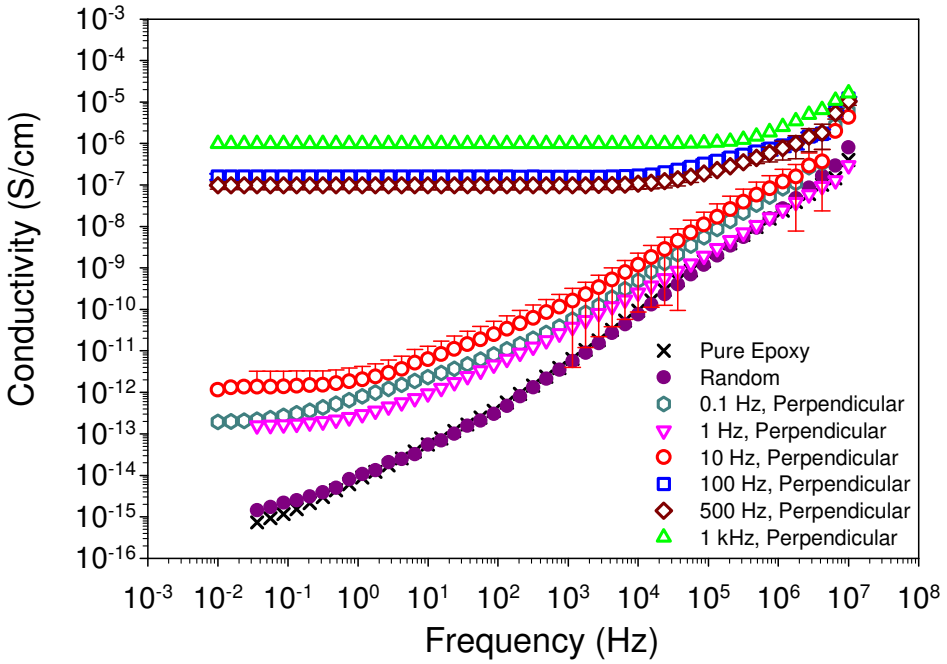

(b)

Figure 5.4. Continued.

These results show that anisotropy in conductivity is dependent on electric field frequency. Degree of anisotropy is measured by dividing parallel conductivity by perpendicular conductivity measured at 0.01 Hz.

$$\text{Anisotropy} = \frac{\sigma_{Parallel}}{\sigma_{Perpendicular}} \qquad 5.1$$

Anisotropy of the nanocomposite processed at 0.1 Hz is 10, which increases to 1000 when processed at 1 Hz electric field. These two nanocomposites behave as insulators in both parallel and perpendicular directions. Anisotropy further increases to 10^6 when the nanocomposite is processed at 10 Hz electric field. This nanocomposite behaves as a conductor in the parallel direction and as an insulator in the perpendicular direction.

Anisotropy decreases to 100 when the nanocomposite is processed at 100 Hz, 500 Hz and 1 kHz electric field. Both these nanocomposites behave as conductors in parallel and perpendicular directions. Parallel and perpendicular electrical conductivity measured at 0.01 Hz is plotted as a function of electric field frequency in Figure 5.5. This data clearly shows anisotropy at different electric field frequencies. This indicates that, depending on the required electrical conductivity, CNF-epoxy nanocomposite can be tailored by applying an AC electric field. The percolation threshold can also be controlled; a composite that is below percolation can be manipulated by applying an AC electric field to achieve percolation. Electric field frequency can also be used to produce unidirectional composites, with large electrical properties in the longitudinal direction of the composite.

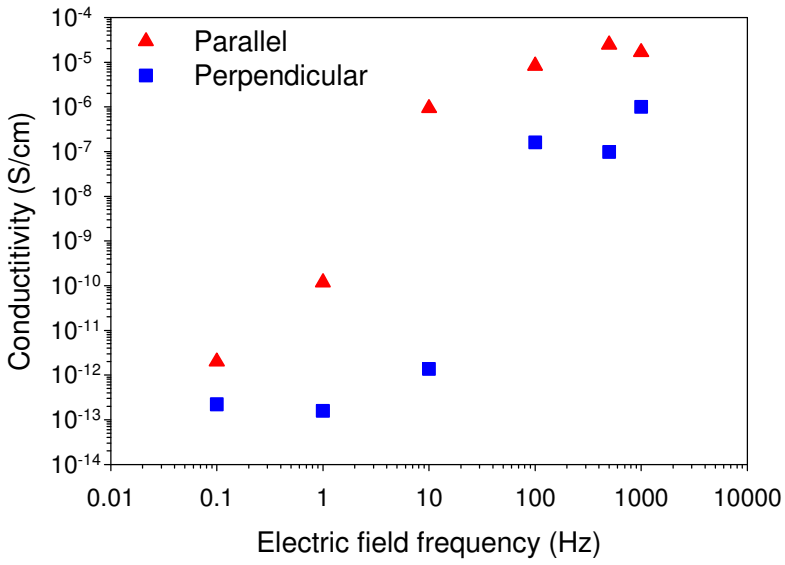

Figure 5.5. Electrical conductivity in the parallel and perpendicular direction of electric field manipulated 0.1 wt% CNF-epoxy polymer nanocomposite measured at 0.01 Hz. Electrical conductivity is plotted as a function of electric field frequency starting from 0.1 Hz to 1 kHz. Magnitude of the AC electric field was 100 V/mm, which was applied for 90 minutes.

Electrical conductivity results are consistent with the digital images and OM images shown in Figure 5.6 and Figure 5.7. A CNF-epoxy nanocomposite manipulated with a 10 Hz electric field shows the CNF network in Figure 5.6a. There are two types of chains, thick chains and thin chains. All the chains are vertical and thick chains are separated by thin chains. Figure 5.6b also shows vertical chains. This type of network resulted in a greater conductivity in the parallel direction compared to the perpendicular direction resulting in a maximum anisotropy. Figure 5.7a shows CNF network in CNF-epoxy nanocomposites manipulated at 1 kHz electric field. There are very thick chains that are interconnected and Figure 5.7b also shows that there is a network that is formed laterally. This type of network resulted in increasing the conductivity in both parallel and perpendicular directions resulting in minimum anisotropy.

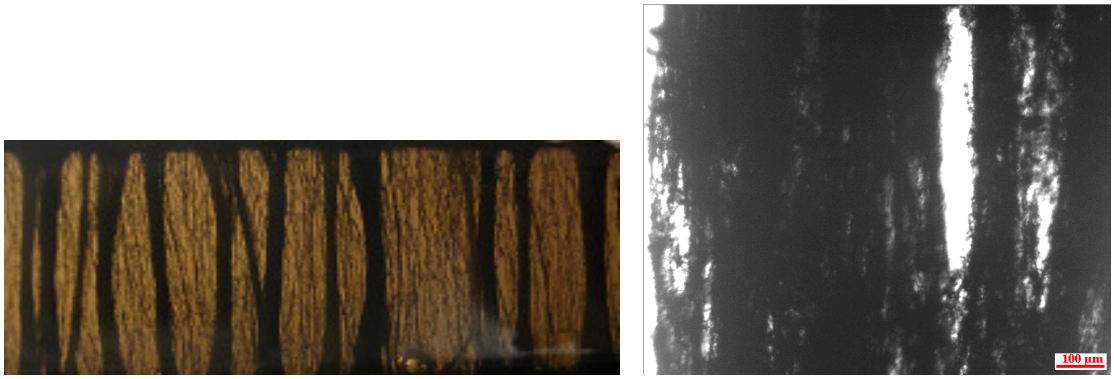

(a) (b)

Figure 5.6. Electric field manipulated 0.1 wt% CNF-epoxy nanocomposite at 10 Hz electric field. (a) digital image and (b) OM at 10x magnification.

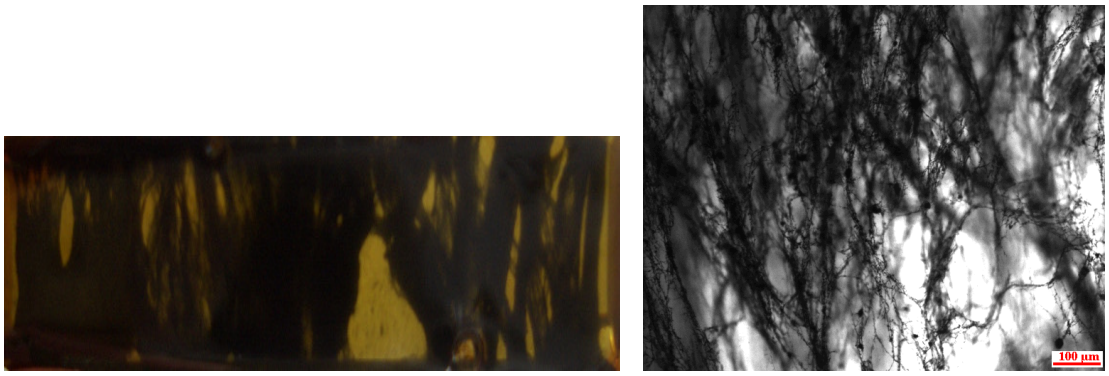

(a) (b)

Figure 5.7. Electric field manipulated 0.1 wt% CNF-epoxy nanocomposite at 1 kHz electric field. (a) digital image and (b) OM at 10x magnification.

The previous results demonstrate that electric field can manipulate the percolation threshold of nanocomposites. In Section 3.2.2, electrical conductivity of CNF-epoxy nanocomposites is measured at different CNF concentrations. 1 wt% CNF-epoxy nanocomposites is below percolation and behaves as an insulator. There is a percolation transition at 1.5 wt% CNF loading and CNF-epoxy nanocomposite is above percolation at CNF loadings that are greater than 2 wt%. Relatively large quantities of CNFs are required to reach percolation, making dispersion a challenge where large CNF agglomerates can occur at these high concentrations. We have seen that electric field manipulated CNF-epoxy nanocomposites can achieve percolation with constant CNF loading that is as low as 0.1 wt% where this percolation is reached by varying the alignment electric field frequency.

5.2 Dielectric constant of electric field manipulated nanocomposites

5.2.1 SWNT-acrylate nanocomposite

Parallel and perpendicular dielectric constant as a function of frequency is shown in Figure 5.8a and b respectively. SWNT-acrylate nanocomposites are manipulated by applying an AC electric field of 300 V/mm for duration of 30 minutes at 10 Hz, 100 Hz and 1 kHz frequency and were processed as described in Section 2.3.1. The random sample has a dielectric constant value that is constant with frequency (dielectric constant is 15 at 0.01 Hz). The parallel dielectric constant of the acrylate nanocomposite subjected to 10 Hz electric field is 45 at 0.01 Hz, which is an increase with respect to the random sample. There is a further increase in dielectric constant to 64 when processed at 100 Hz electric field. There is no change in behavior of the dielectric constant; although the value increases, the trend remains fairly constant with frequency. There is a significant jump in dielectric constant to 390 at 0.01 Hz when processed at 1 kHz electric field. There is also a change in behavior, where the dielectric constant decreases with increase in frequency, indicating a percolation transition. The increase in dielectric constant is due to the SWNT chains that are formed and as the thickness of the chains increase the dielectric constant is influenced by the SWNT bundles. There are thicker chains at 1 kHz compared to 10 Hz, which results in a large increase in dielectric constant. There is no change in perpendicular dielectric constant for electric field manipulated polymer nanocomposites in reference to the random sample. The perpendicular dielectric constant for the random sample, 10Hz, 100Hz and 1 kHz show similar behavior (i.e., constant dielectric constant with measurement frequency

indicating insulating behavior). Dielectric constant is dominated by the polymer matrix in the perpendicular direction due to the absence of a SWNT network. Parallel dielectric constant is greater than perpendicular dielectric constant and anisotropy in dielectric constant increases as the electric field frequency for manipulating acrylate nanocomposites increases from 10 Hz to 1 kHz.

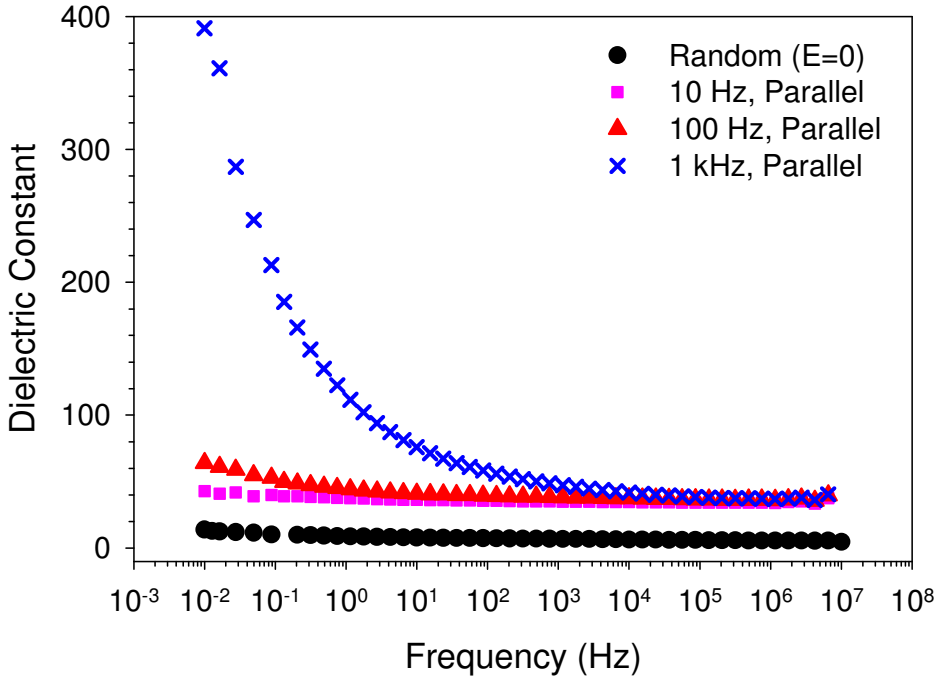

(a)

Figure 5.8. Dielectric constant of electric field manipulated 0.03 wt% SWNT-acrylate polymer nanocomposite as a function of frequency (a) parallel and (b) perpendicular to the electric field. Applied AC electric field was 300 V/mm, which was applied for 30 min.

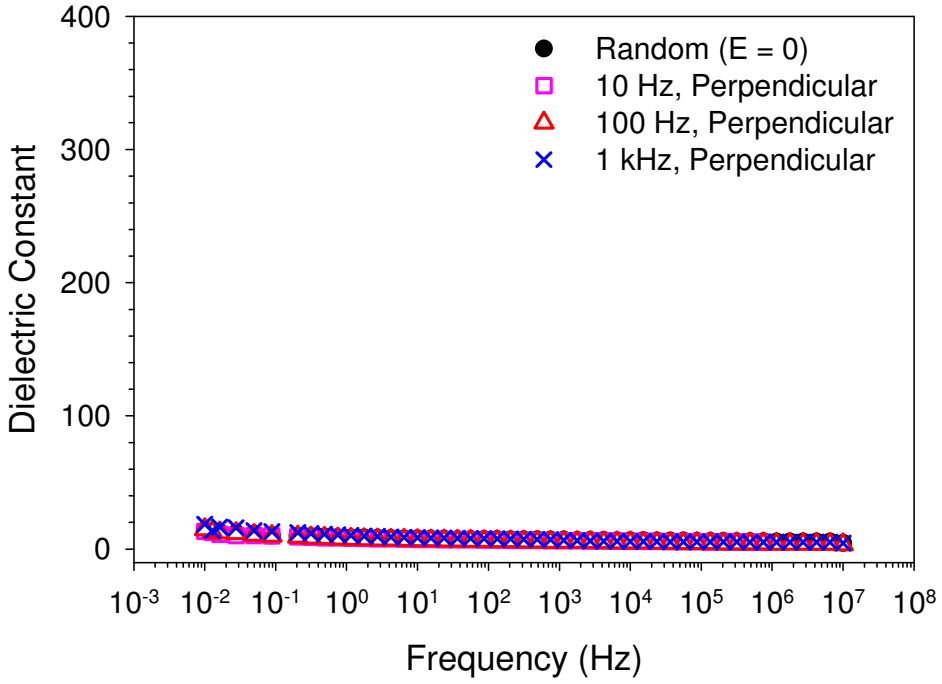

(b)

Figure 5.8. Continued.

5.2.2 CNF-epoxy nanocomposite

Dielectric constant of electric field manipulated CNF-epoxy nanocomposite measured in parallel and perpendicular directions is shown in Figure 5.9a and b respectively. CNF-epoxy nanocomposites are manipulated by applying an AC electric field of 100 V/mm for a duration of 90 minutes at 0.1 Hz, 1 Hz, 10 Hz, 100 Hz, 500 Hz and 1 kHz and were processed as described in Section 2.3.1. The dielectric constant of pure epoxy was 6 and there was no change in this value by the addition of 0.1 wt% CNFs, which was also constant with frequency. For the electric field manipulated 0.1 wt% CNF-epoxy nanocomposites the dielectric constant increased. Parallel dielectric constant for nanocomposites subjected to 0.1 Hz and 1 Hz electric field is 43 and 90 respectively

measured at 0.01 Hz, which decreased with increase in frequency. Dielectric constant decreased from 91 at 0.01 Hz to 15 at 10^6 Hz for the nanocomposite processed at 1 Hz electric field. For the nanocomposites processed at 100 Hz, 500 Hz and 1 kHz frequency the dielectric constant could not be measured below 100 Hz frequency, as the nanocomposite was very conductive with high dielectric losses. In the perpendicular direction there was a very small increase in dielectric constant. Perpendicular dielectric constant was between 15 and 18 at 0.01 Hz for the nanocomposites processed at 0.1 Hz, 1 Hz and 10 Hz electric field. Figure 5.10 shows comparison between parallel and perpendicular dielectric constants measured at 10^3 Hz as a function of electric field manipulated frequency of 0.1 Hz, 1 Hz, 10 Hz, 100 Hz, 500 Hz and 1 kHz. Parallel dielectric constant increases with increase in electric field frequency but perpendicular dielectric constant does not change with electric field frequency. In the parallel direction the CNF chains contribute to the increase in dielectric constant, but in the perpendicular direction the dielectric constant is influenced by the polymer resulting in a small increase in dielectric constant.

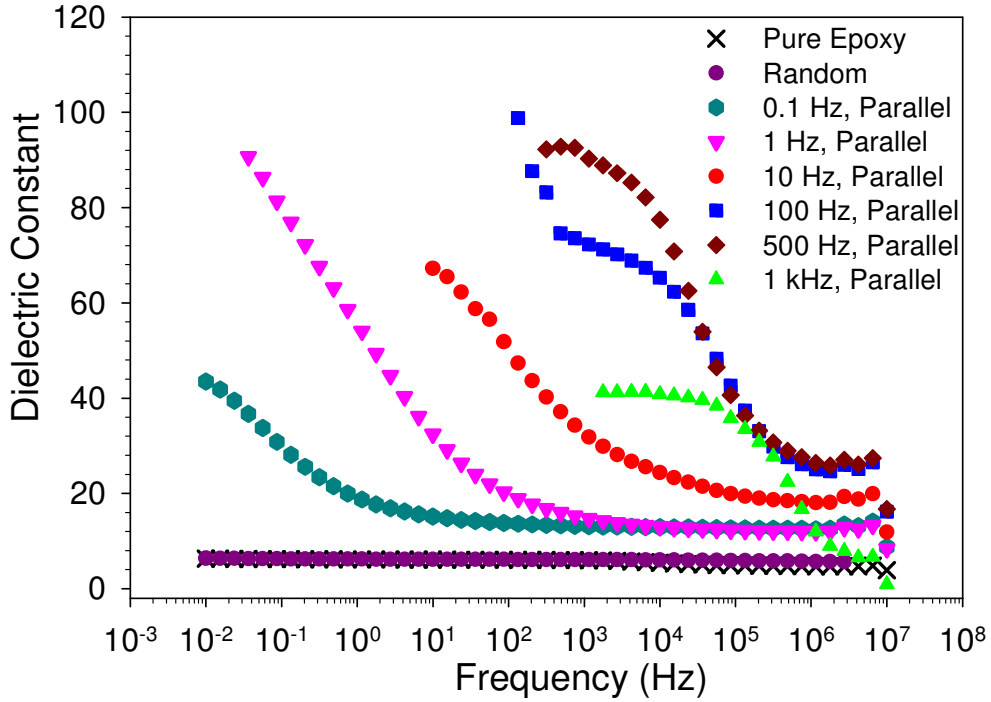

(a)

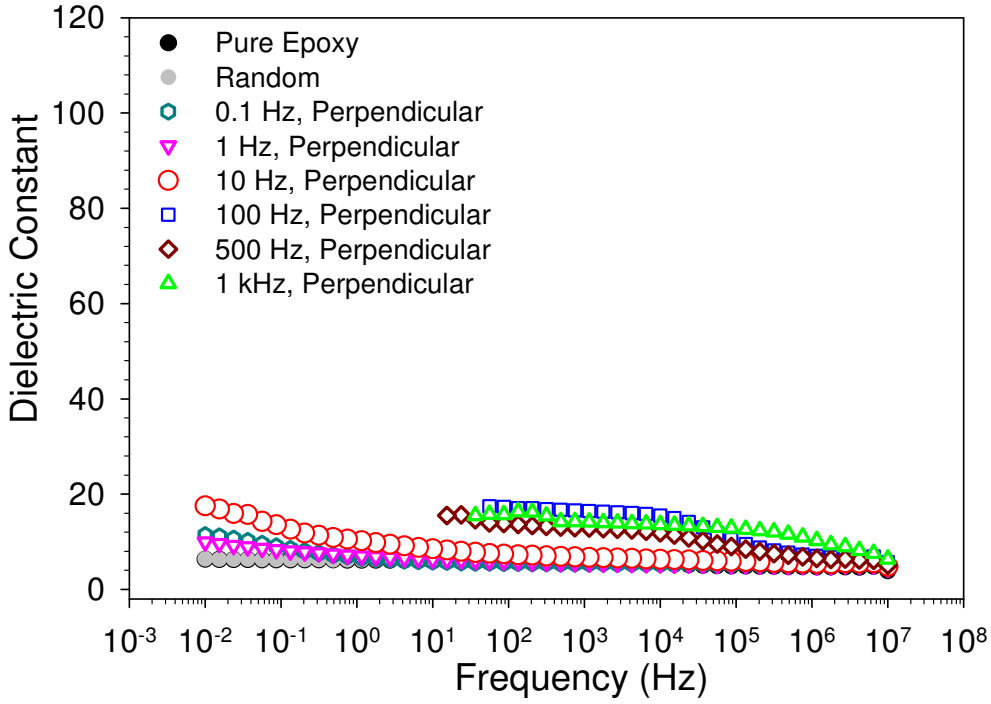

(b)

Figure 5.9. Dielectric constant of electric field manipulated 0.1 wt% CNF-epoxy polymer nanocomposite as a function of frequency (a) parallel and (b) perpendicular to the electric field. Applied AC electric field was 100 V/mm, which was applied for 90 min.

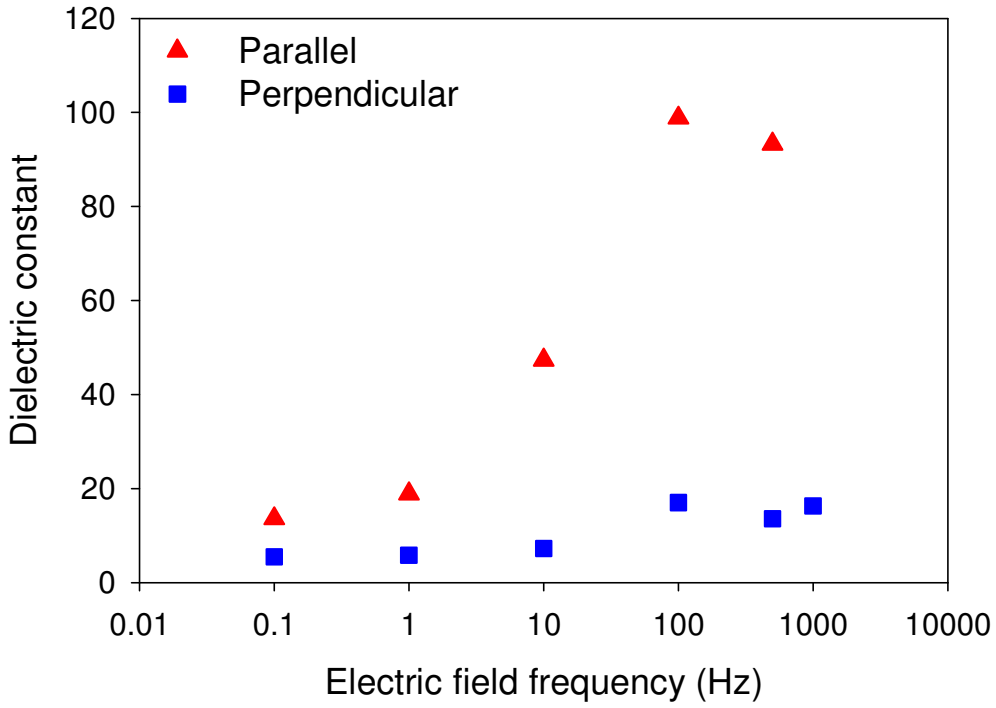

Figure 5.10. Dielectric constant in the parallel and perpendicular direction of electric field manipulated 0.1 wt% CNF-epoxy polymer nanocomposite measured at 0.01 Hz. Electrical conductivity is plotted as a function of electric field frequency starting from 0.1 Hz to 1 kHz. Magnitude of the AC electric field was 100 V/mm, which was applied for 90 min.

5.3 Mechanical properties of electric field manipulated nanocomposites

In Figure 5.11, the storage modulus of 0.03 wt% SWNT-acrylate nanocomposite is measured in two directions: parallel and perpendicular to the applied electric field. Storage modulus of the random sample is 1.2 GPa. Processing the nanocomposite at an electric field frequency of 100 Hz does not increase the storage modulus. The storage modulus value is similar in both parallel and perpendicular directions. The change in microstructure by processing at 100 Hz does not affect the storage modulus measurably. The nanocomposite processed at 1 kHz electric field frequency has a storage modulus of

1.6 GPa in the parallel direction and the perpendicular storage modulus is 1 GPa, as shown in Figure 5.11. There is a 60% increase in storage modulus in the parallel direction in reference to the random sample which indicates that the SWNTs are well aligned and thick chains are formed. However, in the perpendicular direction SWNTs do not contribute to the increase in storage modulus, resulting in a storage modulus comparable to that of the acrylate polymer matrix. A larger increase in storage modulus can be obtained by either modifying the electric field or the SWNT concentration. These results indicate that even the mechanical properties can be enhanced by electric field manipulation of polymer nanocomposites.

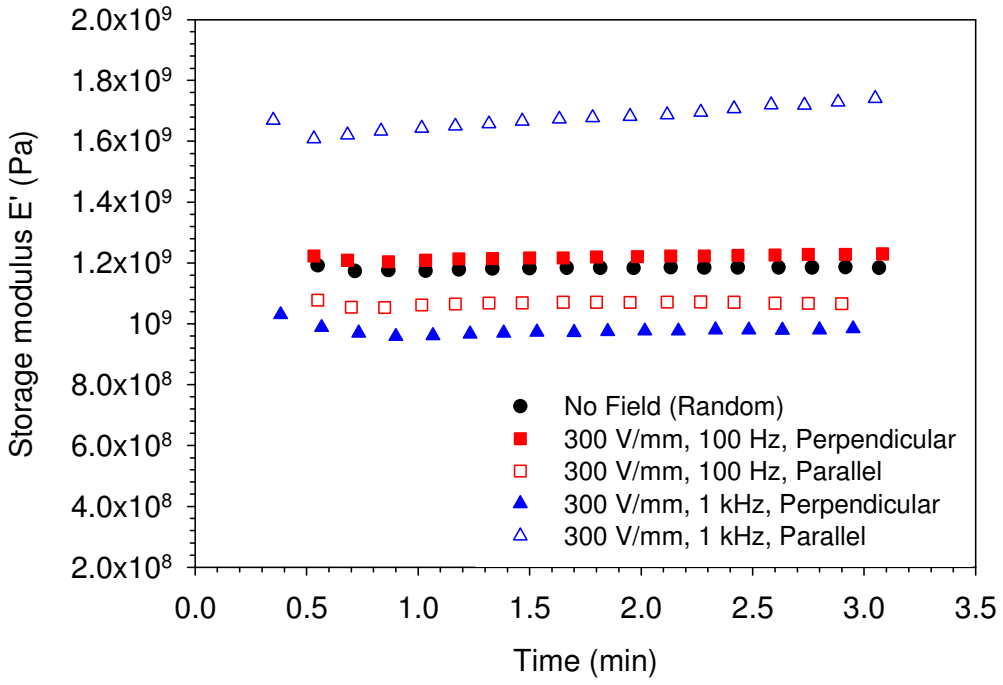

Figure 5.11. Parallel and perpendicular storage modulus of 0.03 wt% SWNT-acrylate polymer nanocomposite processed at 10 Hz, 100 Hz, and 1 kHz electric field frequencies. Magnitude of the AC electric field was 300 V/mm, which was applied for 30 min.

Storage modulus of aligned 0.1 wt% CNF-epoxy do not show an increase compared to unaligned samples in both parallel and perpendicular directions. The concentration of CNFs is too low to enhance the mechanical properties even after alignment. CNFs are not as strong as the SWNTs and a higher concentration of CNFs is likely required to increase the mechanical properties.

6. CONCLUSIONS AND RECOMMENDATIONS FOR FUTURE WORK

The main objective of this work was to improve the physical properties of polymer nanocomposites at low nanoparticle concentration where a homogeneous dispersion is possible. To fulfill this objective, an electric field was used to manipulate a low concentration of well dispersed SWNTs and CNFs in acrylate and epoxy polymers.

As a first step, we focused on dispersion of SWNTs and CNFs in three polymer matrices in order to develop an appropriate processing technique that leads to a homogeneous dispersion without detrimentally affecting the nanoparticle morphology. Two different methods of dispersion were used, solvent-free and solvent-based. A combination of mechanical stirring and sonication was used to separate the large SWNT and CNF agglomerates. Large shear produced by mechanical stirring resulted in smaller SWNT and CNF agglomerates. Increasing the sonication time also resulted in smaller SWNT and CNF agglomerates without detrimentally affecting SWNT and CNF morphology. Homogeneous distribution of SWNT bundles in acrylate polymer was achieved by the solvent-free method. CNFs were dispersed in epoxy polymer by both solvent-free and solvent-based methods, where OM images have shown a better distribution of CNFs by solvent-based method. Predispersion of CNFs in DMAc solvent reduced the CNF agglomerate sizes, which resulted in a better dispersion once the epoxy was added. Similarly, a solvent-based method was used to disperse SWNTs in polyimides, where the polymer is polymerized in the presence of the SWNTs. Percolation study on CNF-

epoxy nanocomposites and SWNT-polyimide nanocomposites have shown low percolation threshold values. CNF-epoxy nanocomposites have shown a percolation transition around 1.5 wt%, which is relatively low for CNF nanocomposites when compared to percolation values reported in the literature, which are as high as 5-10 wt% [1-3]. Percolation threshold of SWNT-polyimide nanocomposites was achieved at 0.06 wt%. Mechanical measurements on SWNT-polyimide nanocomposites showed large enhancement in values. Storage modulus of SWNT-polyimide nanocomposite increased by 113% below T_g and by 480% above T_g at 2 wt% SWNT. The increase in storage modulus indicates homogeneous distribution of SWNTs in polyimide matrix and good SWNT-polyimide interaction. Once a dispersion procedure was optimized for each polymer system, the study moved to the next step, which is electric field-assisted manipulation of SWNTs and CNFs in the polymer solutions.

SWNTs and CNFs were successfully manipulated by means of an AC electric field in acrylate and epoxy polymer solutions. Alignment was observed under an optical microscope to monitor the change in microstructure, which help to identify a two-step process: rotation of SWNT and CNF in the direction of electric field, and chaining of SWNTs and CNFs. Time taken for rotation was dependent on electric field magnitude and viscosity of the polymer, time for rotation decreased with increase in electric field magnitude and with decrease in polymer viscosity. Rotation of SWNT bundles and CNFs was due to the electric field-induced torque. SWNT bundles and CNFs were polarized when AC electric field was applied. Higher polarizability along the long axis

of the high aspect ratio nanoparticle induces a torque, which rotates it in the direction of electric field. Further, we found that extent of SWNT alignment in acrylates following rotation was dependent on AC electric field frequency. ODF developed from experimental polarized Raman spectroscopy data indicated increase in SWNT alignment with increase in AC electric field frequency from 10 Hz to 25 kHz. Increase in electric field magnitude and frequency increases the torque on SWNTs and CNFs resulting in faster and better alignment. Frequency dependence comes from the dielectric permittivity and conductivity of the particle, which appear in the Clausius Mossoti factor, and can be highly dependent on frequency in the case of lossy dielectric particles such as SWNTs and CNFs.

The second step that was observed in the alignment procedure is chain formation of SWNTs and CNFs. After rotation, the nanoparticles attract towards each other forming long chains in the direction of applied electric field and perpendicular to the electrodes. OM images show chain formation increases with increase in magnitude, frequency and duration of applied electric field. For example, in the case of SWNT bundles in acrylate polymer solution no visible chains were formed at 100 V/mm, but chains started to form at 300 V/mm. Very thin chains were formed at low frequencies, namely 1 Hz, 10 Hz and 100 Hz, but as the frequency increased to 1 kHz and higher, thicker chains were formed. Thickness of these chains also increased when the duration of applied electric field was increased above 10 minutes. Chain formation seems to saturate and reach a steady state after 45 hours, as seen in OM images and in-situ electrical measurements. The frequency

dependence of chain formation pointed to dielectrophoresis as the possible driving force. Dielectrophoretic force acts on the polarized nanoparticles, which results in attraction of nanoparticles towards each other. Frequency dependence resides in the Clausius Mossoti factor, which increases with increase in frequency thus, increasing the dielectrophoretic force. In situ electrical measurements show that an optimum AC electric field magnitude, frequency and time were required to increase the electrical and dielectric properties. For example, there was no increase in electrical conductivity and dielectric constant after applying an AC electric field of 300 V/mm for 10 minutes, but there was an increase after 30 minutes because the thickness of chains increased from less than 10 μm to ~70 μm. Electrical conductivity and dielectric constant after 30 minutes also increased as the frequency of applied electric field increased from 10 Hz to 25 kHz. In that frequency range, the thickness of the chains increased from ~30 μm to ~70 μm respectively.

In the final step we demonstrated that it is possible to immobilize the SWNT and CNF alignment in the acrylate and epoxy polymer solutions respectively by initiating curing of the polymer, either chemically or thermally. OM images have shown that the electric field-modified microstructure was retained in both SWNT-acrylate and CNF-epoxy polymer nanocomposites after the electric field was turned OFF. The impact of the resulting microstructure on the physical properties of the nanocomposites were assessed by measuring electrical conductivity, dielectric constant and storage modulus in parallel and perpendicular directions in the solid composites. These physical properties were

dependent on network formation and alignment of SWNTs and CNFs. Electrical conductivity and dielectric constant of the randomly dispersed 0.03 wt% SWNT-acrylate polymer nanocomposites were independent of measurement direction. For the 0.03 wt% SWNT-acrylate nanocomposites subjected to an electric field of 300 V/mm for 30 minutes at 10 Hz, 100 Hz and 1 kHz frequency, conductivity and dielectric constant were measured parallel and perpendicular to direction of electric field. There was an increase in conductivity in the parallel direction when 10 Hz, 100 Hz and 1 kHz electric field frequencies are applied. Highest increase in parallel conductivity, which was by three orders, was seen for the nanocomposite processed at 1 kHz electric field frequency. There was no increase in conductivity measured in the perpendicular direction; their conductivity values were similar to the random sample. Similar behavior was also seen for the dielectric constant measurements.

There was no change in electrical conductivity and dielectric constant of pure epoxy by the addition of 0.1 wt% CNFs. However, there was an increase in conductivity and dielectric constant when 0.1 wt% CNF-epoxy nanocomposite was aligned by applying an AC electric field of 100 V/mm, resulting in anisotropic behavior. Conductivity and dielectric constant values in the parallel direction were greater than the perpendicular direction. Change in conductivity and dielectric constant was dependent on the electric field alignment frequency. There was a three-order increase in parallel conductivity when 0.1 wt% CNF-epoxy nanocomposite was subjected to 0.1 Hz electric field frequency, which further increased by ten orders when subjected to 1 kHz electric field

frequency. Similar trend was seen for conductivity in the perpendicular direction, where a two-order increase was observed when subjected to 0.1 Hz electric field frequency, which further increased by eight orders when subjected to 1 kHz electric field frequency. Anisotropy in conductivity was also dependent on AC electric field frequency. CNF-epoxy nanocomposite processed by applying an electric field of 100 V/mm at 10 Hz frequency had the greatest anisotropy in conductivity. In the perpendicular direction, this nanocomposite was below percolation, while in the parallel direction it was above percolation. Epoxy nanocomposites subjected to 0.1 Hz and 1 Hz electric field frequency were below percolation in both parallel and perpendicular directions. Epoxy nanocomposites subjected to 100 Hz, 500 Hz and 1 kHz electric field frequency were above percolation in both parallel and perpendicular directions. In general, electrical conductivity of 0.1 wt% CNF-epoxy nanocomposite increased from 10^{-12} S/m to 10^{-4} S/m as the electric field frequency was increased from 0.1 Hz to 1 kHz. These experimental results provide information about the impact of alignment on electrical conductivity and also a relationship between processing parameters and the resulting morphology.

Through a variety of characterization techniques, we showed that large improvements in physical properties can be achieved by electric field manipulation of nanoparticle-polymer solutions. Electrical conductivity was increased by 11 orders of magnitude for electric field-manipulated 0.1 wt% CNF-epoxy nanocomposite, reaching a value seen for a randomly dispersed 3 wt% CNF-epoxy composite. Electric field magnitude, frequency

and time can be tuned to achieve desired physical properties at very low nanoparticle loadings.

Recommendations for future work on this topic are described in the following bullets: 1) Regarding dispersion and nanoparticle-polymer interaction, future work could focus on identifying the nature of interaction between SWNT and epoxy and acrylate polymer matrix. This analysis can be done using Raman spectroscopy such as the study done on SWNT-polyimide.[4] The shift in SWNT tangential peak indicates the type of interaction. 2) Regarding the aligned microstructure, the next step should focus on probing the microstructure of SWNTs and CNFs inside the bundles and inside the aligned chains. This can be tackled by using scanning electron microscopy and transmission electron microscopy. 3) Regarding quantifying the electrokinetic and other forces acting on the nanoparticles when subjected to an electric field, especially dielectrophoretic force. This can be done using numerical methods to calculate the local electric field gradient in nanoparticle-polymer solutions. This will provide valuable information in designing materials with specific desired properties. 4) Regarding verifying the reinforcing effect of aligned nanoparticles on the mechanical properties of nanocomposites. This can be verified measuring the storage modulus in parallel and perpendicular direction of electric field manipulated polymer nanocomposites. 5) Regarding testing sensing and actuation capability. This can be done by varying percolation through electric field manipulation of polymer nanocomposites.

REFERENCES

[1] E. Hammel, X. Tang, M. Trampert, T. Schmitt, K. Mauthner, A. Eder, P. Potschke, *Carbon* **2004**, *42*, 1153.

[2] B. A. Higgins, W. J. Brittain, *Eur. Polym. J.* **2005**, *41*, 889.

[3] K. Lozano, J. Bonilla-Rios, E. V. Barrera, *J. Appl. Polym. Sci.* **2001**, *80*, 1162.

[4] K. E. Wise, C. Park, E. J. Siochi, J. S. Harrison, *Chem. Phys. Lett.* **2004**, *391*, 207.

[5] K. Lozano, *JOM* **2000**, *52*, 34.

[6] X. Lu, D. D. L. Chung, *Composites: Part B* **1999**, *30*, 227.

[7] J. Wu, D. D. L. Chung, *Carbon* **2002**, *40*, 445.

[8] J. Chen, M. A. Hamon, H. Hu, Y. Chen, A. M. Rao, P. C. Eklund, R. C. Haddon, *Science* **1998**, *282*, 95.

[9] Z. Jia, Z. Wang, C. Xu, J. Liang, B. Wei, D. Wu, S. Zhu, *Materials Science and Engineering* **1999**, *A271*, 395.

[10] E. T. Mickelson, C. B. Huffman, A. G. Rinzler, R. E. Smalley, R. H. Hauge, J. L. Margrave, *Chem. Phys. Lett.* **1998**, *296*, 188.

[11] X. Gong, J. Liu, S. Baskaran, R. D. Voise, J. S. Young, *Chemical Materials* **2000**, *12*, 1049.

[12] D. Li, H. Wang, J. Zhu, X. Wang, L.Lu, X. Yang, *J. Mater. Sci. Lett.* **2003**, *22*, 253.

[13] T. Chatterjee, K. Yurekli, V. G. Hadjiev, R. Krishnamoorti, *Advanced Functional Materials* **2005**, *15*, 1832.

[14] M. J. O'Connell, S. M. Bachilo, C. B. Huffman, V. C. Moore, M. S. Strano, E. H. Haroz, K. L. Rialon, P. J. Boul, W. H. Noon, C. Kittrell, J. Ma, R. H. Hauge, R. B. Weisman, R. E. Smalley, *Science* **2002**, *297*, 593.

[15] R. J. Chen, Y. Zhang, D. Wang, H. Dai, *Journal of American Chemical Society* **2001**, *123*, 3838.

[16] J. Zhao, J. P. Lu, J. Han, C. K. Yang, *Appl. Phys. Lett.* **2003**, *82*, 3746.

[17] B. X. Yang, K. P. Pramoda, G. Q. Xu, S. H. Goh, *Adv. Funct. Mater.* **2007**, *17*, 2062.

[18] J. N. Coleman, U. Khan, Y. K. Gunko, *Advanced Materials* **2006**, *18*, 689.

[19] J. N. Coleman, U. Khan, W. J. Blau, Y. K. Gunko, *Carbon* **2006**, *44*, 1624.

[20] K. W. Putz, C. A. Mitchell, R. Krishnamoorti, P. F. Green, *Journal of Polymer Science Part B: Polymer Physics* **2004**, *42*, 2286.

[21] P. Potschke, S. M. Dudkin, I. Alig, *Polymer* **2003**, *44*, 5023.

[22] C. Park, Z. Ounaies, K. A. Watson, R. E. Crooks, J. Smith, S. E. Lowther, J. W. Connell, E. J. Siochi, J. S. Harrison, T. L. S. Clair, *Chem. Phys. Lett.* **2002**, *364*, 303.

[23] Z. Ounaies, C. Park, K. E. Wise, E. J. Siochi, J. S. Harrison, *Comp. Sci. Tech.* **2003**, *63*, 1637.

[24] C. A. Martin, J. K. W. Sandler, A. H. Windle, M. K. Schwarz, W. Bauhofer, K. Schulte, M. S. P. Shaffer, *Polymer* **2005**, *46*, 877.

[25] C. Park, J. Wilkinson, S. Banda, Z. Ounaies, K. E. Wise, G. Sauti, P. T. Lillehei, J. S. Harrison, *J. Polym. Sci., Part B: Polym. Phys.* **2006**, *44*, 1751.

[26] T. Prasse, J. Y. Cavaille, W. Bauhofer, *Comp. Sci. Tech.* **2003**, *63*, 1835.

[27] T. Prasse, L. Flandin, K. Schulte, W. Bauhofer, *Appl. Phys. Lett.* **1998**, *72*, 2903.

[28] *British Standards Institution* **2005**, *PAS 71*, 1.

[29] w. m. u. e. 2000/team1/final/main.html. (accessed on July 2008).

[30] M. Endo, Y. A. Kim, T. Hayashi, Y. Fukai, K. Oshida, M. Terrones, T. Yanagisawa, S. Higaki, M. S. Dresselhaus, *Appl. Phys. Lett.* **2002**, *80*, 1267.

[31] S. Iijima, T. Ichihashi, *Nature* **1993**, *363*, 603.

[32] S. Iijima, *Nature* **1991**, *354*, 56.

[33] C. Journet, W. K. Maser, P. Bernier, A. Loiseau, M. Chapelle, A. Lefrant, P. Deniard, R. Lee, J. E. Fischer, *Nature* **1997**, *388*, 756.

[34] C. Journet, P. Bernier, *Applied Physics A* **1998**, *67*, 1.

[35] Z. Shi, Y. Lian, F. H. Liao, X. Zhou, Z. Gu, Y. Zhang, *Journal of Physics and Chemistry of Solids* **2000**, *61*, 1031.

[36] Y. Saito, K. Nishikubo, K. Kawabata, T. Matsumoto, *Journal of Applied Physics* **1996**, *80*, 3062.

[37] A. G. Rinzler, J. Liu, H. Dai, P. Nikolaev, C. B. Huffman, F. J. Rodriguezmacias, *Applied Physics A* **1998**, *67*, 29.

[38] Z. F. Ren, Z. P. Huang, J. W. Xu, J. H. Wang, P. Bush, M. P. Siegal, *Science* **1998**, *282*, 1105.

[39] Z. F. Ren, Z. P. Huang, J. W. Xu, D. Z. Wang, J. G. Wen, J. H. Wang, *Applied Physics Letters* **1999**, *75*, 1086.

[40] Z. P. Huang, J. W. Xu, Z. F. Ren, J. H. Wang, M. P. Siegal, P. N. Provencio, *Applied Physics Letters* **1998**, *73*, 3845.

[41] P. Nikolaev, M. J. Bronikowski, R. K. Bradley, F. Rohmund, D. T. Colbert, K. A. Smith, R. E. Smalley, *Chemical Physics Letters* **1999**, *313*, 91.

[42] G. Tibbetts, D. W. Gorkiewvzz, *Carbon* **1993**, *31*, 809.

[43] S. Iijima, T. Ichlhashi, *Nature* **1993**, *363*, 603.

[44] M. S. Dresselhaus, G. Dresselhaus, P. C. Eklund, R. Saito, *Physics World* **1998**, *January*, 33.

[45] P. M. Ajayan, T. I. Iijima, *Chem. Phys. Lett.* **1993**, *202*, 384.

[46] S. Iijima, T. Ichihashi, Y. Ando, *Nature* **1992**, *356*, 776.

[47] B. I. Yakabson, R. E. Smalley, *Am. Sci.* **1997**, *324*.

[48] F. Li, B. S. Cheng, G. Su, M. S. Dresselhaus, *Applied Physics Letters* **2000**, *77*, 3161.

[49] J. P. Lu, *Journal of Physics and Chemistry of Solids* **1997**, *58*, 1649.

[50] P. G. Collins, P. Avouris, *Scientific American* **2000**, *283*, 62.

[51] X. B. Wang, R. Pethig, T. B. Jones, *J. Phys. D: Appl. Phys.* **1992**, *25*, 905.

[52] X. L. Xiea, Y. W. Maia, X. P. Zhoub, *Materials Science and Engineering R* **2005**, *49*, 89.

[53] F. Du, J. E. Fischer, K. I. Winey, *Journal of Polymer Science: Part B: Polymer Physics* **2003**, *41*, 3333.

[54] B. Safadi, R. Andrews, E. A. Grulke, *J. Appl. Polym. Sci.* **2002**, *84*, 2660.

[55] A. Dufresne, M. Paillet, J. L. Putaux, R. Canet, F. Carmona, P. Delhaes, C. S, *J. Mater. Sci.* **2002**, *37*, 3915.

[56] C. Park, Z. Ounaies, K. A. Watson, R. E. Crooks, J. Smith, S. E. Lowther, J. W. Connell, E. J. Siochi, J. S. Harrison, T. L. S. Clair, *Chem. Phys. Lett.* **2002**, *364*, 303.

[57] M. L. Shofnera, F. J. Rodrıguez-Macıas, R. Vaidyanathan, E. V. Barreraa, *Composites: Part A* **2003**, *34*, 1207.

[58] E. T. Thostenson, T. W. Chou, *Journal of Physics D: Applied Physics* **2002**, *36*, L77.

[59] J. K. W. Sandler, S. Pegel, M. Cadek, F. Gojny, M. V. Es, J. Lohmar, W. J. Blau, K. Schulte, A. H. Windle, M. S. P. Shaffer, *Polymer* **2004**, *45*, 2001.

[60] P. Potschke, S. M. Dudkin, I. Alig, *Polymer* **2003**, *44*, 5023.

[61] A. R. Bhattacharyya, P. Potschke, M. A. Goad, D. Fischer, *Chem. Phys. Lett.* **2004**, *392*.

[62] D. W. Ferguson, E. W. S. Bryant, H. C. Fowler, *ANTEC'98* **1998**, 1219.

[63] J. R. Hagerstrom, S. L. Greene, *Electrostatic Dissipating Composites Containing Hyperion Fibril Nanotubes*, Miami, USA **2000**.

[64] G. D. Liang, S. C. Tjong, *IEEE Transactions on Dielectrics and Electrical Insulation* **2008**, *15*, 214.

[65] S. A. Gordeyev, F. J. Macedo, J. A. Ferreira, F. W. J. v. Hattum, C. A. Bernardo, *Physica B* **2000**, *279*, 33.

[66] M. L. Shofner, F. J. Rodrıguez-Macıas, R. Vaidyanathan, E. V. Barreraa, *Composites: Part A* **2003**, *34*, 1207.

[67] J. Zenga, B. Saltysiak, W. S. Johnson, D. A. Schiraldic, S. Kumara, *Composites: Part B 35* **2004**, *35*, 173.

[68] A. Almasri, Z. Ounaies, Y. S. Kim, J. Grunlan, *Macromolecular Materials & Engineering* **2008**, *293*, 123.

[69] Z. Ounaies, C. Park, K. E. Wise, E. J. Siochi, J. S. Harrison, *Composites Science and Technology* **2003**, *63*, 1637.

[70] M. A. Hamon, J. Chen, H. Hu, Y. Chen, M. E. Itkis, A. M. Rao, P. C. Eklund, R. C. Haddon, *Advanced Materials* **1999**, *11*, 834.

[71] D. E. Hill, Y. Lin, A. M. Rao, L. F. Allard, Y.-P. Sun, *Macromolecules* **2002**, *35*, 9466.

[72] J. Zhu, J. D. Kim, H. Peng, J. Margrave, V. N. Khabashesku, E. V. Barrera, *Nano Lett.* **2003**, *3*, 1107.

[73] C. A. Mitchell, J. L. Bahr, S. Arepalli, J. M. Tour, R. Krishnamoorti, *Macromolecules* **2002**, *35*, 8825.

[74] L. Qu, Y. Lin, D. E. Hill, B. Zhou, W. Wang, Z. Sun, A. Kitaygorodskiy, M. Suarez, J. W. Connell, L. F. Allard, Y. P. Sun, *Macromolecules* **2004**, *37*, 6055.

[75] Y. Lin, B. Zhou, *Macromolecules* **2003**, *36*, 7199.

[76] T. Ramanathan, H. Liu, L. C. Brinson, *Journal of Polymer Science Part B: Polymer Physics* **2005**, *43*, 2269.

[77] J. L. Bahr, J. M. Tour, *J. Mater. Chem.* **2002**, *12*, 1952.

[78] M. Burghard, *Surface Science Reports* **2005**, *58*, 1.

[79] C. A. Dyke, J. M. Tour, *Chemistry A European Journal* **2004**, *10*, 812.

[80] E. T. Mickelson, W. Chiang, J. L. Zimmerman, P. J. Boul, J. Lozano, J. Liu, R. E. Smalley, R. H. Hauge, J. L. Margrave, *Journal of Physical Chemistry B* **1999**, *103*, 4318.

[81] J. Zhao, H. Park, J. Han, J. P. Lu, *Journal of Physical Chemistry B* **2004**, *108*.

[82] E. Bekyarova, M. E. Itkis, N. Cabrera, B. Zhao, A. Yu, J. Gao, R. C. Haddon, *Journal of American Chemical Society* **2005**, *127*, 5990.

[83] Y. J. Kim, T. S. Shin, H. D. Choi, J. H. Kwon, Y. C. Chung, H. G. Yoon, *Carbon* **2005**, *43*, 23.

[84] J. Chen, R. Ramasubramaniam, C. Xue, H. Liu, *Adv. Funct. Mater.* **2006**, *16*, 14.

[85] J. Chen, H. Liu, W. A. Weimer, M. D. Halla, D. H. Waldeck, G. C. Walker, *Journal of American Chemical Society* **2002**, *124*, 9034.

[86] J. C. Grunlan, L. Liu, Y. S. Kim, *Nano Letters* **2006**, *6*, 911.

[87] X. H. Li, B. Wu, J. E. Huang, J. Zhang, Z. F. Liu, H. L. Li, *Carbon* **2002**, *411*, 1645.

[88] M. Sitti, H. Hashmoto, *IEEE/ASME Trans. on Mechatronics* **2000**, *5*, 199.

[89] M. Sitti, *IEEE-NANO* **2001**, *S2.2*, 75.

[90] W. J. Li, N. Xi, W. K. Fung, T. S. Wong, *Encyclopedia of Nanoscience and Nanotechnology* **2004**, *7*, 351.

[91] L. J. Lanticse, Y. Tanabe, K. Matsui, Y. Kaburagi, K. Suda, M. Hoteida, M. Endo, E. Yasuda, *Carbon* **2006**, *44*, 3078.

[92] R. Haggenmueller, H. H. Gommans, A. G. Rinzler, J. E. Fischer, K. I. Winey, *Chemical Physics Letters* **2000**, *330*, 219.

[93] J. R. Wood, Q. Zhao, H. D. Wagner, *Composites Part A: Applied Science and Manufacturing* **2001**, *32*, 391.

[94] T. Kimura, H. Ago, M. Tobita, S. Ohshima, M. Kyotani, M. Yumura, *Advanced Materials* **2002**, *14*, 1380.

[95] B. W. Smith, Z. Benes, D. E. Luzzi, J. E. Fischer, *Applied Physics Letters* **2000**, *77*, 663.

[96] J. Hone, M. C. Llaguno, N. M. Nemes, A. T. Johnson, J. E. Fischer, D. A. Walters, M. J. Casavant, J. Schmidt, R. E. Smalley, *Applied Physics Letters* **2000**, *77*, 666.

[97] N. G. Green, A. Ramos, H. Morgan, *J. Phys. D: Appl. Phys.* **2000**, *33*, 632.

[98] A. Castellanos, A. Ramos, A. Gonzalez, N. G. Green, H. Morgan, *J. Phys. D: Appl. Phys.* **2003**, *36*, 2584.

[99] O. D. Velev, K. H. Bhatt, *Soft Matter* **2006**, *2*, 738.

[100] K. D. Hermanson, S. O. Lumsdon, J. P. Williams, E. W. Kaler, O. D. Velev, *Science* **2001**, *294*, 1082.

[101] R. Kretschmer, W. Fritzsche, *Langmuir* **2004**, *20*, 11797.

[102] S. Lumsdon, E. W. Kaler, J. P. Williams, O. D. Velev, *Appl. Phys. Lett.* **2003**, *82*, 949.

[103] S. O. Lumsdon, E. W. Kaler, O. D. Velev, *Langmuir* **2004**, *20*, 2108.

[104] K. H. Bhatt, O. D. Velev, *Langmuir* **2004**, *20*, 467.

[105] M. Dimaki, P. Boggild, *Nanotechnology* **2004**, *15*, 1095.

[106] M. Dimaki, P. Boggild, *Nanotechnology* **2005**, *16*, 759.

[107] Y. J. Yuan, M. K. Andrews, B. K. Marlow, *Appl. Phys. Lett.* **2004**, *85*, 130.

[108] P. Bahukudumbi, W. N. Everett, A. Beskok, M. A. Bevan, G. H. Huff, D. Lagoudas, Z. Ounaies, *Appl. Phys. Lett.* **2007**, *90*, 224102.

[109] S. O. Lumsdon, D. M. Scott, *Langmuir* **2005**, *21*, 4874.

[110] S. B. Asokan, L. Jawerth, R. L. Carroll, R. E. Cheney, S. Washburn, R. Superfine, *Nano Lett.* **2003**, *3*, 431.

[111] J. Li, Q. Zhang, N. Peng, Q. Zhu, *Appl. Phys. Lett.* **2005**, *86*, 153116.

[112] N. Peng, Q. Zhang, J. Li, N. Liu, *J. Appl. Phys.* **2006**, *100*, 024309.

[113] S. Tung, H. Rokadia, W. J. Li, *Sens. Actuators, A* **2007**, *133*, 431.

[114] D. Wang, R. Zhu, Z. Zhou, X. Ye, *Applie Physics Letters* **2007**, *90*, 103110.

[115] K. Yamamoto, S. Akita, Y. Nakayama, *J. Phys. D: Appl. Phys.* **1998**, *31*, L34.

[116] M. S. Kumar, T. H. Kim, S. H. Lee, S. M. Song, J. W. Yang, K. S. Nahm, E. K. Suh, *Chem. Phys. Lett.* **2004**, *383*, 235.

[117] M. Dimaki, P. Boggild, *Nanotechnology* **2004**, *15*, 1095.

[118] J. Suehiro, G. Zhou, M. Hara, *J. Phys. D: Appl. Phys.* **2003**, *36*, L109.

[119] G. H. Kim, Y. M. Shkel, *J. Mater. Res.* **2003**.

[120] H. Koerner, D. Jacobs, D. W. Tomlin, J. D. Busbee, R. D. Vaia, *Adv. Mater.* **2004**, *16*, 297.

[121] T. Takahashi, T. Murayama, A. Higuchi, H. Awano, K. Yonetake, *Carbon* **2006**, *44*, 1180.

[122] S. A. Wilson, G. M. Maistros, R. W. Whatmore, *J. Phys. D: Appl. Phys.* **2005**, *38*, 175.

[123] E. Svasand, G. Helgesen, A. T. Skjeltorp, *Colloids Surf., A* **2007**, *308*, 67.

[124] Z. Liang, J. Goua, C. Zhang, B. W. L. Krame, *Materials Science and Engineering A* **2004**, *365*, 228.

[125] T. B. Jones, *Electromechanics of Particles*, Cambridge University Press, Cambridge, **1995**.

[126] H. Morgan, N. G. Green, *AC Electrokinetics Colloids and Nanoparticles*, Research studies Press Ltd, Baldock, England **2003**.

[127] H. A. Pohl, *Dielectrophoresis*, Cambridge University Press, Cambridge **1978**.

[128] B. J. John, L. D. Russell, *Electron Microscopy: Principles and Techniques for Biologists*, Bartlett Publishers, Sudbury, MA, **1999**.

[129] S. Kirkpatrick, *Reviews of Modern Physics* **1973**, *45*, 574.

[130] P. Potschke, S. M. Dudkin, I. Alig, *Polymer* **2003**, *44*, 5023.

[131] A. Jorio, M. A. Pimenta, M. S. S. Dantas, *Physical Review Letters* **2000**, *84*, 1820.

[132] M. S. Dresselhaus, G. Dresselhaus, A. Jorio, A. G. S. Filho, R. Saito, *Carbon* **2002**, *40*.

[133] R. Pérez, S. Banda, Z. Ounaies, *J. Appl. Phys.* **2008**, *103*, 074302.

[134] Z. Ounaies, C. Park, J. Harrison, "Single wall carbon nanotube polymer composites: investigating their percolative behavior and physical performance", presented at *ASME International Mechanical Engineering Congress & Exposition*, Anaheim, CA, **2004**.

[135] L. X. Benedict, S. G. Louie, M. L. Cohn, *Physical Review B* **1995**, *52*, 8541.

[136] T. Ebbesen, H. Lezec, H. Hiura, J. Bennett, H. Ghaemi, T. Thio, *Nature* **1996**, *382*, 54.

[137] C. Zhou, J. Kong, H. J. Dai, *Appl. Phys. Lett.* **2000**, *76*, 1597.

[138] H. A. Pohl, *J. Appl. Phys.* **1951**, *22*, 869.

VITA

Name: Sumanth Banda

Address: Department of Aerospace Engineering, H. R. Bright Building, Rm 701, Ross Street- TAMU 3141, College Station, TX, 77843-3141

Email address: sumanthb@gmail.com

Education: Bachelor of Technology (B. Tech), Jawaharlal Nehru Technological University, India, 2002.
M.S. Virginia Commonwealth University, Richmond, VA, 2004.
Ph.D. Texas A&M University, College Station, TX, 2008

Journal publications:

S. Banda, Z. Ounaies, "Electric field alignment of SWNT-polymer nanocomposites", Manuscript in preparation.

R. Perez, S. Banda, Z. Ounaies, "Determination of the Orientation Distribution Function (ODF) by Polarized Raman Spectroscopy in aligned SWNT polymer", accepted in Journal of Applied Physics, 2008.

S. Banda, Z. Ounaies, C. Park. 2006, "Dynamic Mechanical Analysis of Single Wall Carbon Nanotube Polyimide Composite Thin Films", submitted to *Composites Science & Technology*.

C. Park, J. Wilkinson, S. Banda, Z. Ounaies, 2006, "Aligned single wall carbon nanotube polymer composites using an electric field" *Journal of Polymer Science Part B: Polymer Physics,* 44, 1751.

Conference proceedings:

S. Yun, J. H. Kim, **S. Banda**, Z. Ounaies, K. Kim, "Alignment of multi-walled carbon nanotubes in cellulose EAPap by electric fields" Proceedings of SPIE Proceedings of SPIE: Smart Structures and Materials, Volume 6526.

Z. Ounaies, A. Almasri, **S. Banda**, J. Grunlan, 2006, "*Active nanocomposite polymers: enhancing sensing and actuation performance*" Multifunctional nanocomposites International Conference ASME, Honolulu, HI.

S. Banda, Z. Ounaies, 2005, "Electric field alignment of single wall carbon nanotubes in polymers" *Proceedings of SPIE: Smart Structures and Materials*, Volume 5761.

S. Banda, Z.Ounaies, C. Park, J. Wilkinson, and J. Harrison., 2004, "Aligned carbon nanotube-polymer composites: investigating their electrical and physical characteristics", *Proceedings of SPIE: Smart Structures and Materials*, Volume 5387.